THE PHYSICAL AND CHEMICAL PROPERTIES OF THE SURFACE OF VENUS

by

Stewart David Nozette

B.S. The University of Arizona
(1979)

SUBMITTED TO THE DEPARTMENT OF
EARTH AND PLANETARY SCIENCES
IN PARTIAL FULFILLMENT OF THE
REQUIREMENTS OF THE
DEGREE OF

DOCTOR OF PHILOSOPHY

AT THE

MASSACHUSETTS INSTITUTE OF TECHNOLOGY

November 1982

Signature of Author . . . . . .
Department of Earth and Planetary
Sciences
November 2, 1982

Certified by. . . . . .
John Lewis, Thesis Supervisor

Certified by. . . . . .
Gordon Pettengill, Thesis Supervisor

Accepted by . . . . . .
Ted Madden
Chairman, Department Committee

THE PHYSICAL AND CHEMICAL PROPERTIES OF THE SURFACE OF VENUS

by

Stewart David Nozette

Submitted to the Department of Earth and Planetary Sciences on November 2, 1982, in Partial Fulfillment of the Requirements of the Degree of Doctor of Philosophy

ABSTRACT

Experimental studies of aeolian transport on Venus, using a scale-modeling technique, indicate that observed surface winds are sufficient to move sedimentary particles of about 0.3 mm or less in diameter. Measurements of radar reflectivity indicate that portions of the surface are covered by material with low bulk density, possibly wind-blown sediments. Transport of chemically weathered material by wind may also affect the local composition of the lower atmosphere. The buffering of atmospheric gases in some regions of the surface is only possible for a restricted mineral assemblage.

Radar determination of the surface dielectric constant by the Pioneer Venus radar mapper for at least one area of the surface, Theia Mons, suggests that the surface contains conductive material, probably iron sulfides. Laboratory measurements of the dielectric constants of terrestrial sulfide bearing rocks indicate that sulfide inclusions present at 15% by weight provide a good match to the dielectric constant inferred for Theia Mons. Theia Mons and other high-dielectric constant areas could be a source of sulfur bearing compounds previously suggested to explain the composition of the clouds of Venus.

In this thesis one possible model for geochemical transport is presented, transport of weathering products from high to low elevation. However, we are still ignorant of the relative importance of this process, and of the possible existence of others. Further insight into the physical and chemical nature of Venus will have to await more detailed exploration by spacecraft and laboratory investigation of chemical weathering.

Thesis Supervisors: John S. Lewis
Title: Professor of Planetary Science

Gordon H. Pettengill
Professor of Planetary Physics

ACKNOWLEDGEMENTS

I must acknowledge many people who played a crucial role in the preparation of this thesis.

I would like to express my gratitude to all members of my thesis committee, especially John Lewis and Gordon Pettengill, for their guidance and attention to this work. I must also express extreme gratitude to Peter Ford for his unique talents, and thorough understanding and tutelage, of the various aspects of the Pioneer Venus radar data reduction. I would also like to thank Eric Eliason, for his brief tour through the land of image processing, and for supplying the images used in my thesis. I must also thank John Southard for providing a reasonable experiment to study aeolian transport on Venus. I also thank M. B. Fegley and Ron Prinn for enlightening discussions. In addition, I must thank W. Westphal for aid in dielectric measurements.

It would be impossible to mention all of the individuals responsible for the success of the Pioneer Venus Project, which supplied the data that form the basis of this thesis. Therefore, I would like to extend my gratitude to all members of the Pioneer Project, both at NASA Ames, and NASA Headquarters, especially Larry Colin and Henry Brinton.

I would also like to thank Laurel Wilkening, and Geoff Briggs, for their encouragement in a time of rapidly changing direction for the U.S. space program.

Most importantly, I would like to extend my warmest appreciation to my parents, Morris and Helen Nozette, for their unyielding support through the tough times, and ups and downs of the NASA planetary program. More than anything, this thesis is a product of their support.

My gratitude is also extended to Mr. Francis Doughty, Ms. Barbara Langford, and to Ms. Dorothy Frank for typing and preparing the thesis.

TABLE OF CONTENTS

Table of Figures

List of Tables

I. Introduction

In the first two and a half decades of space exploration no fewer than nineteen separate spacecraft have been launched toward Venus. In spite of this extensive exploration, our understanding of the Venus surface remains sketchy and incomplete. The harsh and challenging surface conditions, and the obscuring clouds, have hindered direct observation. Yet, some conclusions are possible. This work represents a compilation of previous knowledge about the nature of the Venus surface, integrated with new ideas. A synthesis is attempted of our knowledge about the surface-atmosphere interaction on Venus, including: spacecraft radar observation, laboratory investigation of the dielectric properties of rocks, theoretical speculation on the chemistry of Venus, and experimental studies of surface aeolian transport. Such a synthesis requires an approach in the true spirit of planetary science and exploration, combining physics and chemistry with astronautics and engineering. Unfortunately, there exist many gaps in our understanding of Venus. These gaps may remain for at least six years, due to a hiatus in Venus exploration by the United States. The present hiatus serves as a useful time to look back on what has been learned, and to devise some new theories which can help us understand our present data and offer predictions which may be tested in the future.

The thesis is divided into three major sections. The first will review our current knowledge of the physical and chemical nature of the Venus atmosphere, and present some new ideas regarding the chemical interaction between atmosphere and surface with particular attention to using Pioneer Venus and Venera data in a model of chemical weathering on Venus. This section will address such questions as: what minerals are stable on which portions of the Venus surface, and what role does the surface play in regulating the composition of the Venus atmosphere?

The second section will focus on physical studies of the Venus surface made by the Pioneer Venus radar mapper, though measurements of radar altitude, roughness, and dielectric constant which allow new speculations on the gross physical and chemical characteristics of a large portion of the surface.

Since similar data are available for the Moon and Mars, we may compare the relationships between radar observations and the other characteristics observed directly on these planets, namely the regolith distribution and density and texture of the surface. The results of measurements of the dielectric constants of selected rocks is also reported.

Section three describes the results of a dynamic experiment scale-modeling aeolian transport on Venus. Aeolian transport provides a possible link between chemical weathering and some surface properties observed by radar.

Experiments on transport were conducted at the MIT Experimental Sedimentology Laboratory using materials which dynamically model the aeolian environment appropriate to selected elevations on Venus. These results indicate that aeolian transport is possible on Venus and can be invoked to explain some aspects of the distribution of surface regolith and weathering products.

The end of Section Three will summarize the basic conclusions of this thesis, and point the direction for further research. The exploration and understanding of Venus is an open-ended problem, and this thesis has only touched on a small portion of it.

Table 1. Venus Spacecraft Exploration

Spacecraft	Launch Date	Milestone
Mariner 2	August 27, 1962	First successful planetary flyby
Venera 4	June 12, 1967	First data from Venus atmosphere
Mariner 5	June 14, 1967	First fully instrumented flyby of Venus
Venera 5	January 5, 1969	Failed to reach surface
Venera 6	January 10, 1969	Failed to reach surface
Venera 7	August 17, 1970	First data from surface
Venera 8	March 27, 1972	Measured light on surface; first chemical analysis
Mariner 10	November 3, 1973	First dual planet mission (with Mercury)
Venera 9	June 14, 1975	Surface image and analysis
Venera 10	June 14, 1975	Surface analysis
Pioneer Venus 1	May 20, 1978	Extensive observation from orbit
Pioneer Venus 2	August 8, 1978	Four atmospheric probes
Venera 11	September 9, 1978	Atmospheric analysis
Venera 12	September 14, 1978	Atmospheric analysis
Venera 13	October 29, 1981	Extensive chemical analysis of surface
Venera 14	November 1, 1981	Analysis of surface

II. Interaction Between Atmosphere and Surface

A. Purpose

The harsh conditions found on Venus preclude extensive petrologic and geochemical investigation of the surface. One way to gather insight on the nature of the surface is to examine the atmosphere surface interaction using the methods of chemical thermodynamics. Given the known composition of the atmosphere, and geologically reasonable assumptions about what minerals may be present in rocks at the surface, some insight into chemical weathering processes is possible. Recent spacecraft data on surface composition can further constrain the problem. Another important motivation is to assess a possible role of the surface in regulating the composition of the atmosphere. The high surface temperatures found on Venus, combined with a lack of biological activity, suggest that chemical equilibrium may be approached near the atmosphere surface boundary in some regions of the surface. This assumption is the starting point for the investigation of atmosphere surface interaction on Venus.

B. Structure of the Venus Atmosphere

In order to study the atmosphere-surface interaction on Venus we must know the composition and structure of the atmosphere. The existence of a substantial atmosphere around Venus was first surmised in the late 18th century from the brilliance of the reflected sunlight. Since then,

many workers have attempted to unravel the nature, structure and composition of that atmosphere.

Observers in the 19th century searched for evidence of O_2 and H_2O. Claims of detection were made, but all were unreliable. We know today that these early investigations were actually reporting detection of terrestrial H_2O and O_2; in fact, the atmosphere above the Venus reflecting layers contains little of these gases.

Adams and Dunham (1932) made the first reliable detection of CO_2 in the Venus atmosphere using the 100-inch reflector at Mount Wilson. They discovered three bands at 782, 788, and 869μm which they attributed to Venusion CO_2. This result was confirmed by the laboratory work of Adel and Dennison (1933) and Adel and Slipher (1934). The CO_2 content above the reflecting layer was estimated by the latter to be about 3km-atm; by contrast the Earth's atmosphere has a total CO_2 column density of only 2.6m-atm.

The year 1967 marked the beginning of spacecraft examination of the detailed structure of the Venus atmosphere, with the arrival of Venera 4 and Mariner 5. Mariner 5 permitted the first successful radio occultation measurement of the atmosphere, while Venera 4 reported on in-situ conditions above 20km altitude. Neither spacecraft obtained a direct measurement of the surface conditions, but adiabatic extrapolation of their data using the Earth-based-radar-determined surface radius suggested a

surface pressure of about 90 bars and a temperature in excess of 700°K.

Later Soviet entry probes Venera 5-10 succeeded in establishing the conditions at the Venus surface, yielding a temperature of 750±20K and a pressure of 90±20 bars, with an atmosphere composed mostly of CO_2. The most detailed information concerning the structure of Venus atmosphere is given by Seiff et al. (1980). Using data from the four Pioneer Venus entry probes, which made in situ measurements from an altitude of 126km to impact, at four widely separated sites. For unknown reasons the temperature sensors on all four probes failed to operate below 12km altitude, while the pressure sensors reported faithfully throughout. Seiff et al. report an extrapolation of temperatures downward from the failure altitude by comparing the observed temperature-pressure profile above 12 km against a CO_2, N_2 adiabat ($\gamma \cong 1.4$). In the observed region, the data match the theoretical curves within several percent, an accuracy which is adequate for thermochemical calculations.

Probe altitude and temperature are plotted for all four probes in Figures 1 and 2. Altitudes were determined by assuming hydrostatic equilibrium:

$$dp = -\rho g dz \qquad (1)$$

Altitude is then defined by:

$$Z = \int_{p}^{p_o} \frac{\delta RT}{p\mu g(z)}\, dp \qquad (2)$$

where p and T are local atmospheric pressure and temperature, g(z) = local acceleration of gravity, R is the universal gas constant, δ is a non-ideal gas correction factor and μ is the mean molecular weight. Evaluation of the integral from the surface pressure (p_o) to p yields the altitude. The integral is evaluated numerically from the observations using tables of δ. Seiff *et al.* report an error of 0.5% in altitude, taking into account uncertainties in all the variables. Figure 3 gives a comparison of the lower atmospheric temperature profiles obtained by Venus 9 and 10 and the two Pioneer Venus probes.

Figure 1

Temperature in the Venus atmosphere as a function of altitude, as measured by the four Pioneer Venus Entry probes.

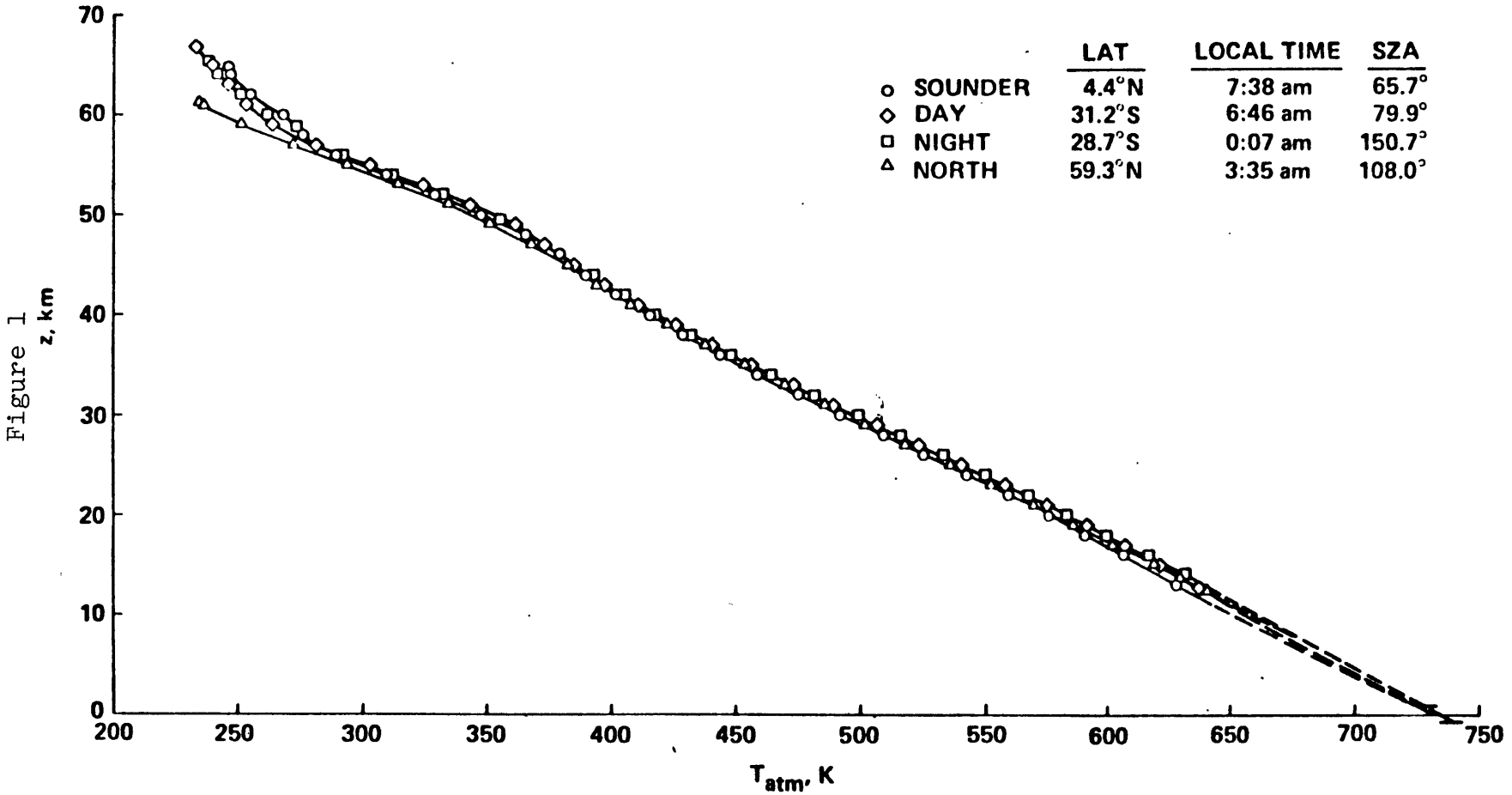
LAT
LOCAL TIME
SZA
SOUNDER 4.4°N 7:38 am 65.7°
DAY 31.2°S 6:46 am 79.9°
NIGHT 28.7°S 0:07 am 150.7°
NORTH 59.3°N 3:35 am 108.0°
z, km
70
60
50
40
30
20
10
0
200
250
300
350
400
450
500
550
600
650
700
750
T atm, K

Figure 1

Figures 2 and 3

Pressure as a function of altitude as measured by Pioneer Venus entry probes. Fig. 3, comparison of temperature as measured by the Pioneer Venus and Venera probes.

Figure 2

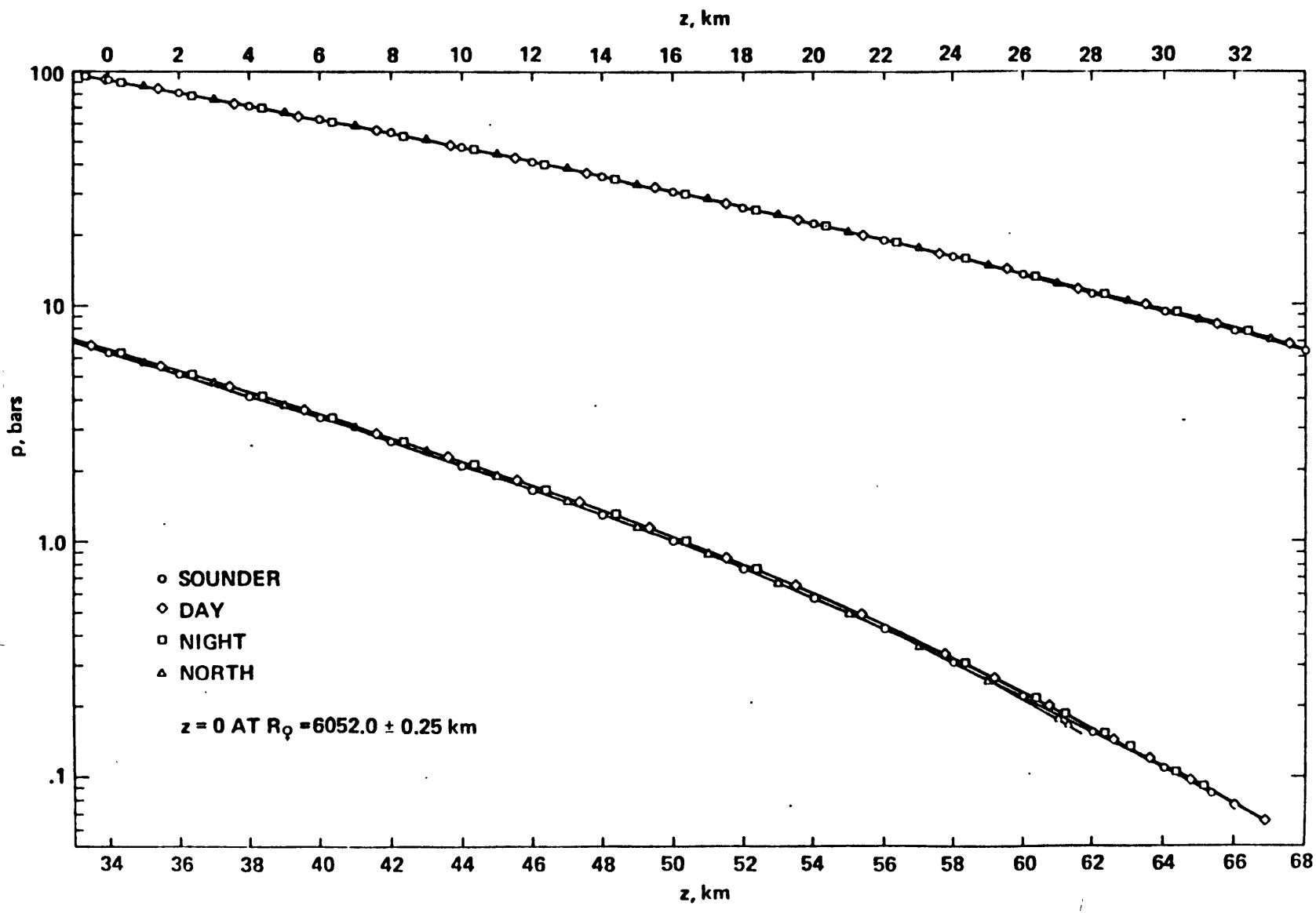
z, km
0
2
4
6
8
10
12
14
16
18
20
22
24
26
28
30
32
100
10
1.0
.1
p, bars
SOUNDER
DAY
NIGHT
NORTH
z = 0 AT R♀ =6052.0 ± 0.25 km
34
36
38
40
42
44
46
48
50
52
54
56
58
60
62
64
66
68
z, km

Figure 3

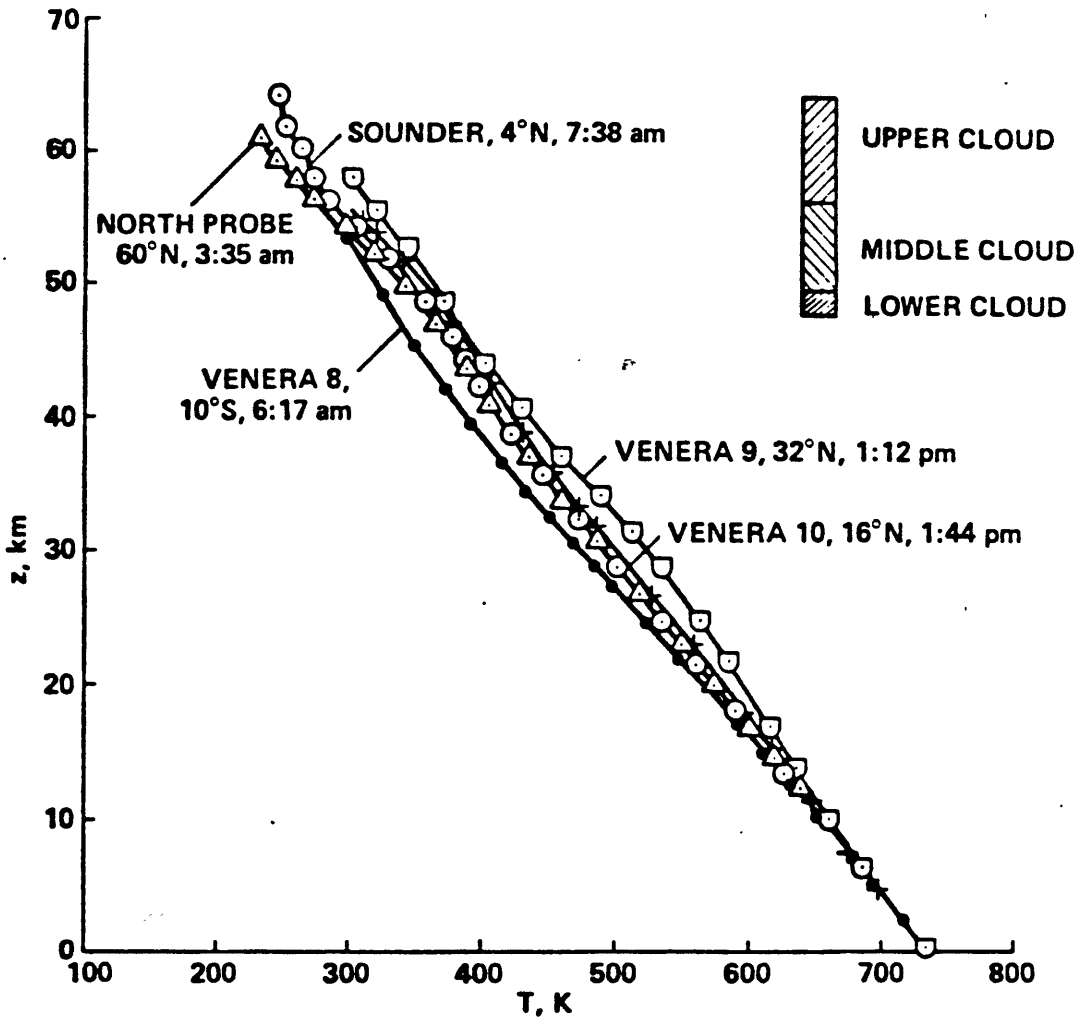
70
60
50
40
30
20
10
0
z, km
100
200
300
400
500
600
700
800
T, K
SOUNDER, 4°N, 7:38 am
NORTH PROBE
60°N, 3:35 am
VENERA 8,
10°S, 6:17 am
VENERA 9, 32°N, 1:12 pm
VENERA 10, 16°N, 1:44 pm
UPPER CLOUD
MIDDLE CLOUD
LOWER CLOUD

C. Composition of the Venus Atmosphere

As we have seen, CO_2 is the major constituent of the Venus atmosphere. Arguments as to why this should be were first put forward by Belton et al. (1967), Connes et al. (1967), and Moroz (1968). Earth-based observers of the period were also very interested in the abundance of H_2O in the Venus atmosphere, especially because of their hope that Venus could be an abode for life. The atmosphere above the clouds turned out to be extremely dry (Belton and Hunten, 1969); however, Earth-based measurements could provide no answer to the water vapor abundance below the clouds. O_2 was identified in the nightglow of the upper atmosphere in 1977 (Barker, 1975), with a mixing ratio above the cloud deck of about 1 ppm.

The presence of H in the exosphere was first confirmed by Mariner 5 (Barth et al., 1967). Most relevant to the evolution of H_2O on Venus was the failure of Wallace et al. (1971) to detect D. Measurement of D has been carried out by the Venera 9 and 10 orbiters, using a D absorption cell (Von Zahn et al., 1981), although no positive detection of D is reported.

Donahue et al. report that the droplet of H_2SO_4 which clogged the mass-spectrometer leak during the descent of the large Pioneer-Venus ("sounder") probe, contains an enrichment of D. They argue that this droplet must contain a substantial contribution of Cytherian water and note that the HDO/H_2O count ratio increased sharply after the droplet

clogged the leak, and stayed high after the leak reopened. The actual value of HDO/H_2O is about $3\text{-}5\times10^{-3}$, as contrasted to a terrestrial value of $\sim3\times10^{-4}$. Since there is probably a terrestrial and Cytherian component present in these data, and since the ratio of the two is not known, the data constrain HDO/H_2O on Venus to be $2.8\times10^{-2}\text{-}3.6\times10^{-3}$ by arguing that the terrestrial component should decrease as it is outgased during the descent, while the observed ratio increased.

Most mechanisms of escape from a planetary atmosphere discriminate strongly against the loss of deuterium, with the exception of hydrodynamic flow which would carry HD away equally as rapidly as H_2. However, when the mixing ratio of H_2 in the atmosphere falls below 2% HD will no longer be swept along. Subsequent loss of hydrogen by Jeans escape would produce an enrichment of D. At present, the Venus atmosphere contains two orders of magnitude less hydrogen than the critical 2% required for hydrodynamic escape. Thus a hundred-fold enrichment of D over H (as compared with Earth) is consistent with the initial presence on Venus of at least 1% of a terrestrial ocean of water.

McElroy *et al.* (1982) suggest that a mass 2 ion detected by the Pioneer Venus orbiter ion mass spectrometer is D^+, not H_2^+, with a relative abundance of 10^{-2} that of H.

They note that postulating D^+ provides a simpler explanation of their data than providing sources and sinks of the right magnitude for H_2^+. This value is close to the Donahue value. McElroy estimates an escape rate for H of 10^7 cm^{-2} sec^{-1} over an H_2O lifetime of $9x10^8$ years if atmospheric H_2O is the dominant reservoir. This would allow hydrogen to grow from 200ppm to 2% in $4.2x10^9$ years, which implies an initial abundance for H_2O on Venus of $8x10^2 g\text{-}cm^{-2}$. These measurements, of course, cannot reveal how much additional H_2O (above 0.3% of the terrestrial value) was initially present.

In-situ measurement of H_2O was first attempted by the Venera 4, 5, and 6 spacecraft (Vinogradov et al., 1973). Later spacecraft, including the Pioneer-Venus large probe, have attempted to measure the in-situ H_2O abundance using a mass spectrometer. Mass spectrometers have difficulty in the Venus environment both because chemically reactive species (H_2O, SO_2, O) tend to adsorb and react with the walls, and because the huge dynamic range of the ambient pressure is difficult to accomodate. Hoffman et al. (1980) give a review of the improvements in mass spectrometer capabilities: unfortunately, these improvements have been only partially successful.

A more fruitful approach to measurement of H_2O abundance was identified by Moroz et al. (1976, 1980). They employed narrow band photometers to measure the brightness ratio of the 0.87μm and 0.82μm bands of CO_2 and H_2O,

respectively. Preliminary results by Moroz et al. (1980) from the Venera 11 and 12 spacecraft indicate that the H_2O vapor mole fraction varied from 200ppm in the clouds to 20ppm at the surface, see (Von Zahn et al., 1982).

Young (1981) has analyzed the same spectra and suggests that the data are consistent with a constant H_2O mixing ratio of 100ppm between surface and clouds. Moroz (Von Zahn et al., 1982) does not agree with this interpretation, and maintains that the H_2O mixing ratio must be less than 100ppm at the surface. The most recent determination of H_2O abundance at the surface by the Venera 13 and 14 landers reveal less than 20ppm mixing ratio, with a possibility of less than 1ppm (Moroz et al., 1982).

The Pioneer-Venus sounder probe mass spectrometer reported an H_2O vapor mixing ratio of 500ppm above the clouds, but it is thought that some of this water vapor may have arisen from sources within the instrument. A conservative upper limit of 1,000ppm was reported by Hoffman et al. (1980). As described above, the input port to the instrument was blocked in the cloud region by a droplet which emitted H_2O and SO_2, the normal breakdown products of sulfuric acid. When the leak reopened at a lower altitude the H_2O abundance appeared to increase.

The Pioneer Venus gas chromatagraph shows a similar pattern of H_2O abundance (Oyama et al., 1980) but was unable to measure H_2O abundance near the surface. The water

abundance picture is complicated by conflicting data. It seems that the optical technique of Moroz is the least sensitive to contamination by sulfuric acid cloud droplets. A low reading can only be explained by a low column abundance of H_2O. However, the data analysis involved in the optical method is not simple, and there is not a unique solution. Laboratory studies of the optical properties of H_2O and CO_2 under Venus conditions could conceivably clear up some of the uncertainty. However, at present we cannot disregard the clear implication of a low (<20ppm) H_2O abundance at the surface.

HCl and HF were discovered in the Venus atmosphere by Connes et al. (1967). Connes reported mixing ratios of HCl and HF at 6×10^{-7} and 10^{-8}, respectively. Young (1972) refined analysis of these spectra and derived an HCl mixing ratio of $4.2 \pm 0.7 \times 10^{-7}$ or $6.1 \pm 0.6 \times 10^{-7}$ depending on whether the HCl lines are formed at the 36mbar or the 50mbar effective pressure level.

Remote Sensing of the Upper Venus Atmosphere

Spectroscopic Water Abundance Measurements

Source	W*	Waterbands mm	Altitude of observer	Instrument
Connes et al. (1967)	< 20	1.2-2.5	0.7km	Fourier interferometer
Owne (1967)	< 16	0.82	ground-based	Spectrometer
Schorn et al. (1969)	< 16-40	0.82	ground-based	Spectrometer
Kuiper et al. (1969	2	1.4/1.9/2.7	12.2km	Fourier interferometer
Fink et al. (1972)	0.4±0.1	1.4/1.0/2.7	12.2km	Fourier interferometer
Gull et al. (1974)	< 8	0.82	14.6km	Spectrometer
Traub (1974) Carlton	< 1	0.82	ground-based	Fabry-Perot interferometer
Barker et al. (1975)	< 0.3-25	0.82	ground-based	Spectrometer

* Vertical column abundance above clouds in mm of precipitable water vapor at STP.

In-Situ Measurement of Water Abundance Below the Clouds Since 1975

Spacecraft	Technique	Venus Altitude 0km	22km	42km	52km	Source
			(ppm)			
Venera 9 and 10	narrow band photometers			300		Moroz et al. (1976)
Venera 11 and 12	scanning spectrophotometers	20	60	150	200	Moroz et al. (1979)
Venera 11 and 12	scanning spectrophotometers	100	100	150	200	Young et al. (1981)
Pioneer Venus Sounder Probe	mass spectrometer	< 1,000				Hoffman et al. (1980)
Pioneer Venus Sounder Probe	gas chromatograph		1,350	5,200	< 600	Oyama et al. (1980)
Venera 11 Lander	mass spectrometer	76	67			Istomin et al. (1980)
Venera 12 Lander	mass spectrometer	130	52			Istomin et al. (1980)
Venera 12 Lander	gas chromatograph	≤ 100	≤ 100	≤ 100		Gelman et al. (1980)
Venera 13 Lander	gas chromatograph	≤ 20ppm	≤100ppm	≤700ppm		Moroz et al. (1982)
Venera 14 Lander	gas chromatograph	≤ 10ppm				Moroz et al. (1982)

The chemistry of sulfur and its compounds has perhaps the most important influence on the chemical weathering of rocks at the surface. The sulfur-bearing species now positively identified in the atmosphere include sulfur dioxide gas, concentrated sulfuric acid droplets, and, more tentatively, elemental sulfur, hydrogen sulfide, and carbonyl sulfide.

The photochemistry of sulfur compounds on Venus has been studied extensively by Prinn (1973) and Florensky et al. (1978). They suggest a photochemical region within and above the clouds where solar UV produces thermodynamically unstable oxidized sulfur compounds. Prinn (1979) suggested that this region might extend down to 10km above the surface. A region probably exists near the surface which contains thermodynamically stable compounds; the composition of the atmosphere must reflect rates of reaction there, as well as the degree and rates of mixing.

Sulfur dioxide has been detected in the Venus atmosphere by ground-based observations (Barker et al., 1979), as well as by in-situ spacecraft measurements. Table 4 gives a summary of SO_2 measurements.

Table 4

Mole Fractions of SO_2 (ppm)

0 km	22km	42km	52km	69km	Technique	Source
				0.02-0.06	ground-based spectroscopy	Barker (1979)
				0.1-0.8	IUE	Conway et al. (1979)
				0.1	PV-OUV	Esposito et al. (1979)
			4ppm		PV-OUV	Winich and Stewart ( )
	185±43	176	600		PV-GC	Oyama et al. (1980)
300	300		10		PV-MS	Hoffman et al. (1980)
130±35					Venera 12-GC	Gelman et al. (1979)
<20	<400				Venera 13	Moroz et al. (1982)
<20	<400				Venera 14	Moroz et al. (1982)

Prinn (1971, 1973, 1975) suggested that SO_2 was an intermediate product in the photochemical formation of H_2SO_4 from COS and H_2S. It is generally held that the clouds of Venus are produced by the photochemical oxidation of sulfur gases (COS, H_2S, SO_x), followed by addition of atmospheric water to produce sulfuric acid, thought to be the major cloud constituent. Moroz et al. (1979) reported optical detection of elemental sulfur and chlorine compounds. Silicate particles have also been suggested as cloud particles. Prinn (1978) suggested that because of slow mixing between the surface thermochemical zone and the upper atmospheric photochemical zone, SO_2 produced by photochemistry would dominate both COS and H_2S, and be the principal cloud precursor. Venera 11 and 12 observations reveal that SO_2, not COS or H_2S, is the dominant sulfur-bearing compound between 22km and 50km (cloud base), with a mixing ratio is ~150ppm.

Carbonyl sulfide (COS) was predicted to be the dominant sulfur-bearing gas by Lewis (1970). It has not been detected by the Pioneer Venus experiment, but an upper limit of 2-3ppm above 22km has been given by Hoffman et al. (1980). Venera 13 and 14 results suggest a possible COS concentration of 40±20ppm, and an H_2S concentration of 80±40ppm, below 22km.

The dominance of COS or SO_2 at the surface bears directly on the types of rock weathering to be expected. A number of workers (Mueller, 1963, 1965; Urey, 1956; Lewis,

1970; Florensky et al., 1978; Khodakovsky et al., 1979; Barsukov et al., 1980; Lewis and Kreimendahl, 1980) propose that equilibrium exists between the lower atmosphere and the surface, and have examined the consequences of this hypothesis for surface and atmospheric composition.

Lewis and Kreimendahl (1980), and Barsukov et al. (1980) have suggested the following buffer as a regulator of the oxygen abundance in the lower atmosphere.

$$FeS_2 + 2CaCO_3 + 7/2\ O_2 \rightarrow 2CaSO_4 + FeO + 2CO_2 \quad (A)$$

Lewis and Kreimendahl (1980) have calculated the equilibrium relationship of the sulfur-bearing gases and their abundance relative to O_2, and have concluded that the total mixing ratio of sulfur gases (SO_2 + COS + H_2S) decreases rapidly with increasing O_2. This equilibrium relationship is illustrated graphically in Figure 4. For increasing O_2 (which corresponds to increasing FeO in the crust) the concentration of sulfur-bearing gases declines drastically. The equilibrium relationship suggests that the surface of Venus lies within the stability field wustite, given the known abundance of sulfur bearing gases.

A total mixing ratio for sulfur gases of 150ppm would require a surface FeO activity <1/10 that of Earth. The terrestrial FeO activity is roughly 0.1 in most igneous rocks. These calculations suggest that, under equilibrium, a mildly oxidizing crust is completely at odds with the observed concentration of SO_2. An equilibrium situation

predicts that H_2S and COS would predominate over SO_2, while the observed SO_2 mixing ratio at 22km altitude is 10 times that predicted by Lewis and Kreimendahl.

These observations suggest that reactions with surface rocks would take up SO_2 until only 1/10 of what is observed actually remains. Since we have few measurements of the surface composition, COS could be the dominant species right at the surface, and the relevant atmospheric-surface equilibrium may exist. Preliminary measurements reported by Venera 13 and 14 from the surface do reveal the presence of COS and H_2S, strengthening this suggestion.

Another possibility is that COS and H_2S are converted into SO_2, but SO_2 cannot be converted back into $CaSO_4$ fast enough to be reconverted into COS and H_2S. This reconversion would have to take place geologically and could be slow. If disequilibrium prevails, then SO_2 would be a powerful igneous rock weathering agent, but atmosphere-surface reactions may not regulate sulfur.

Figure 4

Equilibrium abundances of sulfur gasses as a function of oxygen partial pressure. The total sulfur gas abundance decreases rapidly as a function of increasing oxygen partial pressure. Notice that an oxidized crust, to the right of the wustite-hematite boundary, results in a lower sulfur gas abundance than reported for the atmosphere at 22km altitude by Venera 11 and 12.

Figure 4

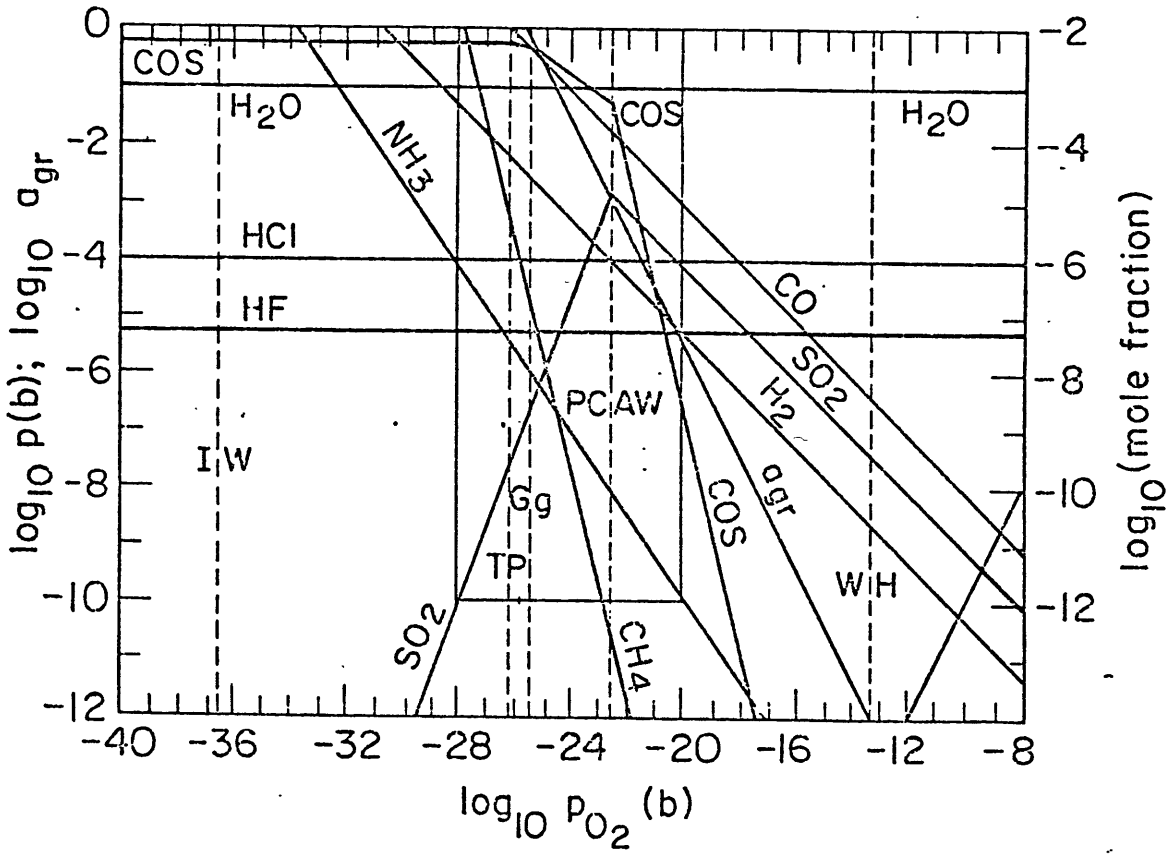
COS
H2O
HCl
HF
IW
NH3
COS
H2O
CO
SO2
H2
PC
AW
Gg
TP
SO2
CH4
COS
agr
WH
log10 p(b); log10 agr
log10 pO2 (b)
log10(mole fraction)
0
-2
-4
-6
-8
-10
-12
-40
-36
-32
-28
-24
-20
-16
-12
-8

Barsukov et al. (1980) note that the sulfur gas abundance near surface may be further complicated by rapid large scale atmospheric circulation. The very near surface region (100's of meters above) is the reactive zone for chemical weathering. The lower atmosphere composition may reflect only "quasi equilibrium" present locally near the surface due to rapid mixing (relative to rates of gas-solid reactions) and photo-oxidation of sulfur gases higher in the atmosphere.

Because of these complications Prinn (in Von Zahn et al., 1982) suggests that it is more informative to view sulfur gas abundances in the lower atmosphere as the product of a cycle combining inputs and outputs from various sources and sinks. Tectonic activity, large scale mixing, and chemical weathering and photochemistry will all be part of the overall sulfur cycle.

Figure 5 outlines a current view of the sulfur cycle on Venus. Prinn (in Von Zahn et al.) suggested that the geological cycle involves the reaction of pyrite to produce reduced gases COS and H_2S.

$$FeS_2 + 2H_2O \rightarrow FeO + 2H_2S + 1/2\ O_2$$

$$FeS_2 + 2CO_2 \rightarrow FeO + 2COS + 1/2\ O_2$$

COS and H_2S will be converted into SO_2 by the net photochemical reactions

$$2H_2S + 3O_2 \rightarrow 2H_2O + 2SO_2$$

$$2COS + 3O_2 \rightarrow 2CO_2 + 2SO_2$$

SO_2 will then build up beyond its equilibrium pressure and the following reactions may occur:

$$CaAl_2Si_2O_8 + SO_2 + CO_2 \rightarrow CaSO_4 + Al_2SiO_5 + SiO_2 + CO$$

$$CaMgSi_2O_6 + SO_2 + CO_2 \rightarrow CaSO_4 + MgSiO_3 + SiO_2 + CO$$

Anhydrite ($CaSO_4$) can then be converted into pyrite by reaction (A). It is not known if the conversion of SO_2 into $CaSO_4$ and then to FeS_2 can actually proceed fast enough to maintain atmosphere-surface equilibrium. Production of sulfur gases may be dominated by volcanic activity, and may not balance reincorporation by surface weathering. In order to maintain an atmospheric steady state abundance of sulfur gases, some source must be present.

Figure 5

The current view of the cycles of sulfur on Venus, after Prinn in Von Zahn et al., 1982.

Figure 5

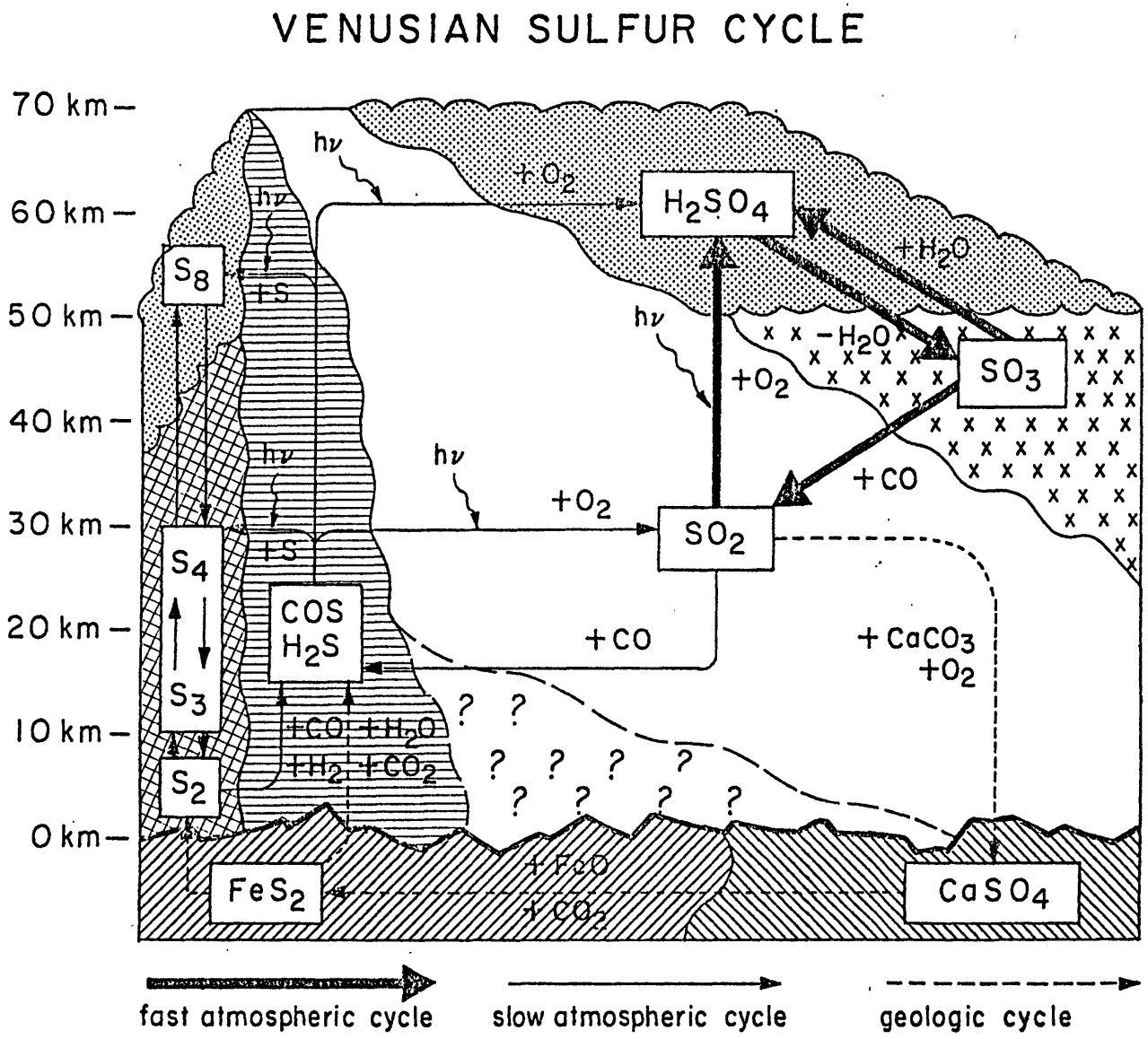
VENUSIAN SULFUR CYCLE
70 km
60 km
50 km
40 km
30 km
20 km
10 km
0 km
hν
+O2
H2SO4
+H2O
S8
+S
-H2O
SO3
+O2
+CO
SO2
S4
S3
S2
COS
H2S
+CO
+CaCO3
+O2
+CO +H2O
+H2 +CO2
?
+FeO
+CO2
FeS2
CaSO4
fast atmospheric cycle
slow atmospheric cycle
geologic cycle

D. The Composition of the Venus Surface

Our present knowledge of the rocks on Venus comes from measurements of natural radioactivity and from surface photographs transmitted by Soviet landers. Venera 8, 9, and 10 measured the gamma ray emission of the surface. Venera 8 and Venera 10 measured the density of the surface using a gamma-ray densitometer, which they reported to be 2.8 ± 0.1 g/cm^3. The actual error may be greater due to calibration uncertainties (Surkov et al., 1976). Venera 8 reported a density of $1.5 g/cm^3$, (Vinogradov et al., 1973) which is lower than expected for solid rock.

The abundances of K, U, and Th are shown in Table 4, and are plotted in Figure 6 relative to the composition of other solar system rocks. The comparison indicates that Venus rocks are different from primitive meteorites, and have experienced differentiation. The Venera 9 and 10 radioactive compositions are similar to those of terrestrial basaltic rocks, and have been interpreted as evidence for such rocks on Venus.

The Venera 9 site is characterized photographically (Fig. 7) by an abundance of slab-like boulders 40-80cm across. Some blocks are as large as 2m. Florensky et al. (1977) suggest that several rocks at the Venera 9 site contain features suggestive of layering, but the low resolution in the images makes this hypothesis tentative. Almost all the rocks in the Venera 9 image show little surface texture, except for one rock in the lower right hand

portion of the scene, which shows light and dark splotches. A large number of small fragments less than 10cm in diameter are visible, which may be derived from the larger boulders. The rocks and boulders appear to rest on a fine-grained substrate whose individual components are unresolved.

The panorama of the Venera 10 landing site is characterized by large flat rocks separated by regolith. Smaller patches of "platform rocks" are sprinkled within the regolith. These may be fragments broken off larger rocks, or partially uncovered bedrock (Florensky et al., 1977). The rocks beneath the Venera 10 lander appear smooth and unmarked with only occasional fractures and grooves, and are quite similar to the individual boulders at the Venera 9 site.

Selivanovitch (1976) reports low (less than 3%) albedos at both Venera 9 and 10 landing sites. The rocks at the Venera 9 site have albedos of 5%, while some rocks at the Verera 10 site have albedos approaching 12%.

Garvin (1981) reports evidence of dust being kicked up during Venera 9 and 10 touchdown, similar to that observed on Mars during Viking landings. Mechanical properties of the surface at both sites were estimated using the gamma-ray spectrometer-densitometer (Leonovich et al., 1977), yielding a bearing strength for individual rocks on the surface of ~400kg/cm^2. The strength of the surface beneath Venera 9 was found to be similar, suggesting that it is composed of well compacted rocks and chips.

During the preparation of this thesis new data became available from the Venera 13 and 14 landers. Photographs from both sites also show slab-like rocks covering a flat surface. However, the Venera 13 site appears to contain cloddy soil, while rocks cover most of the surface seen by Venera 14. The interpretation of these images is still very tentative at this time. Weathering is evident in the Venera 14 scene. However, more loose dust and soil blanket the surface in the Venera 13 scene. Both landers obtained color photographs of the surface, and these revealed a brown discoloration, possibly the result of weathering. This observation suggests that weathering processes may produce low albedo substances. One terrestrial mineral with low albedo is magnetite. However, chemical weathering on Venus may produce dark substances with no terrestrial analog.

The two landers also obtained X-ray fluorescence measurements at each site, with results as seen in Table 5. The high potassium levels in the Venera 13 analysis is indicative of alkali basalt, while the Venera 14 analysis is suggestive of a tholeiitic basalt, similar to that found on the terrestrial ocean floor. The high radioactivity seen at the Venera 8 site may also be due to alkali basalt, rather than granite as was originally suggested by the Soviets.

It is not feasible to use the techniques of chemical thermodynamics to predict or explain the detailed appearance of surface rocks and soils. However, it may be possible to say something about what compounds may be produced by

weathering from the primary rocks inferred to be present at the Venera 13 and 14 sites. The X-ray flouresence analyses conducted do not yield information on what minerals are present, only major element chemistry. These analyses may be used as a starting point for analysis of chemical weathering on Venus provided assumptions are made as to the minerals present.

Figure 6

The concentration of uranium, potassium, and thorium measured by the Venera 9 and 10 landers, compared with other solar system results. The Venera measurements are more indicative of differentiated rocks.

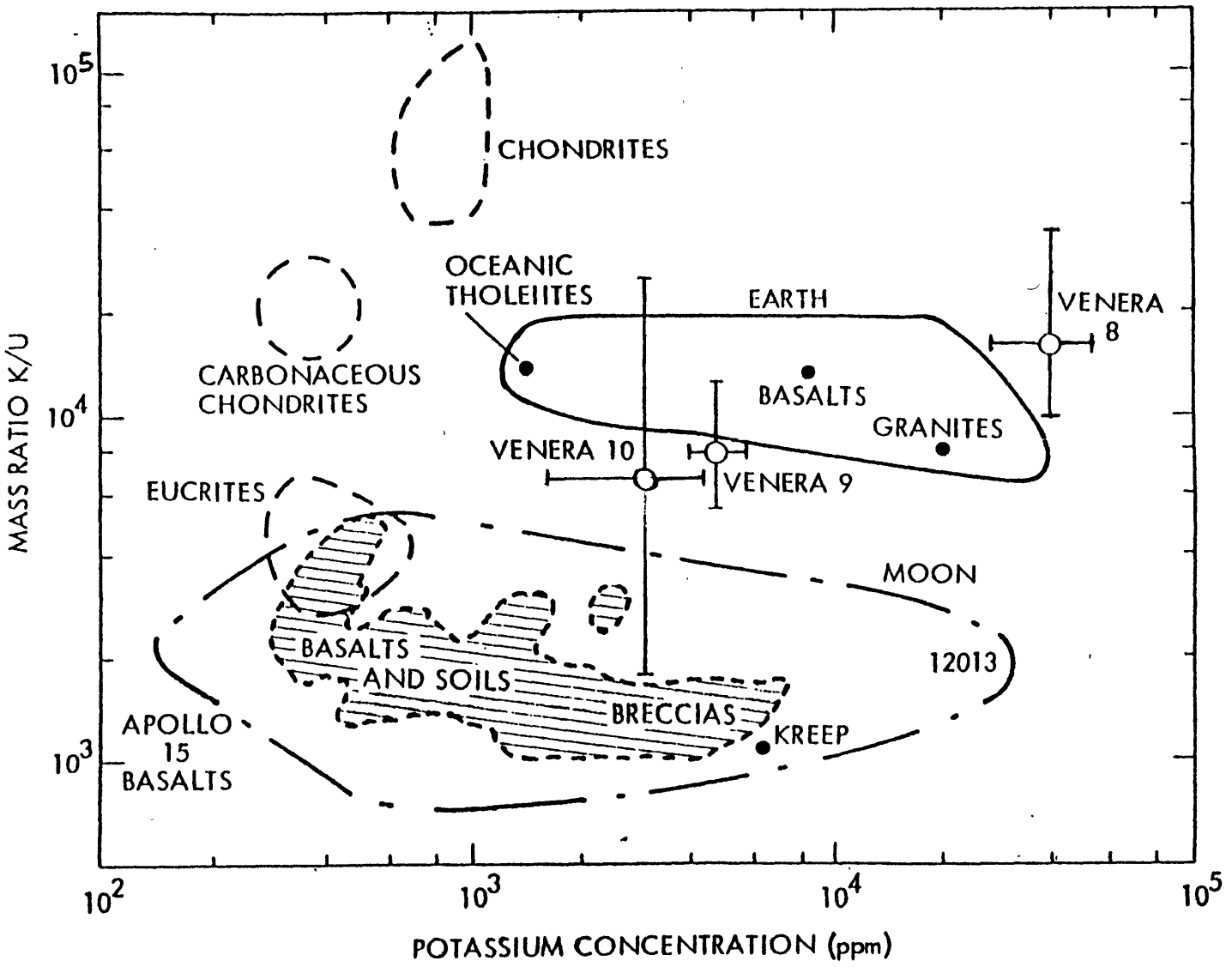
CHONDRITES
OCEANIC
THOLEIITES
EARTH
VENERA
8
CARBONACEOUS
CHONDRITES
BASALTS
GRANITES
VENERA 10
VENERA 9
EUCRITES
MOON
BASALTS
AND SOILS
BRECCIAS
12013
KREEP
APOLLO
15
BASALTS
MASS RATIO K/U
10^5
10^4
10^3
10^2
10^3
10^4
10^5
POTASSIUM CONCENTRATION (ppm)

Figure 6

Figure 7

Surface panoramas from Venera 9 (top) and Venera 10 (bottom).

Figure 7

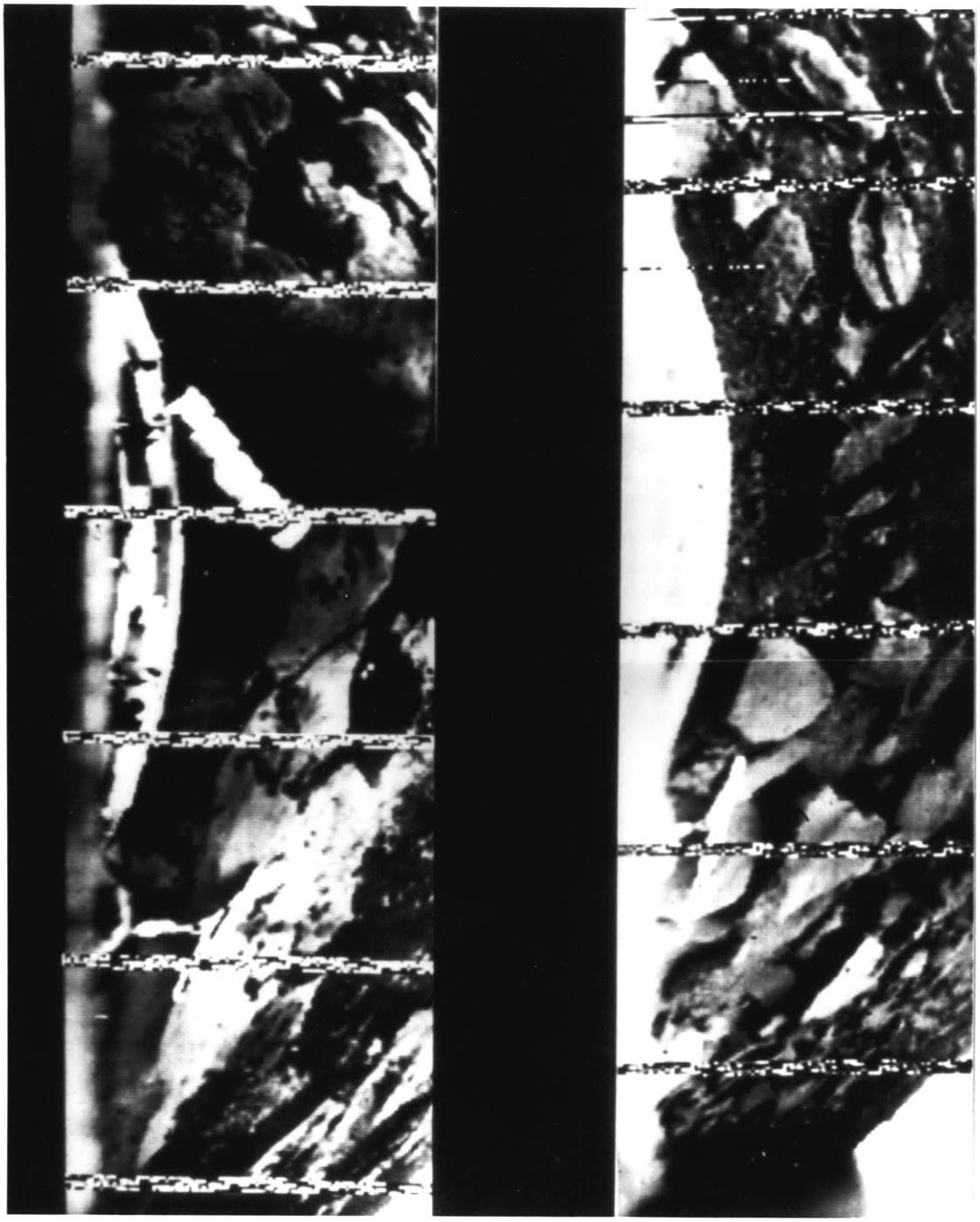

Table 5

Venera Measurements of Uranium, Thorium, and Potassium Abundances (Surkov, 1977)

Venera	U($\times 10^{-4}$wt.%)	Th($\times 10^{-4}$wt.%)	K(wt.%)	K/U($\times 10^4$)
8	2.2±0.7	6.5±0.2	4.0±1.2	$1.82^{+1.65}_{-0.85}$
9	0.60±0.16	3.65±0.42	0.47±0.08	$0.78^{+0.47}_{-0.27}$
10	0.46±0.26	0.70±0.34	0.30±0.16	$0.65^{+1.65}_{-0.46}$

Venera X-Ray Fluorescence Measurements

	Venera 13 (wt.%)	Venera 14 (wt.%)
MgO	10±6	8±4
Al_2O_3	16±4	18±4
SiO_2	45±3	49±4
K_2O	4±0.8	0.2±0.1
CaO	7±1.5	10±1.5
TiO_2	1.5±0.6	1.2±0.4
MnO	0.2±0.1	0.16±.08
FeO	9±3	9±2

E. Chemical Weathering on Venus

1. Methodology of Study

Given our current ignorance of the physical and chemical state of the atmosphere-surface boundary, all we may do is calculate how known rock-forming minerals would behave when exposed to the Venus atmosphere. A qualitative hypothesis will emerge as to the types of weathering reactions which are possible, but no insight is possible on which reactions do indeed occur. There are two separate questions that must be addressed. The first asks what happens to various types of rock exposed to the Venus atmosphere at various locations on the surface. The second asks whether solid-gas equilibrium reactions affect the composition of the lower atmosphere. We will not be able to address the rates at which landforms degrade, or the relative ages of features, due to our almost total lack of knowledge of the kinetics of gas-solid reactions involving rock-forming minerals under Venus conditions.

Weathering on Venus must proceed in an entirely different fashion than on the other terrestrial planets with atmospheres: Earth and Mars. On Venus there is no liquid H_2O; on Mars, which also has a CO_2 atmosphere, chemical weathering will also proceed via gas-solid reactions. However, important differences must be noted. Gooding (1978) has conducted a theoretical evaluation of chemical weathering on Mars using the same thermodynamic principles used here for Venus.

There the similarity ends: the conditions of low temperatures and pressures on Mars result in a stable weathering assemblage consisting of montmorillonite type clays, along with sulfates, oxides, and carbonates. The surface of Mars is known to be highly oxidized, and large amounts of liquid water may have been present at some time in the past, so it is possible that weathering of rocks has been hastened by its presence. In addition, unlike Venus, photochemical reactions are possible on the surface of Mars.

On Earth, most chemical weathering involves liquid water, so naturally most research on the subject has been aimed at aqueous reactions and alterations. Liquid water may act as a reactive medium, and also facilitates reactions between solid minerals and atmospheric gases, as well as aqueous ions. Liquid water will also transport weathering products, which accounts for leaching processes which change the composition of rocks during chemical weathering. Expansion of water during freezing, and swelling of minerals by hydration, also hastens the breakdown of primary igneous minerals. An equilibrium assemblage on Earth would be very difficult, if not impossible, to define precisely. In reality the actual final equilibrium will not be of great importance, because on Earth we commonly deal with partially completed processes.

For this reason our knowledge of chemical weathering is highly qualitative. We may know what happens chemically in

the decay of a rock, but we have no means of predicting what the state of the rock will be at some time in the future, even given our extensive experience with terrestrial weathering. The task on Venus is much more difficult. We do know that, even on Earth, dry air causes rocks to decay only slowly, as is attested by the preservation of four-thousand-year-old inscriptions in Egypt. Elevated temperatures on Venus will hasten the decay of dry rock (Krauskopf, 1973).

Data available today from the Venera 13 and 14 Landers imply a range of rock forming minerals found in terrestrial igneous rocks. Therefore, these minerals will be the starting point for a discussion of weathering on Venus. Data available on gas composition require the examination of a number of cases, and a number of possible reactions. The simplest case to explore first is the reaction of a pure phase as a crystal in a rock with a single atmospheric gas. Next, an assemblage of phases may be reacted with one or several atmospheric gases. Some reactions will result in an exchange of gases, and these are most likely to affect the local atmospheric composition. Finally, since not all minerals will be present as pure phases in real rocks, the effects of activities less than unity on chemical weathering must be discussed.

Khodakovsky et al.(1979) and Barsukov et al.(1980) employ a different method. They employ a numerical technique to minimize the free energy in a system of

selected minerals, and the system is open with respect to gases. It will be instructive to examine the qualitative and quantitative differences between this approach and the examination of selected individual weathering reactions involving assemblages known to be stable in igneous rocks.

Table 6

Reactive Components of the Lower Atmosphere of Venus

Gas	Mole Fraction of Total Atmosphere	Observation
CO_2	0.96	Mariner, Pioneer Venus, Venera
CO	$10^{-4} \rightarrow 10^{-5}$	Spectroscopic, Pioneer Venus
H_2O	$10^{-6} \rightarrow 10^{-4}$	Pioneer Venus, Venera, Spectroscopic
HF	10^{-8}	Spectroscopic
HCl	10^{-6}	Spectroscopic
SO_2	$\sim 2 \times 10^{-4}$	Pioneer Venus, Spectroscopic, Venera
COS	$4 \times 10^{-5} \rightarrow 2 \times 10^{-6}$	Pioneer Venus, Venera
H_2S	$8 \times 10^{-5} \rightarrow 3 \times 10^{-6}$	Pioneer Venus, Venera

Table 7

Minerals and Activities Common to Igneous Rocks

Mineral	Range of Activity
Fosterite	~ 0.9
Fayalite	~ 0.1
Ferrosilite	~ 0.1
Diopside	~ 0.8-0.9
Enstatite	~ 0.9-1
Orthoclase	~ 0.95-1
Anorthite	0.4-0.7
Albite	0.6-0.3
Magnetite	1
Quartz	1

Venus Weathering Reactions - Summary

Reactions Involving CO_2	Equilbrium Gas Pressure Within Venus Bounds
$CaSiO_3 + CO_2 = CaCO_3 + SiO_2$	Yes
$CaMgSi_2O_6 + CO_2 = CaCO_3 + MgSiO_3 + SiO_2$	No
$CaMgSi_2O_6 + CO_2 = CaSiO_3 + MgCO_3 + SiO_2$	No
$CaMgSi_2O_6 + 2CO_2 = CaMg(CO_3)_2 + 2SiO_2$	No
$2CaMgSi_2O_6 + Mg_2SiO_4 + 2CO_2 = CaMg(CO_3)_2 + 4MgSiO_3$	Yes
$Mg_2SiO_4 + 2CO_2 = 2MgCO_3 + SiO_2$	Yes
$Mg_2SiO_4 + CO_2 = MgCO_3 + MgSiO_3$	Yes
$CaAl_2Si_2O_8 + CO_2 = CaCO_3 + Al_2SiO_5 + SiO_2$	No
$CaMg(CO_3)_2 + SiO_2 = CaCO_3 + MgSiO_3 + CO_2$	Yes
Reactions Involving H_2O	
$2CaAl_2Si_2O_8 + 5MgSiO_3 + SiO_2 + H_2O = Ca_2Mg_5Si_8O_{22}(OH)_2 + 2Al_2SiO_5$	Yes
$2CaMgSi_2O_6 + 3MgSiO_3 + SiO_2 + H_2O = CaMg_5Si_8O_{22}(OH)_2$	Yes

Reactions Involving HF	Equilbrium Gas Pressure Within Venus Bounds
$KAlSi_3O_8 + 3MgSiO_3 + 2HF = KMg_3AlSi_3O_{10}(F)_2 + 3SiO_2 + H_2O$	Yes
$CaAl_2Si_2O_8 + 2HF = CaF_2 + Al_2SiO_5 + SiO_2 + H_2O$	No
$MgSiO_3 + 2HF = H_2O + MgF_2 + SiO_2$	No
$CaMgSi_2O_6 + 2HF = CaF_2 + MgSiO_3 + H_2O + SiO_2$	No
$CaMgSi_2O_6 + 2HF = MgF_2 + CaSiO_3 + H_2O + SiO_2$	No
$CaSiO_3 + 2HF = CaF_2 + SiO_2 + H_2O$	No
$CaF_2 + 2HF = CaF_2 + 2HCl$	No
$CaCO_3 + 2HF = CaF_2 + CO_2 + H_2O$	No
Reactions Involving HCl	
$CaMgSi_2O_6 + 2HCl = CaCl_2 + MgSiO_3 + H_2O + SiO_2$	No
$2NaAlSi_3O_8 + 2HCl = 2NaCl + Al_2SiO_5 + 5SiO_2 + H_2O$	Yes
Reactions Involving COS	
$CaCO_3 + COS + 2CO_2 = CaSO_4 + 4CO$	(?)
$Fe_2SiO_4 + 4COS = 2FeS_2 + SiO_2 + 2CO_2 + 2CO$	(?)
Reactions Involving SO_2	
$CaAl_2Si_2O_8 + SO_2 + CO_2 = CaSO_4 + Al_2SiO_5 + SiO_2 + CO$	Yes
$CaMgSi_2O_6 + SO_2 + CO_2 = CaSO_4 + MgSiO_3 + SiO_2 + CO$	Yes
$Mg_2SiO_4 + 2SO_2 = 2MgSO_4 + SiO_2$	No

2. Variation of Weathering Over the Surface

The important weathering reactions are grouped according to the gases and minerals involved. Since we do not know what type of rocks are present, a wide range of reactions are possible. However, the Venera 10 and 14 analyses are indicative of basalt. Carbonization of mafic and ultramafic rocks may occur via:

$$Mg_2SiO_4 + CO_2 = MgCO_3 + MgSiO_3 \quad (1)$$

olivine (forsterite) — magnesite — enstatite

$$2Mg_2SiO_4 + CaMgSi_2O_6 + 2CO_2 = CaMg(CO_3)_2 + 4MgSiO_3 \quad (2)$$

diopside — dolomite

$$CaSiO_3 + CO_2 = CaCO_3 + SiO_2 \quad (3)$$

wollastonite

(Urey, 1952)

The stability fields of these reactions are plotted in Figure 8 along with the Venus P-T curve observed by Seiff et al. It is seen that reaction of mafic minerals with atmospheric CO_2 is thermodynamically more favorable at the higher elevations on Venus. The effect of non-unit activities on reactions 1-3 is also shown. It can be seen that lowering the activity of the primary mineral raises the altitude where weathering will be favored. These weathering reactions will most likely occur at the highest elevations on Venus.

Figure 8

Equilibrium partial pressure of CO_2 as a function of temperature for carbonitization of mafic minerals. Note the favoring of reaction at higher elevations. The numbers refer to the reactions listed on the previous page. Variation effects for reasonable mineral activities are also shown.

Figure 8

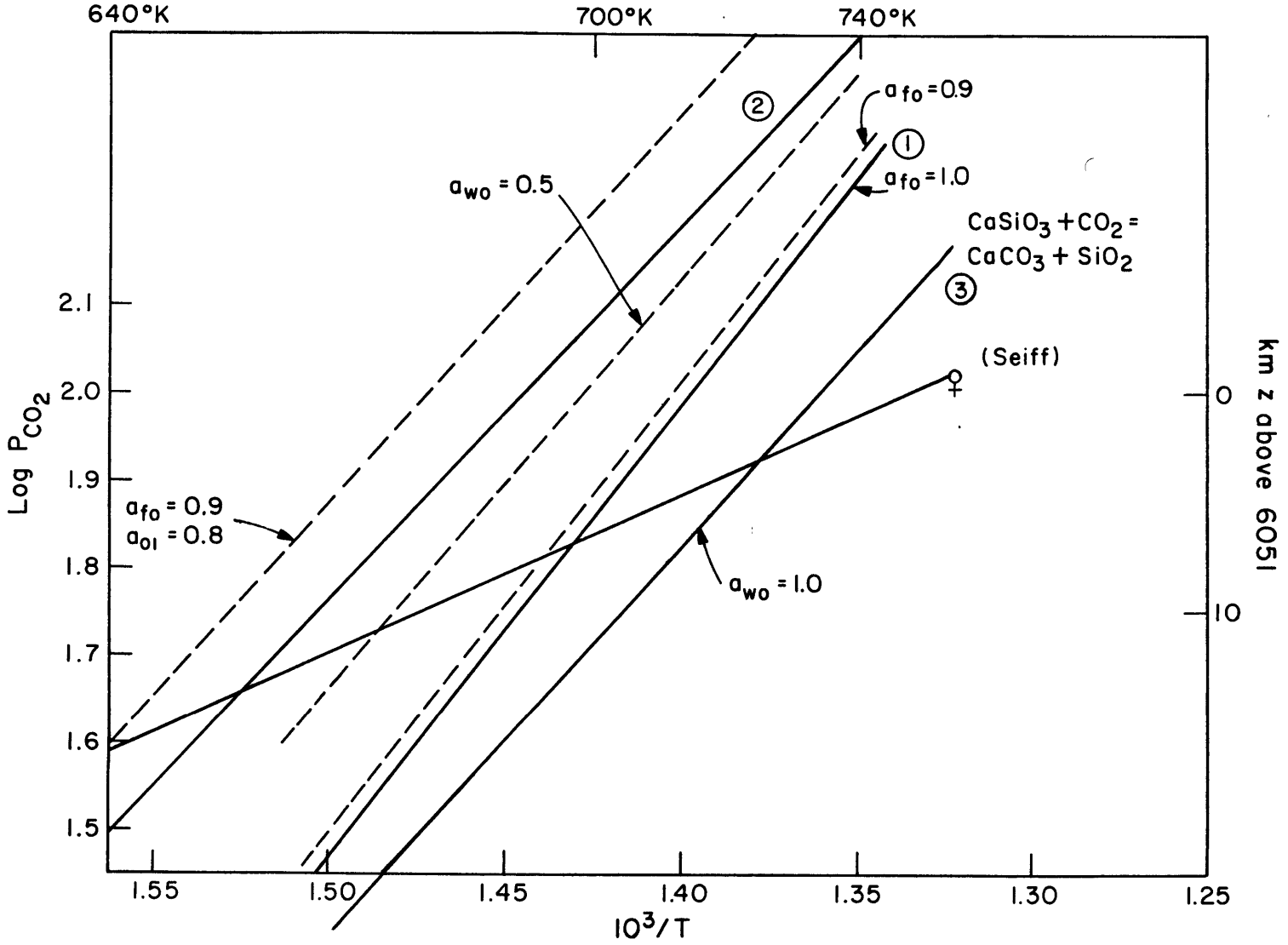
640°K
700°K
740°K
a_{fo} = 0.9
a_{fo} = 1.0
a_{wo} = 0.5
$CaSiO_3 + CO_2 = CaCO_3 + SiO_2$
(Seiff)
a_{fo} = 0.9
a_{ol} = 0.8
a_{wo} = 1.0
Log P_{CO_2}
2.1
2.0
1.9
1.8
1.7
1.6
1.5
1.55
1.50
1.45
1.40
1.35
1.30
1.25
$10^3/T$
km z above 6051
0
10

Water vapor may also act as a weathering agent. Again mafic minerals are included since they seem to be plausible on the Venus surface.

$$2CaMgSi_2O_6 + 3MgSiO_3 + SiO_2 + H_2O = Ca_2Mg_5Si_8O_{22}(OH)_2 \quad (4)$$

diopside — tremolite

$$2CaAl_2Si_2O_8 + 5MgSiO_3 + SiO_2 + H_2O = Ca_2Mg_5Si_8O_{22}(OH)_2 + 2Al_2SiO_5 \quad (5)$$

plagioclase — andalusite

The stability range of these weathering reactions is shown in Figure 9, assuming a constant mixing ratio of H_2O of 100 ppm. Again, these reactions tend to the right at higher elevations. Since plagioclase and diopside are present in many igneous rock types, including tholeitic basalt, these reactions may be reasonable weathering reactions.

Tremolite formation is only possible for a realtively high X_{H2O} (100ppm). Data from the Venera 11-14 landers indicate that hese reactions will not be important due to low (<20ppm) water abundance in the lower atmosphere.

In addition, mineral activities typical of terrestrial basalts further negate the importance of the altitude variation effects on tremolite formation.

Figure 9

Weathering reactions involving tremolite formation as function of altitude, for a constant mixing ratio of $H_2O \sim 10^{-4}$. Tremolite formation requires water abundance greater than that reported by the Venera 11-14 landers, and high (a greater than 0.9) activities for the primary minerals involved in the reaction.

Figure 9

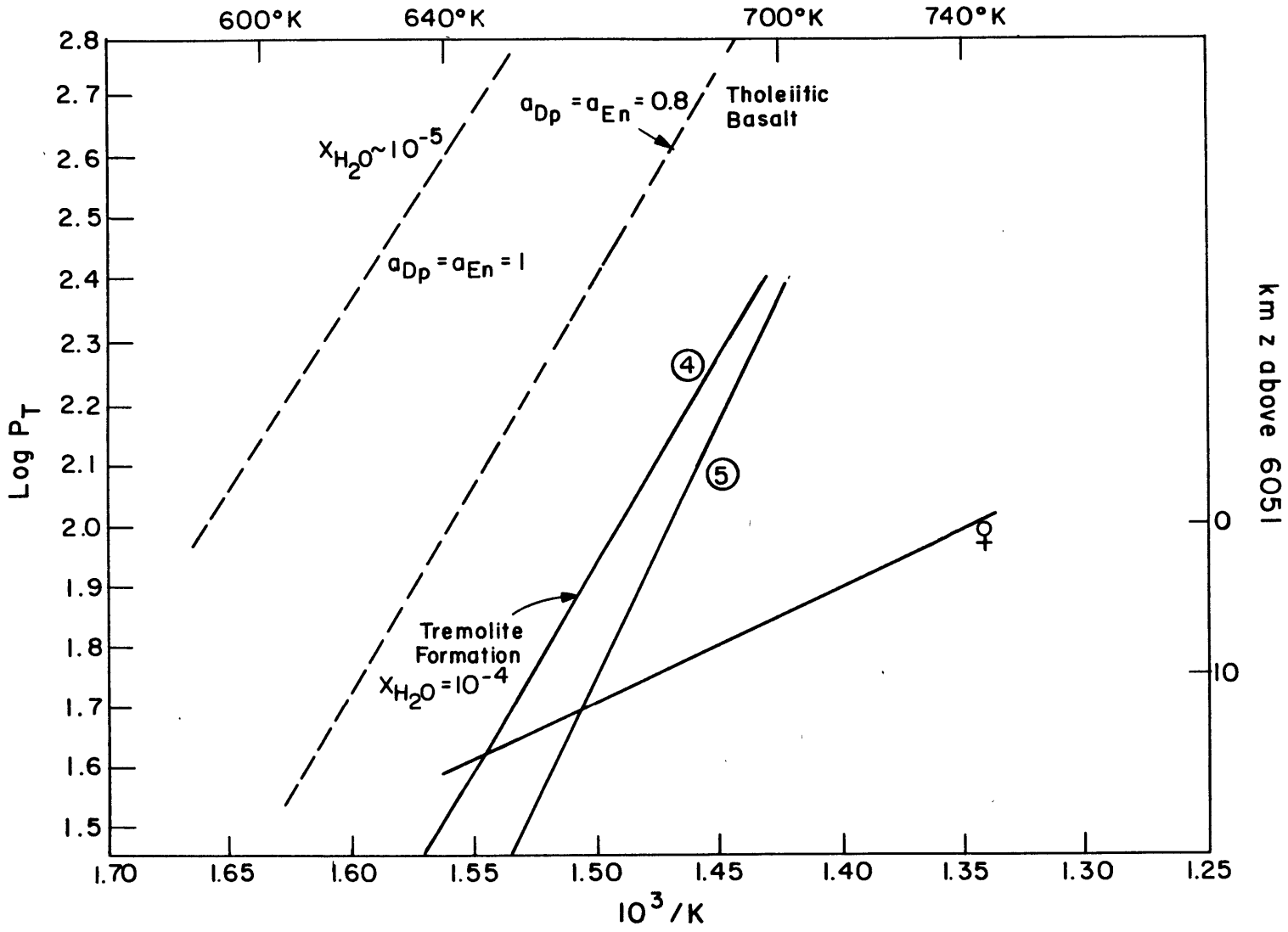
600°K
640°K
700°K
740°K
2.8
2.7
2.6
2.5
2.4
2.3
2.2
2.1
2.0
1.9
1.8
1.7
1.6
1.5
Log P_T
$X_{H_2O} \sim 10^{-5}$
$a_{Dp} = a_{En} = 0.8$
Tholeiitic Basalt
$a_{Dp} = a_{En} = 1$
④
⑤
♀
Tremolite Formation
$X_{H_2O} = 10^{-4}$
0
10
km z above 6051
1.70
1.65
1.60
1.55
1.50
1.45
1.40
1.35
1.30
1.25
$10^3/K$

Weathering reactions may also play a role in regulating the atmospheric composition of Venus. As we have seen SO_2 may react with igneous minerals in the following manner.

$$CaAl_2Si_2O_8 + SO_2 + CO_2 = \underset{\text{anhydrite}}{CaSO_4} + Al_2SiO_5 + SiO_2 + CO \quad (7)$$

$$CaMgSi_2O_6 + SO_2 + CO_2 = CaSO_4 + MgSiO_3 + SiO_2 + CO \quad (8)$$

The range of equilibrium gas abundances for these reactions may be calculated by noting

$$K_T \cong \frac{P_{CO}}{P_{CO_2} P_{SO_2}} \cong \frac{X_{CO} P_{TOT}}{X_{CO_2} P_{TOT} X_{SO_2} P_{TOT}} \cong \frac{X_{CO}}{X_{CO_2} X_{SO_2} P_{TOT}}$$

$$X_{CO} \cong X_{CO_2} X_{SO_2} P_{TOT} K_T$$

Given $X_{CO_2} = 0.96$ and P_{TOT} and K_T we can plot a range of equilibrium for these reactions as seen in Figure 10. The ranges of equilibrium at 740°K are actually quite similar to the range of gas abundances actually observed.

Figure 10

Equilibrium of CO and SO_2 in reactions involving plagioclase. The range of gas abundance is close to the actual values observed. The effect of non-unit activity for anorthite is also depicted.

Figure 10

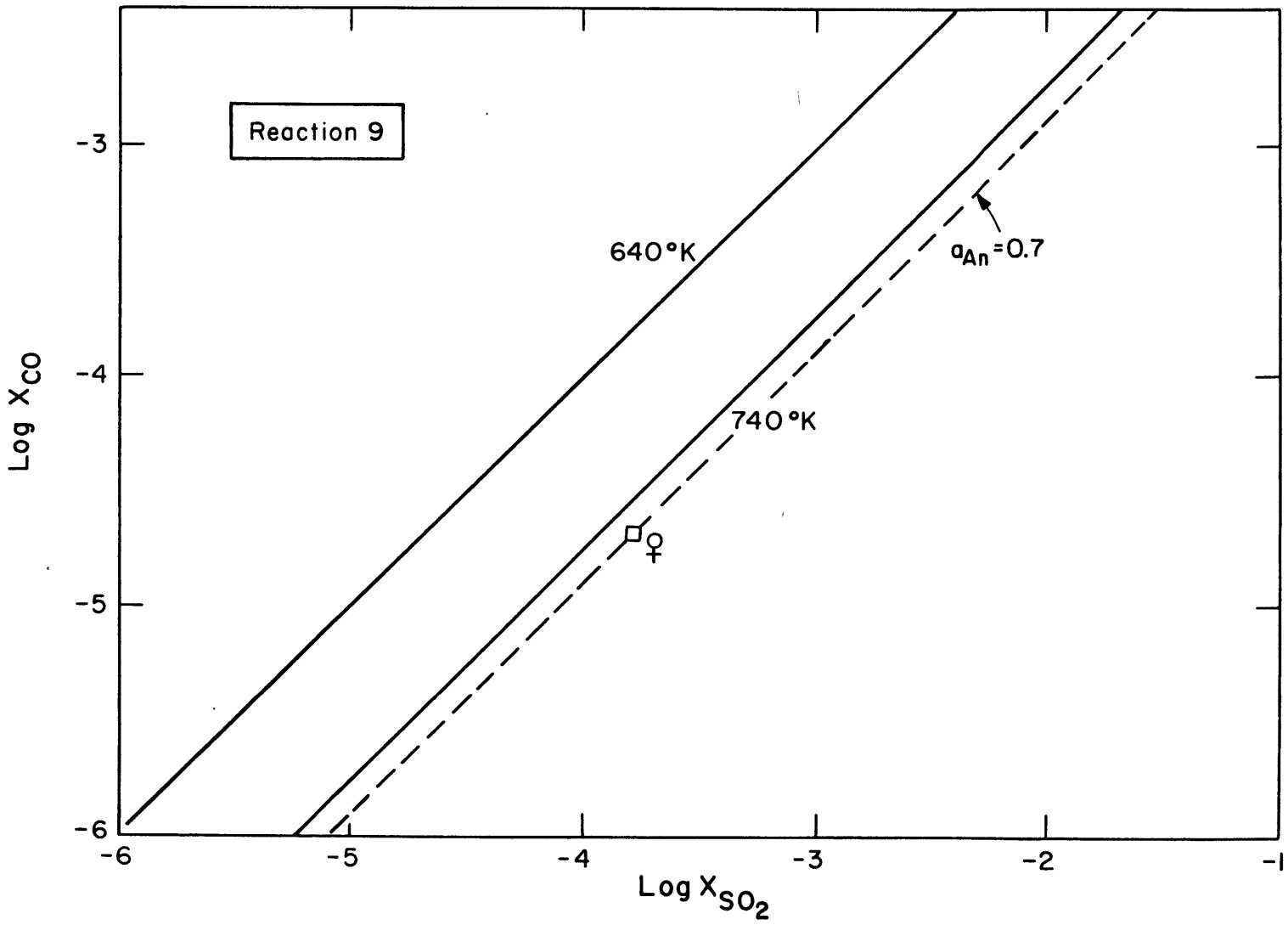

The same argument may be made for the following weathering reactions involving halogen gases.

$$KAl_3Si_3O_8 + 3MgSiO_3 + 2HF =$$

orthoclase

$$KMg_3Al_3Si_3O_{10}(F)_2 + H_2O + 3SiO_2$$

fluorophlogopite (9)

The altitude of equilibrium for this reaction is given in Figure 11 assuming constant mixing ratios of HF and H_2O with altitude. Figure 12 gives the equilibrium variations of HF and H_2O for reaction (9).

In Figure 14 the surface hypsometric curve of Venus is plotted over the equilibrium boundaries for several gas-solid weathering reactions, with variable water vapor concentration.

Other Halogen Reactions

$$2NaAlSi_3O_8 + 2HCl(g) = 2NaCl + Al_2SiO_5 + 5SiO_2 + H_2O \quad (10)$$

$$P_{H_2O} = P^2_{HCl}\, K(T)$$

$$K_{740} = 6.94 \times 10^2$$

$$K_{640} = 2.53 \times 10^4$$

$$X_{H_2O}\, P_{TOT} = P^2_{TOT}\, X^2_{HCl}\, K(T)$$

$$X_{H_2O} = P_{TOT}\, X^2_{HCl}\, K(T)$$

The range of equilibrium water pressures for this reaction may be seen in Figure 13.

$$X_{HCl} = \left| \frac{X_{H_2O}}{KTP_T} \right|^{1/2}$$

This discussion of weathering has first assumed solid gas equilibrium and unit activity for the reacting solids, then has soufht to find where on the actual Venus surface the equilibrium exists. It is reasonable to assume that igneous mineral assemblages of the type examined (minerals for which thermodynamic data are available), will experience disequilibrium conditions at many points of the surface. This suggests that the breakdown of rocks is more likely (that is, more weathering reactions are possible) at higher elevations.

Figure 11

Altitude dependence of phlogopite formation calculated for constant mixing ratio of HF, and two mixing ratios of H_2O.

Figure 11

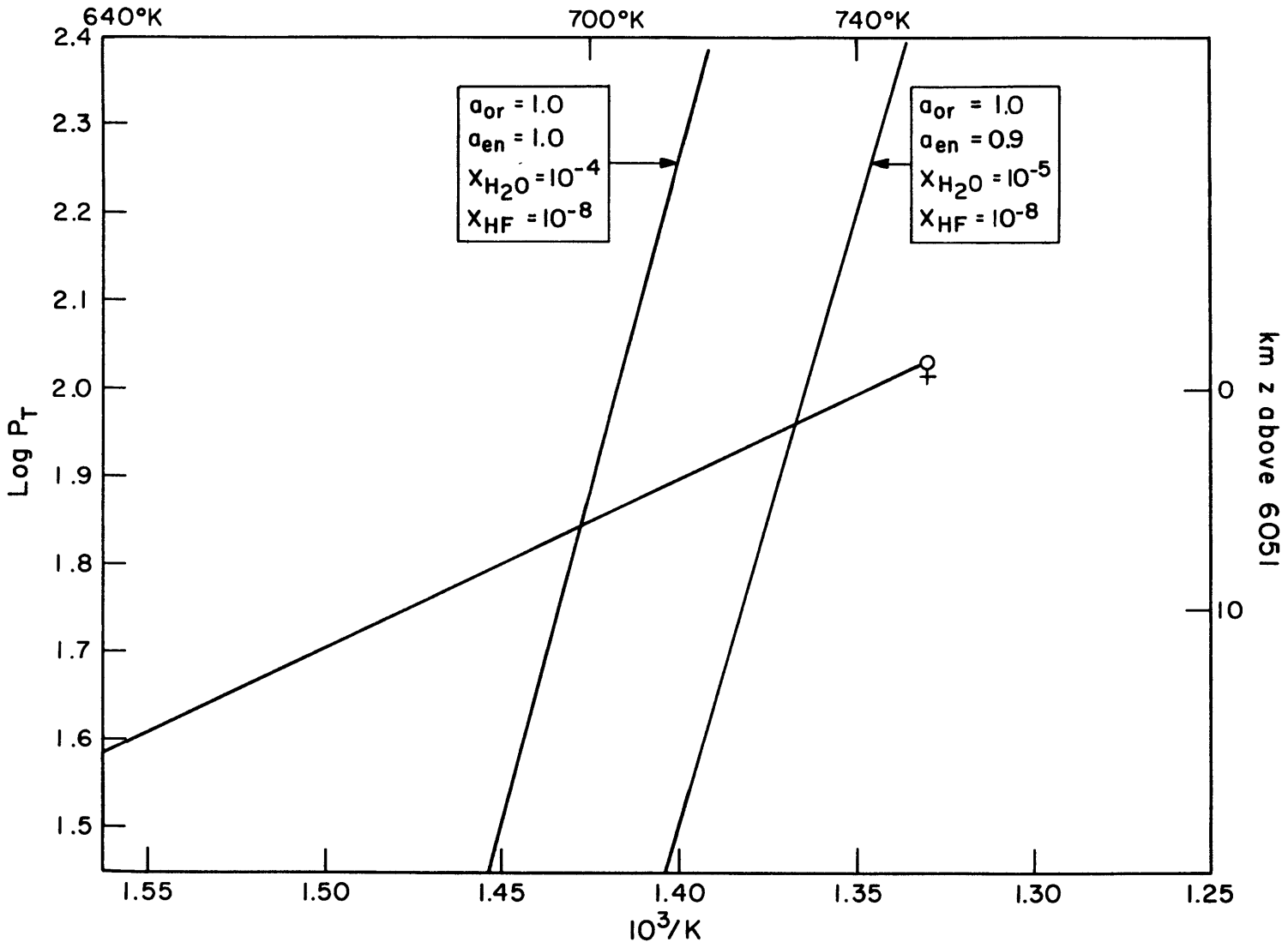
640°K
700°K
740°K
2.4
2.3
2.2
2.1
2.0
1.9
1.8
1.7
1.6
1.5
Log P_T
a_{or} = 1.0
a_{en} = 1.0
$X_{H_2O} = 10^{-4}$
$X_{HF} = 10^{-8}$
a_{or} = 1.0
a_{en} = 0.9
$X_{H_2O} = 10^{-5}$
$X_{HF} = 10^{-8}$
♀
0
10
km z above 6051
1.55
1.50
1.45
1.40
1.35
1.30
1.25
$10^3/K$

Figures 12 and 13

Equilibrium gas abundance variation for phlogopite formation. The 740°K relation provides a close match for a possible gas abundance. Figure 13 shows equilibrium gas abundance for resetion of alfite and HCI.

Figure 12

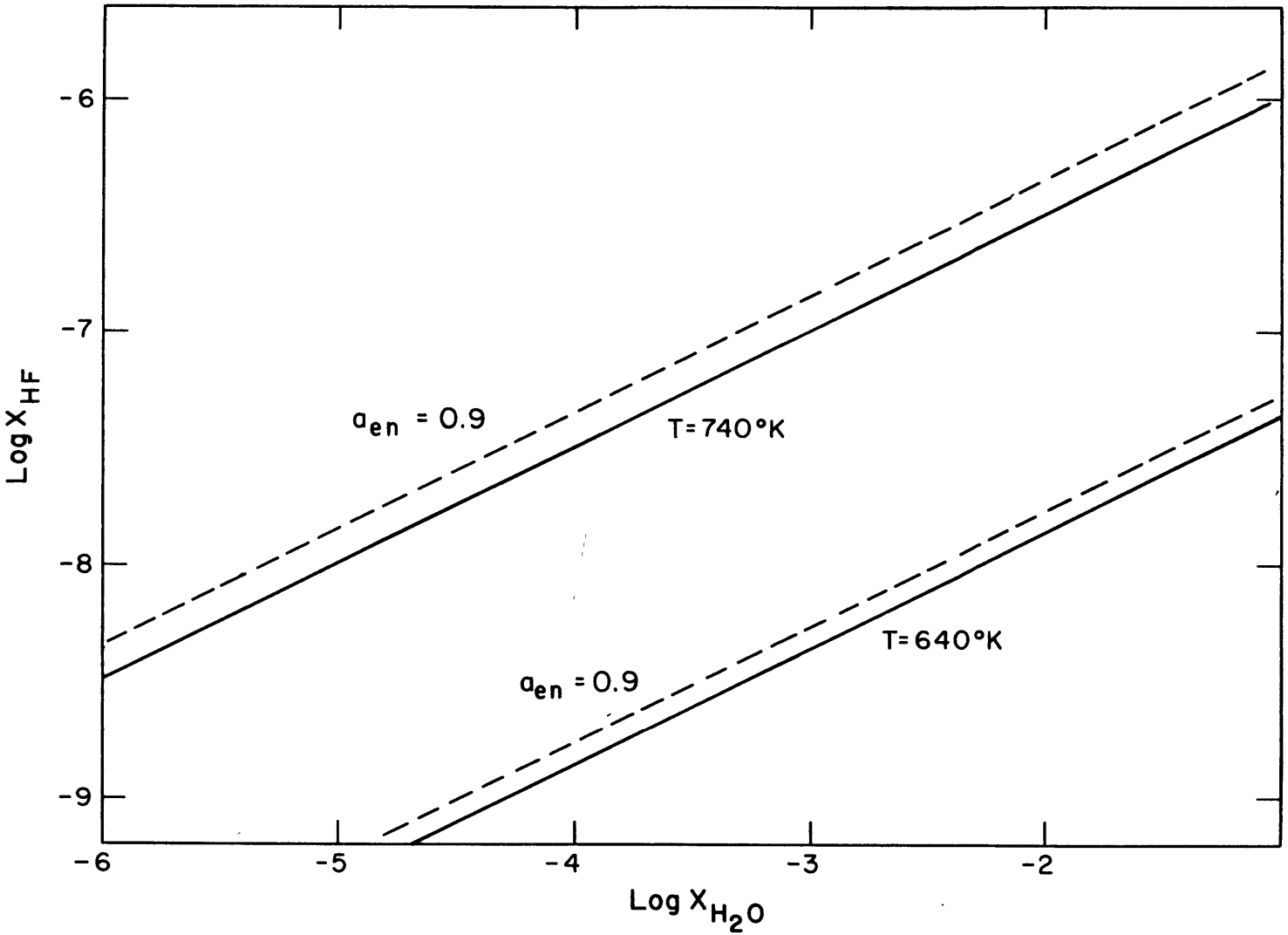

Figure 13

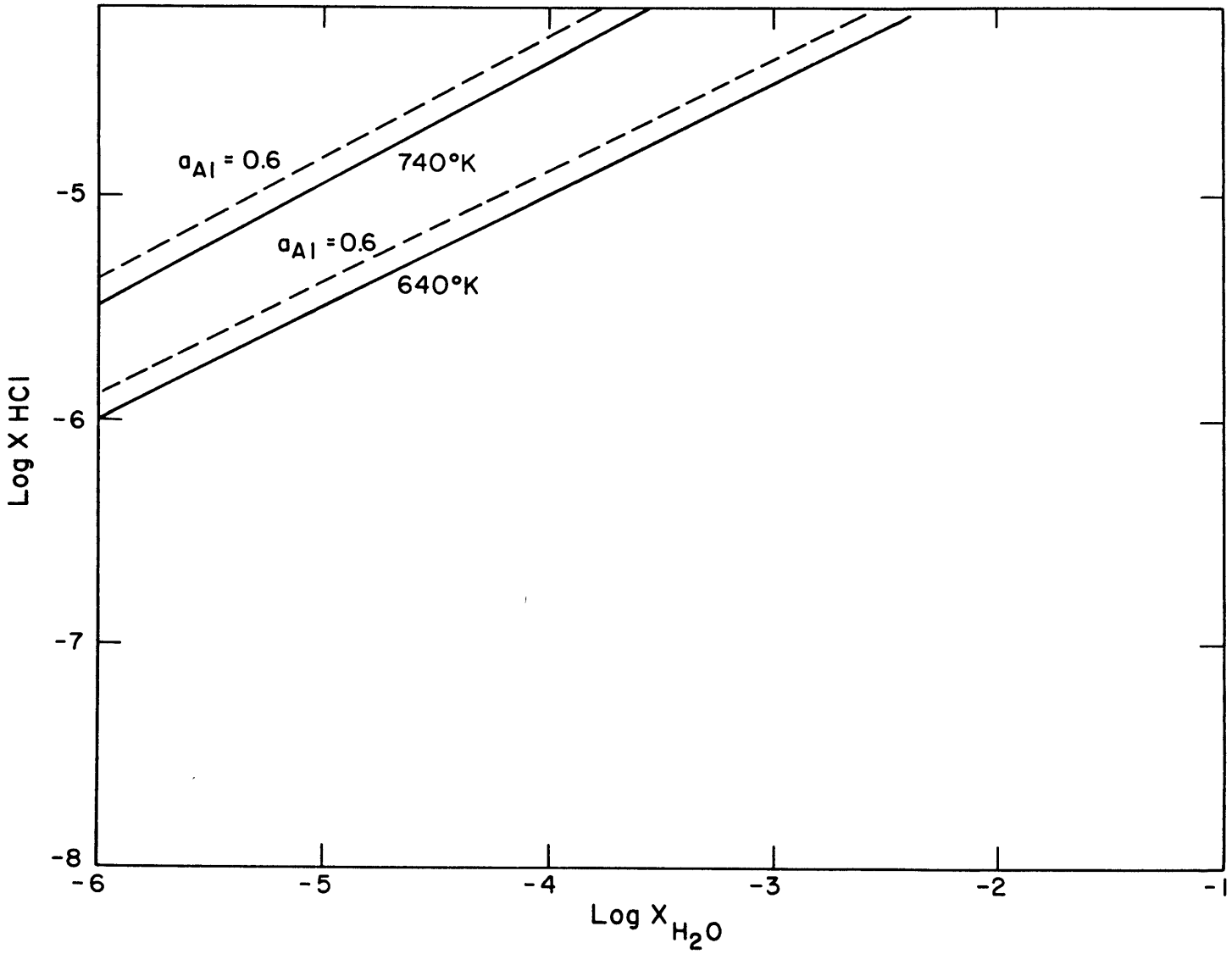

As to the effect of gas-solid weathering reactions on lower atmosphere composition, the most we can say is that some weathering reactions evolve an equilibrium partial pressure of gas at elevations found on the Venus surface. Therefore, it is entirely plausible that the lateral variation of abundance of minor gases (H_2O, HF, SO_2) is affected by the local mineralogy of the surface. Transport of weathering products from one area to another can also affect the local atmospheric composition. For example, carbonates produced on Maxwell Montes (T≈640K, P~45bar) would evolve CO_2 in the lowlands if carried there, with a partial pressure close to ambient CO_2 pressure. Of course, the mixing of the atmosphere, as well as other non-equilibrium processes (volcanic eruption) may complicate the actual situation. Still, it seems remarkable coincidence that plausible geochemical processes do indeed yield several of the observed gas abundances.

The buffering of gas species would only require a centimeter of dirt covering the surface with a high CaO activity. Lewis (1970) and Nozette and Lewis (1982) note that a 50 cm regolith layer containing 30% CaO could remove the entire amount of atmospheric water.

Figure 14

Altitude variation for several weathering reactions as a function of altitude; calculated for a range of possible gas abundances. The low H_2O abundances measured by the Soviet landers indicate that tremolite formation may not occur on Venus.

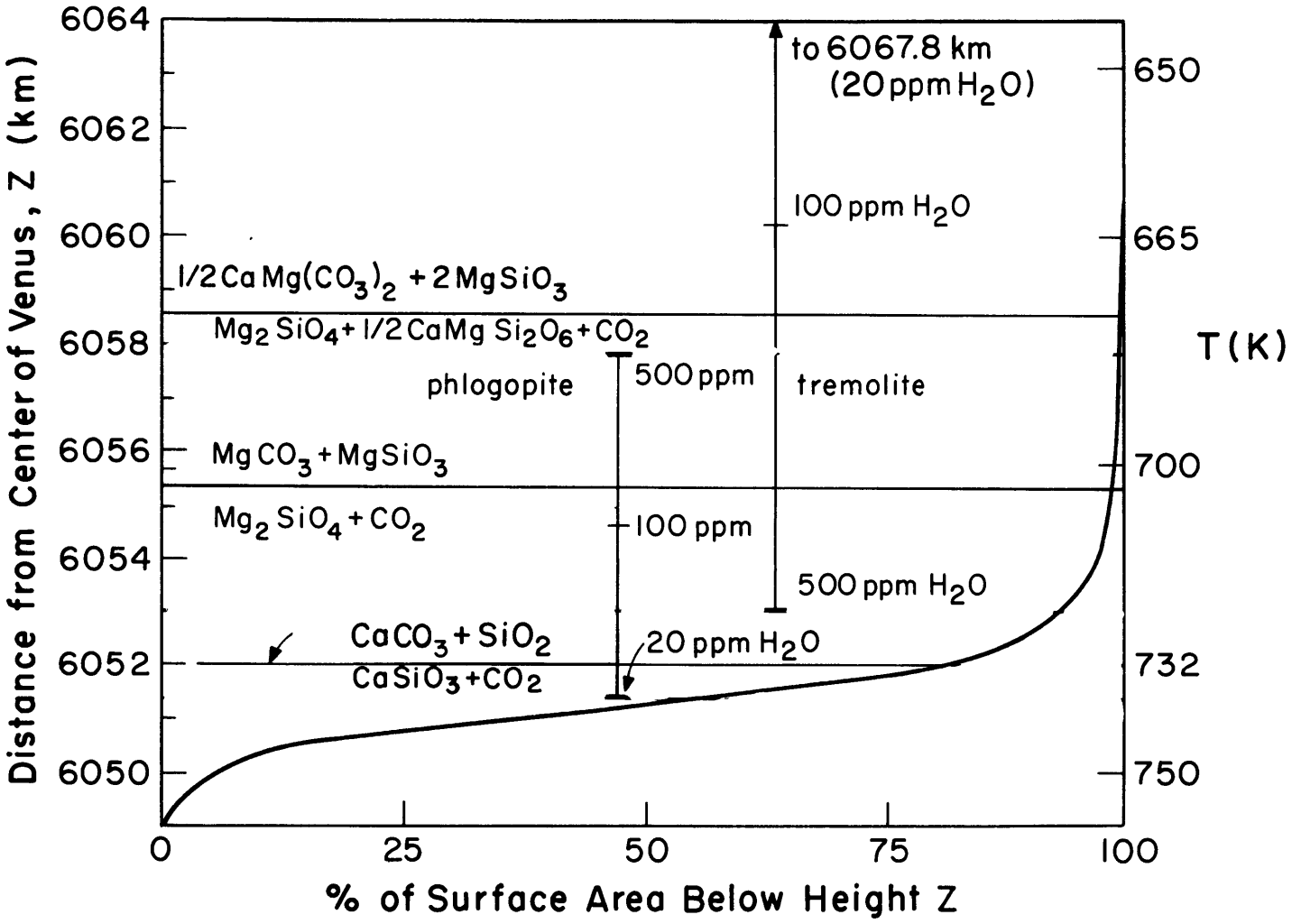
6064
6062
6060
6058
6056
6054
6052
6050
Distance from Center of Venus, Z (km)
to 6067.8 km
(20 ppm H_2O)
100 ppm H_2O
$1/2\,CaMg(CO_3)_2 + 2MgSiO_3$
$Mg_2SiO_4 + 1/2\,CaMgSi_2O_6 + CO_2$
phlogopite
500 ppm
tremolite
$MgCO_3 + MgSiO_3$
$Mg_2SiO_4 + CO_2$
100 ppm
500 ppm H_2O
$CaCO_3 + SiO_2$
$CaSiO_3 + CO_2$
20 ppm H_2O
650
665
700
732
750
T(K)
0
25
50
75
100
% of Surface Area Below Height Z

Figure 14

3. Kinetics Effects

The preceeding discussion of chemical weathering has not addressed the crucial question of reaction kinetics. How fast do the reactions discribed occur, and can a quasi-equilibrium be approached? In fact, many effects will work to disrupt an approach to equilibrium. Reactions will require a finite time to occur, and this time may be much larger than the time scale of perturbing processes such as atmospheric circulation, volcanic eruption, or mass transfer. In addition, the reactants must communicate chemically for sufficient time for reaction to occur. This last condition probably best justifies the assumption about restricting the complexity of mineral assemblages involved in possible weathering reactions.

Data on reaction kinetics involving minerals and gases under Venus conditions are scarce. The most studied reactions are reactions involving CO_2, since they are similar or identical to metamorphic reactions occurring on Earth. Weathering reactions are likely to involve several distinct steps and mechanisms, requiring constituents to diffuse to and from the site of reaction. Each of these steps will have its own rate constant, with its own activation energy.

The experimental energy of activation E* may be related to the rate constant k by the general expression

$$\frac{\partial \mathrm{Ln}k}{\partial T} = \frac{E^*}{RT^2}$$

where the E* measured depends on the conditions of the experiment. If we assume that no change in volume during reaction then we may approximate $E^* = \Delta H^* + RT$. Mueller and Krindelbaugh (1973), and Kridelbaugh (1973) estimate E* by assuming ΔH^* (enthalpy of activation) is not less than the heat of reaction. They then consult thermodynamic data to estimate

E^* (700) $\geq$ 21,258 cal

E^* (1100) $\geq$ 20,424 cal

for the formation of wollastonite. These values assume that the chemical step controls the rate, not the diffusion step, which may be slower.

Experimental study of the wollastonite reaction by Kridelbaugh (1972) indicates that for anhydrous conditions, the formation of wollastonite depends strongly on CO_2 pressure, temperature, and grain sizes of reactants. At Venus conditions or 1500psi, Mueller and Kridelbaugh simply assume that the activation energy is directly proportional to pressure, and extrapolate from data taken at higher pressure. A proportionality correction gives E* at 700°K of 22,555 cal, greater than the activation energy deduced from heat of reaction.

Harker and Tuttle (1956) noted that the reaction is accelerated by the presence of trace amounts of water. But no catalyst can lower the energy barrier below the endothermic heat of reaction. Thus, under Venus conditions wollastonite formation must have an activation energy

approaching 20Kcal/mole. However, water on Earth acts to reduce the diffusion barrier.

We have discussed reaction rates for decarbonization of calcite and quartz, which may be different than the rate of the reverse reaction. By assuming an activation energy of 20kcal/mole, Mueller and Kridelbaugh claim several hundred years reaction time at 700°K, and 10^7 years at 400°K. Using the same method, one calculates that on the higher mountain tops (640°K) the reaction would be about an order of magnitude slower than in the lowlands, assuming similar rates in both directions. These rates based on crude estimates, but probably within the correct order of magnitude.

The reaction times deduced are short geologically, but may be much longer than disrupting processes such as atmospheric circulation and local volcanic eruption. Unfortunatley no data exist for any other weathering reactions discussed.

The most important reaction rates to be explored would be the reactions involving sulfur and halogen gases. The dominance of SO_2 over reduced sulfur gases in the lower atmosphere does imply that rates of incorporation into surface minerals are much slower than rates of production of SO_2 by photochemial processes in the upper atmosphere. However, Venera 13 and 14 gas chromatograph measurements do show COS and H_2S as dominant species right at the surface.

Provided these data are reliable, they imply a very thin quasi-equilibrium zone right at the surface with reactions that are catalysed by the surface rocks. However, caution must be applied to this hypothesis.

F. Conclusions and Directions for Future Work

It is noteworthy to compare the results of investigation of separate mineral equilibria with the results of Barsukov et al (1980). They employ a global minimization of free energy for a system of igneous rock forming minerals, open with respect to atmospheric gases (except the halogen gases), and offer predictions of the stable mineral assemblages that result. For reactions involving basalt in contact with a water rich (X_{H2O} 1.35×10^{-3}) at 750°K, tremolite is predicted, while it is absent for low ($X_{H2O} < 10^{-5}$) water vapor abundances, consistent with results for single equilibria. Barsukov et al.(1980), also predict the production of anhydrite from both basalt and rhyolite, and the coexistence of sulfides and sulfates in weathered basalts, again consistent. They do not predict stable assemblages of carbonate minerals, calcite and dolomite, but since the primary rocks included in the analysis are not alkali rich, this is not unexpected. Calcite and dolomite would be expected for weathering at lower temperatures and pressures, and wollastonite would be produced as as secondary product. Barsukov et al.(1980) do not investigate the role of the halogen gases in rock weathering. Based on a single equilibrium (phlogopite formation) HF should be a powerful weathering agent of alkali-bearing basalts. The only connection that may be made to actual observation is the weathered appearance of the terrain surrounding the Venera 13 site, a site reported

to have a high (4%) K_2O concentration. Any connection between the appearance and equilibrium calculation is speculative at this time.

Future work on chemical weathering and atmospheric interaction must address the question of kinetics through actual laboratory experiments, involving realistic gas mixtures and analytic study of altered minerals. Furthermore, existing data on lower atmosphere composition must be carefully analysed and refined so as to lessen ambiguous and contradictory conclusions.

III. Radar Investigation

A. Background

Radar can measure the physical scale of Venus surface structure, as well as electrical properties of the Venus surface, since the radar cross section is proportional to the physical cross section of the target, and is related to target surface geometry and electrical properties. In order to separate these effects and interpret the received echoes, a parameterized model of the surface scattering is needed. Using this model, the parameters may be estimated from weighted least-square analysis, and the parameters may then be interpreted in terms of surface morphology and composition.

The scattering of electromagnetic waves by a surface which has a sharp dielectric interface (e.g., air and rock) may be described by two processes. A specular or coherent scattering is produced by reflections from surfaces which are smooth on the scale of a wavelength. In the case of most planetary surfaces, this type of reflection is assumed to be produced by small facets oriented on the surface so that the law of reflection is satisfied locally. Theoretical models for this type of scattering assume a wrinkled or undulating surface whose local radius of curvature is on the order of, or larger than, the observing wavelength. Reflection from such a surface is called quasi-specular to differentiate it from reflection by a perfectly smooth surface.

Hagfors (1967) derived the following expression which is applicable to the quasi-specular case:

$$\sigma_o(\theta) = C\rho_o/2 \ (\cos^4\theta + C \sin^2\theta)^{-3/2}$$

where σ_o is a dimensionless radar cross section, ρ_o is the Fresnel reflection coefficient at normal incidence and C is a constant related to the decrease of σ_o with increasing angle of incidence, θ. Hagfors reports that for $C>>1$, the r.m.s. slope of the surface (in radians) is approximated by $C^{-1/2}$. This slope may vary with wavelength, λ, since structure smaller than about $\lambda/2\pi$ will not contribute to the quasi-specular scattering.

The previous discussion allows interpretation of the quasi-specular reflection. To the extent that the surface is not smooth at the wavelength scale, the assumptions used in deriving the Hagfors model break down. In fact, the actual Venus surface is best represented by the sum of a specular and diffuse component. The diffuse component (caused by subwavelength sized surface roughness) dominates reflection at incidence angles greater than about ~20°, the quasi-specular component usually dominates at smaller angles.

Thus, the observed radar cross section depends on three parameters: intrinsic reflectivity, roughness at subwavelength dimensions, and undulations on a many-wavelength scale. The relative magnitude of each may be separated if observations are available over a suitably

large range of incidence angles. By combining Earth-based observations at large scattering angles with Pioneer Venus spacecraft radar data taken near normal incidence, the separate contributions of intrinsic reflectivity and surface roughness at several scales may be estimated.

B. Earth-Based Radar Observations

1. Arecibo

12.6-cm-wavelength observations of Venus, carried out by Campbell and Burns (1980) at the Arecibo Observatory in 1975 and 1977, have imaged the surface at resolutions ranging from 20km near the equator to 5km at high latitudes. Due to a near commensurability between the rotation period and the synodic period of the Venus-Earth system, approximately the same portion of Venus is mapped at each inferior conjunction. The sub-Earth track, however, does vary between 9°N and 9°S from conjunction to conjunction.

Arecibo observations allow measurements of $\sigma_o(\theta)$ from near normal incidence out to 65°, the largest angle measured to date. At 12-cm wavelength the Hagfors law is obeyed to about 25°, with a C factor typically of 175 (4° rms slope). Campbell and Burns report that beyond 40° incidence angle $\sigma_o(\theta)$ goes as $\cos^{3/2}\theta$. At very large angles of incidence (as at small) the observed cross section depends sensitively on large-scale slope.

The rapid variation of the scattering with incidence angle allows high surface resolutions at low angles where

the echo per unit surface area is strong. Unfortunately, the echo "signature" highlights quite different aspects of a surface feature when viewed at different angles, thus complicating its interpretation.

In the Arecibo radar images, Lakshmi Planum, a low reflectivity region 1,200 km in diameter centered at (67°N, 330°), and the neighboring Maxwell Montes to the east, dominate the higher latitudes, as may be seen in Figure 15. Before the Pioneer Venus altimetry, this area was interpreted as a basin, not an elevated plateau several kilometers above the surrounding terrain. The Lakshmi Planum appears smooth at the centimeter scale to which the high incidence Arecibo observations are sensitive.

Maxwell Montes, on the other hand, appears to be extremely rough on the centimeter scale. Observations at 70cm by Jurgens and Dyce (1970) revealed that the radar echo from Maxwell was almost completely depolarized, consistent with centimeter-scale roughness. A 100-km-diameter dark (i.e. smooth) circular feature is observed inside the eastern edge of Maxwell; a hint of a smaller circular feature (~40 km) may be seen within the larger one.

Beta Regio is the most prominent feature in the equatorial portion of the Arecibo maps, with two components, Rhea Mons (33°N, 283°) and Theia Mons (23°N, 281°). The latter has been seen in earlier radar observations and described by Campbell *et al.* (1979) and Goldstein *et al.* (1978). Saunders and Malin (1977) suggested that Theia

might be a volcano based on its estimated altitude and circular symmetry. Ray-like flow patterns are observed emanating from Beta Regio.

Alpha Regio (located at 35°S, 3°E) is the most prominent feature in the southern hemisphere seen at Arecibo. Its prominence stems from a very rough surface, which displays a series of SW to NE linear features, spaced at about 20 km.

Campbell and Burns report a number of circular features, both large and dark, and small and bright, which they claim may be either impact or volcanic craters. They have suggested that over 30 of these features are impact craters, and have compared their sizes and shapes to craters observed on the Moon, Mercury, and Mars. The crater-like features are characterized by diffuse scattering at high incidence angles and some of them have an internal bright spot, usually not perfectly centered.

The assumed Venus impact craters tend to have a bright annular region surrounding them, brighter and larger than the region surrounding lunar craters of comparable size. These features appear randomly distributed over the mapped surface.

The size-frequency distribution of the crater-like features was also reported by Campbell and Burns, and compared to lunar and Martian distributions. From a knowledge of the rate and size distribution of the assumed impacting bodies, and correcting for the effects of gravity

and atmospheric drag, a time of accumulation or age may be estimated. By assuming a cratering rate similar to that affecting the Moon, we infer an age of 600 m.y. - 800 m.y. Because of possible systematic error in the identification of impact craters as the incidence angle changes, this age may be greatly in error. But the results point toward a younger surface for Venus than for the Moon, Mercury and Mars. Given the poor resolution and possible mis-identification of impact craters on Venus, however, an age determination based on crater statistics must be viewed as premature.

Figure 15

Arecibo radar image of a portion of the Venus surface. Maxwell is the bright pork chop shaped feature in the upper right, Beta Regio is the prominent feature at 30° north and 280°-285° west. Alpha Regio lies astride the origin of longitude at 25° south.

Figure 15

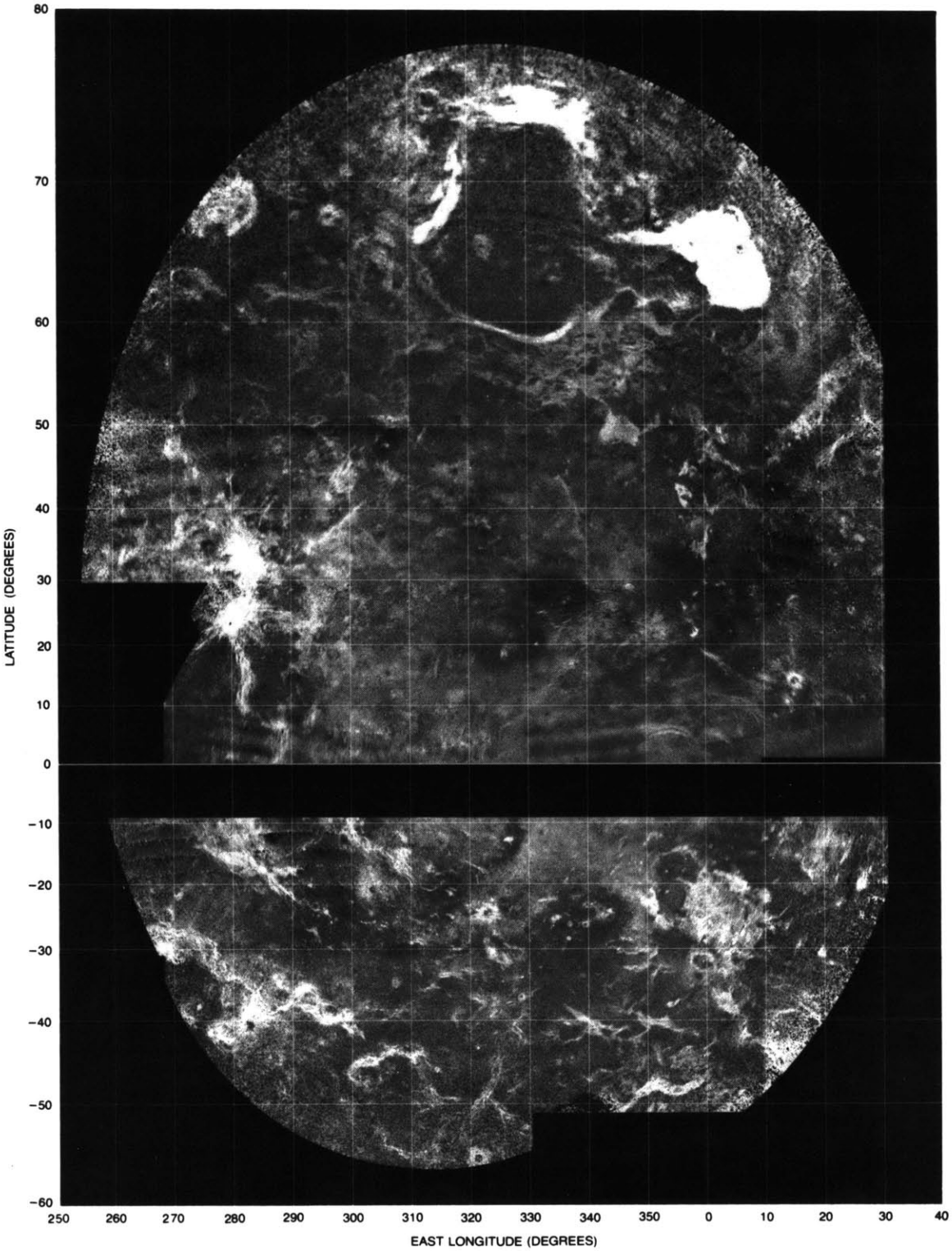
80
70
60
50
40
30
20
10
0
-10
-20
-30
-40
-50
-60
LATITUDE (DEGREES)
250
260
270
280
290
300
310
320
330
340
350
0
10
20
30
40
EAST LONGITUDE (DEGREES)

2. Goldstone

Jurgens et al.(1980) report measurements of Venus topography and reflectivity, using a three-station interferometer system. The interferometric system used at Goldstone allows a determination of altitudes and scattering efficiency for areas near the sub-Earth point at a linear surface resolution of better than 10 km. The radar images produced by the Goldstone group cover areas no more than 8° from the sub-radar point, i.e. no more than 8° from normal incidence. They also note that a smooth region will appear bright at near normal incidence, dark at higher incidence angle, while a rough surface behaves in just the opposite way. The brightness at normal incidence is also influenced by the Fresnel coefficient, so at normal incidence a surface may look dark because its dielectric constant is low, or it is rough, or both. Jurgens et al. have not attempted to separate the effects of altitude, roughness, and dielectric constant. They note that differences in apparent reflectivity do exist.

The radar maps display a variety of structure, showing, among other objects, a bright circular feature some 400 to 500 km in diameter near 41°S, 336°, with an irregular shape. The feature may be a crater: it possesses a bright ring.

Pioneer Venus Radar Observations

1. Experiment Description and Operation

The ground-based radar studies, while extremely useful, are limited by their lack of altitude coverage away from the equator, and the wide variation in the incidence angle of observation. In addition, only a portion of the surface of Venus is accessible to ground-based radar observation. For these reasons, NASA sent the Pioneer-Venus spacecraft in 1978 to orbit Venus carrying a small radar altimeter. The basic objective was to measure the distance from spacecraft to surface, while tracking the spacecraft to determine its distance from the center of Venus. The known geometric relationship among these quantities yields the planetary radius at the point observed.

The orbital parameters of the spacecraft determine the range of coverage possible. The orbit has an eccentricity of 0.84, a period of 24 hours, an inclination of -106°, and a perapsis altitude of about 160 km (although this changes due to solar perturbations). Radar observations are limited to that portion of the orbit where useful echoes are obtained, generally below 4,700 km. The spacecraft is spin stabilized, with the spin axis pointing close to the south ecliptic pole, so radar observations are possible only during that portion of the spin period when the planetary nadir lies in the beamwidth of the antenna, about 1 sec out of each 12 sec spin period.

Near periapsis the orbital velocity of about 10 km/sec

separates each radar measurement by about 120 km. Since Venus rotates about 1.5°/day (about 150 km at the equator) the daily orbital tracks are separated by 1.5° in longitude. During the extended mission it was possible to interleave the new tracks between those from an earlier rotation to obtain denser grid coverage. The orbital inclination (in the north) combined with the altitude constraint (in the south) limit observation to the region between 74°N and 63°S, about 93% of the planetary surface. Only the polar regions escape coverage.

The instrument has two modes of observation, altimetric and imaging. The altimetric mode operates when the antenna is pointing straight down at the planetary nadir, while the imaging mode is engaged while the antenna is rotated away from nadir, before and after altimetric observation, by the spacecraft spin. The imaging mode operates only below 550 km altitude, and produces a delay-Doppler map of radar cross-section similar to that of the Arecibo images. Samples of receiver noise are taken when the antenna is directed near nadir, and again at 180° from nadir, to sample the system temperature while observing the planet and space, respectively. Since the temperature of space and the planet are assumed to be known, the receiver performance may be verified.

D. Pioneer Venus Radar Results

1. Global Altimetry and Roughness

The Orbiter radar has returned over 200,000 discrete measurements of altitude. From the near-global data set, three types of average planetary radius have been obtained:

(1) The mean radius, or first moment of the distribution: 6051.9 km.

(2) The modal radius, or most probable value: 6051.4 km.

(3) The median radius, i.e. the value for which half the planet lies above, half below: 6051.6 km.

All topographic contour maps in this thesis are referenced to the median radius.

The global topography of Venus is markedly unimodal, as compared with Earth's bimodal distribution, as seen in Figure 16. The maximum relief measured by the Pioneer Venus radar is about 13.5 km, and the median and modal elevations are nearly equal, again in contrast with Earth.

At first glance, the global topography of Venus is very dissimilar to that of Earth. A comparison between Figure 17 and 18 shows that the Pioneer Venus radar would indeed be capable of observing the major features of Earth's topography, namely, continents, ocean basins, midocean ridges, mountainous belts, and subduction zones. Of course, we cannot simply remove the terrestrial oceans and compare the two planets. The oceans produce a topographic load which would disappear, and temperature differences between Venus and Earth would also tend to even out the topography.

Removal of the ocean load and elevated temperatures would still not totally explain the apparent lack of similarity between Venus and Earth topography, since this effect would account for only about 20% of the difference. Head et al. (1981) note that many complex geologic features would completely escape detection at Pioneer Venus resolution, and that terrestrial plate tectonics would not be uniquely determined. Since Venus contains a variety of features very different from those of the smaller planets (Moon and Mars), many tectonic processes may operate on Venus. Only high resolution images of Venus will clarify the details.

Figure 16

Topographical comparison between Venus and Earth. The Venus distribution is unimodal, as compared to the bimodal terrestrial distribution.

Figure 16

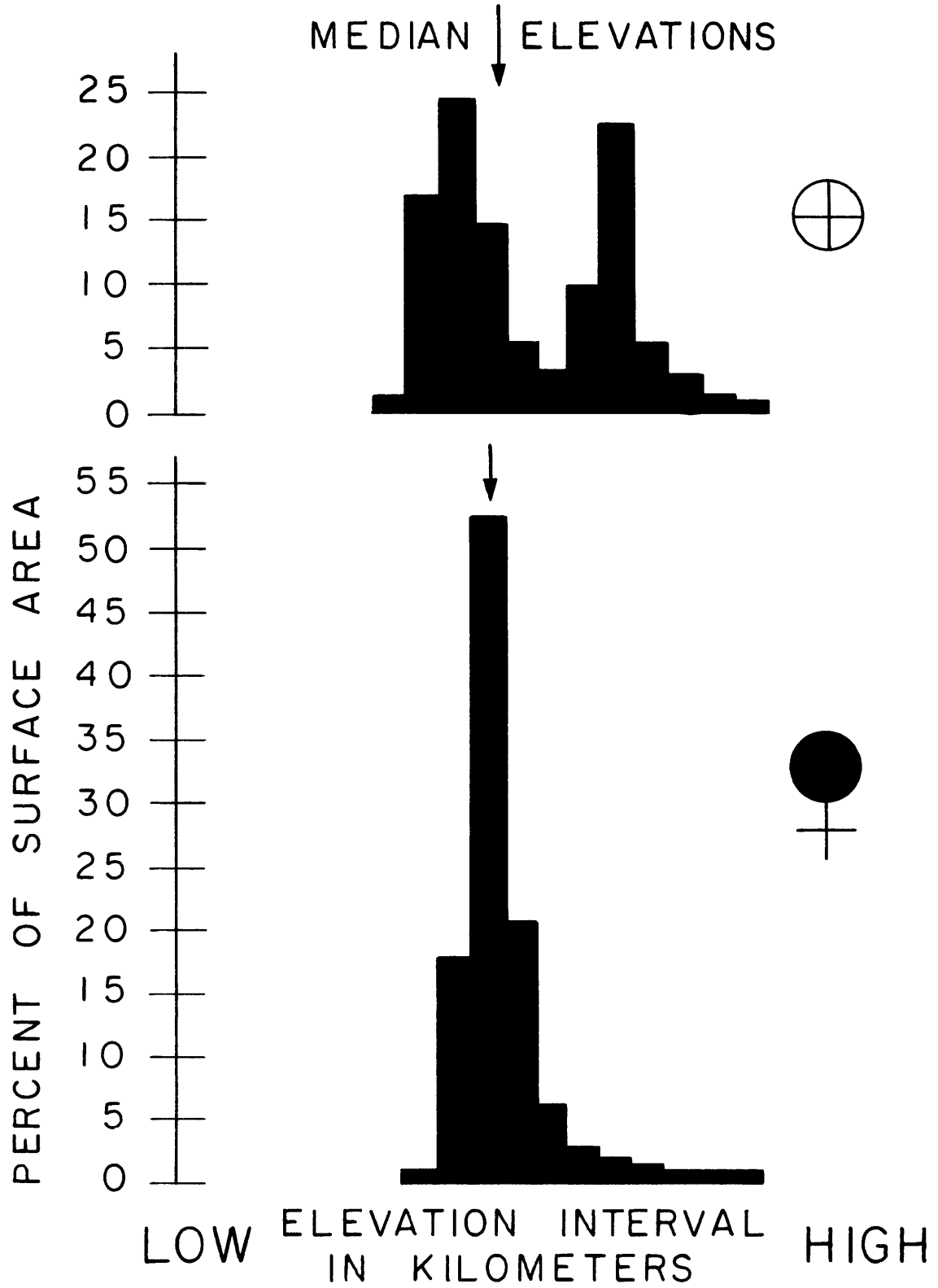
MEDIAN ELEVATIONS
25
20
15
10
5
0
55
50
45
40
35
30
25
20
15
10
5
0
PERCENT OF SURFACE AREA
LOW
ELEVATION INTERVAL IN KILOMETERS
HIGH

Figure 17

The Venus topography as measured by the Pioneer Venus radar mapper, displayed in Mercator projection. Ishtar Terra, the northern continent, and Aphrodite Terra in the equatorial region are the most prominent features. Beta Regio consists of two separate parts, Rhea and Theia Mons.

Figure 17

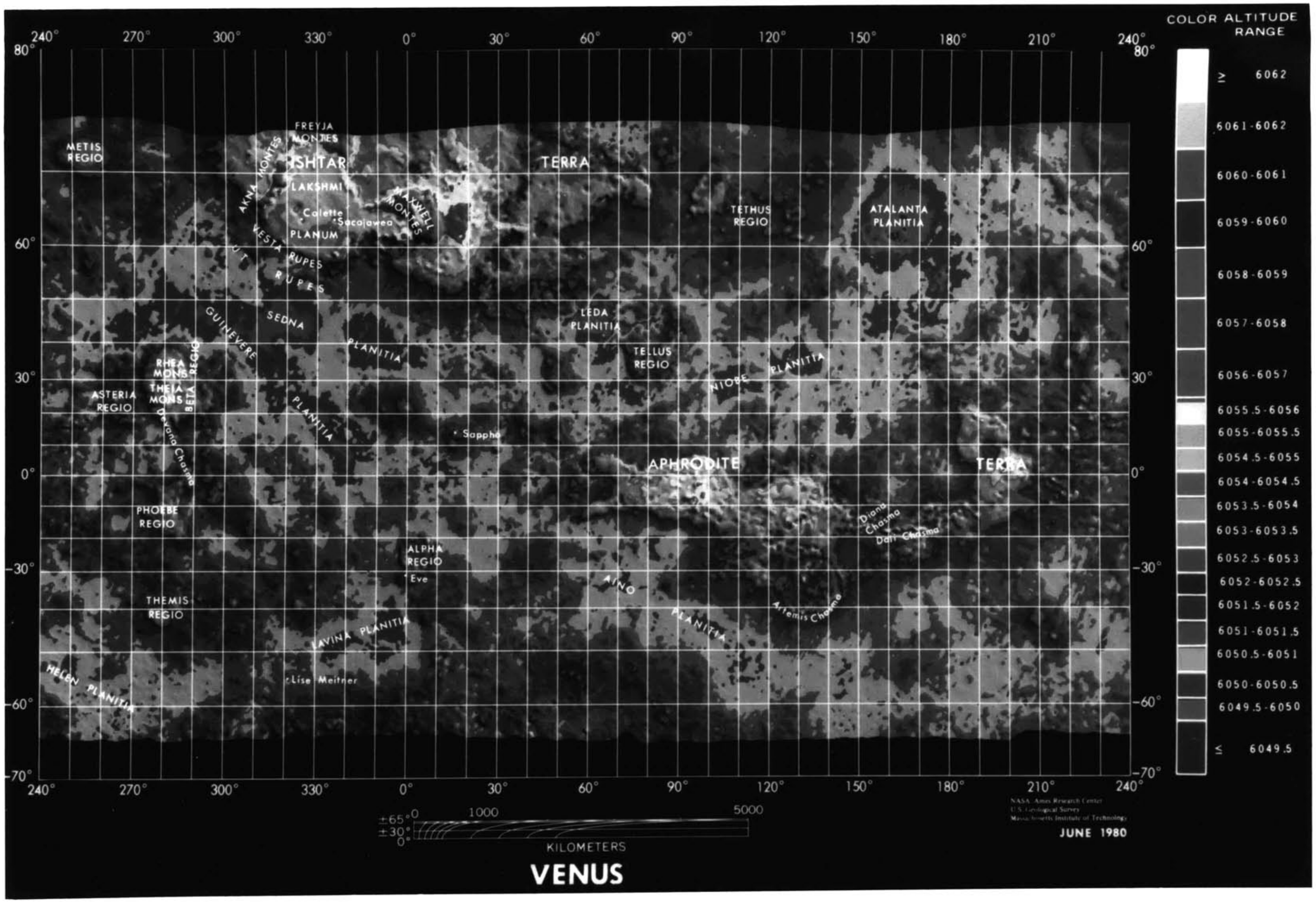
COLOR ALTITUDE RANGE
≥ 6062
6061-6062
6060-6061
6059-6060
6058-6059
6057-6058
6056-6057
6055.5-6056
6055-6055.5
6054.5-6055
6054-6054.5
6053.5-6054
6053-6053.5
6052.5-6053
6052-6052.5
6051.5-6052
6051-6051.5
6050.5-6051
6050-6050.5
6049.5-6050
≤ 6049.5
METIS REGIO
FREYJA MONTES
ISHTAR
TERRA
AKNA MONTES
LAKSHMI
MAXWELL MONTES
Colette
Sacajawea
PLANUM
VESTA RUPES
UT RUPES
TETHUS REGIO
ATALANTA PLANITIA
SEDNA
PLANITIA
GUINEVERE
PLANITIA
LEDA PLANITIA
TELLUS REGIO
NIOBE
PLANITIA
RHEA MONS
THEIA MONS
BETA REGIO
ASTERIA REGIO
Devana Chasma
Sappho
APHRODITE
TERRA
PHOEBE REGIO
Diana Chasma
Dali Chasma
ALPHA REGIO
Eve
AINO
PLANITIA
Artemis Chasma
THEMIS REGIO
LAVINA PLANITIA
Lise Meitner
HELEN PLANITIA
KILOMETERS
JUNE 1980
VENUS

Figure 18

Terrestrial topography displayed at Pioneer Venus resolution. The outlines of terrestrial continents, mountain chains, and oceans are visible, but the tectonic organization is not uniquely determined (Arvidson, 1981).

Figure 18

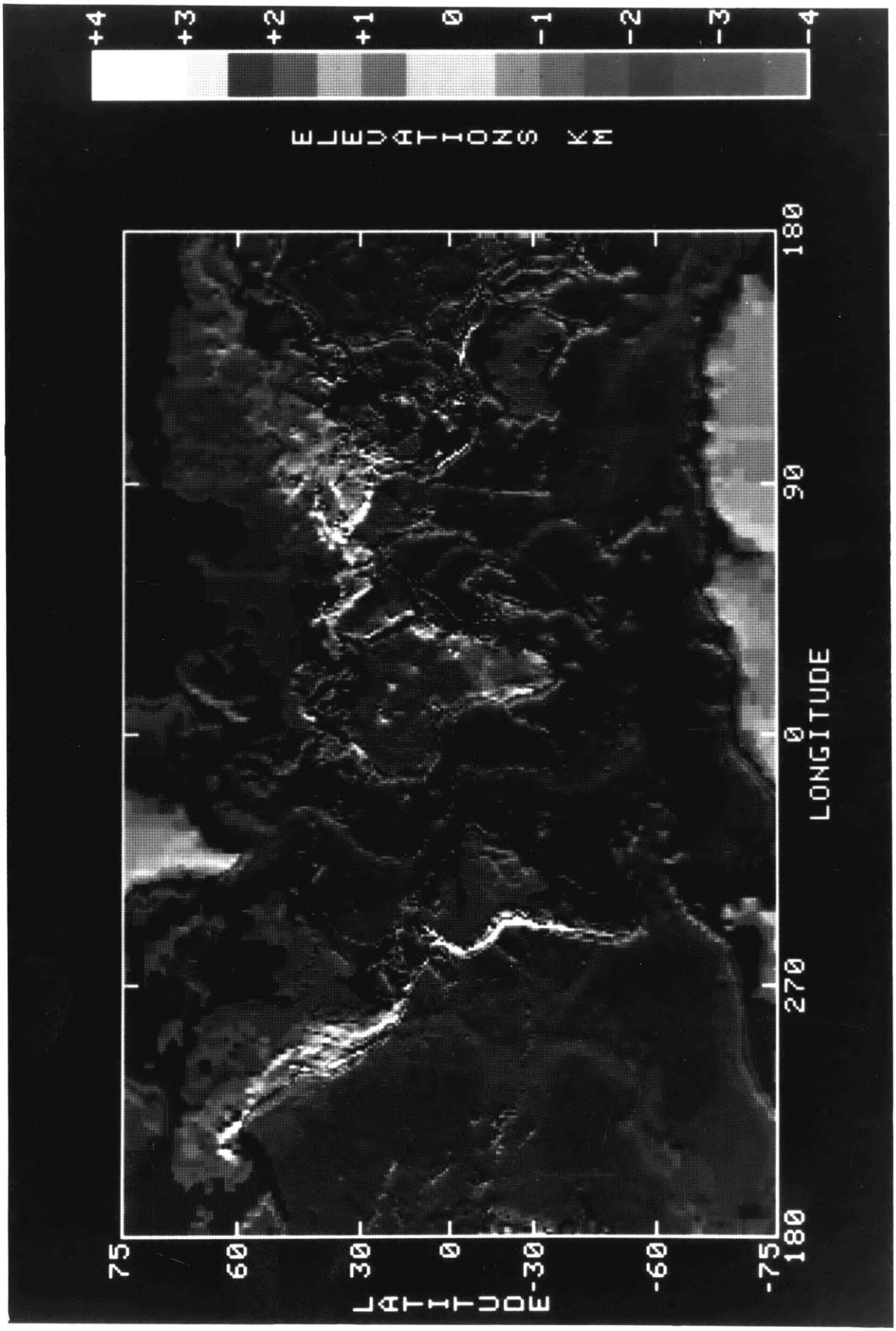
+4
+3
+2
+1
0
-1
-2
-3
-4
3X OZONE/CM
75
60
30
0
-30
-60
-75
LATITUDE
180
270
0
90
180
LONGITUDE

Most of the surface of Venus has been described as a rolling terrain (Masursky et al., 1980), characterized by topography with low local relief (<2 km) over thousands of kilometers lateral extent. Figure 19 shows the surface with contours 1 km above, and 1 km below the median radius. Most of the low terrain lies within broad, irregular, shallow basins, many of which are adjacent to areas of higher elevation.

Atalanta Planitia, is the lowest extensive area on Venus, located in the northern hemisphere. The other striking low, Diana Chasma, consists of a series of long, narrow troughs. Because of their narrowness, they are probably poorly sampled by the course net of altimetric measurements, and may actually be deeper. From the hypsometric diagram we see that the areas of high elevation (> 4 km) are not a large fraction (< 5%) of the total. Their relief, however, is more striking than the relief of the low regions.

The ground-based radar images (from both Arecibo and Goldstone) reveal that some of the high and low topographic features are characterized by radar brightness higher and lower than the mean, respectively. The ORAD images also show this effect (see Fig. 20); the basin areas generally appear radar dark. There are exceptions to this correlation, Alpha Regio is not a striking topographic high, yet it appears bright in Earth-based and Pioneer Venus observations at meter and centimeter scale.

Some of the roughest areas (on the meter and centimeter scale) appear to be prominent topographic highs: Maxwell Montes, Aphrodite Terra, Beta Regio, Akna Montes, Freyja Montes, and Vesta Rupes (the slope of Lakshmi Planum). Alpha Regio, Phoebe Regio, Themis Regio, and Metis Regio, also appear rough on the cm scale). It is probable that higher horizontal resolution than that now available in Earth-based images (5-10 km) would show small-scale slopes which lie below the resolution of the Pioneer Venus radar. McGill et al. (1982), suggest that the apparent roughness of these areas may not be slopes at all, but are rippled dunes of wind transported material, or surface roughness produced by faults, folds, or other tectonic features.

Figure 19

Major geologic provinces on Venus, the highlands, basins, and rolling plains, and the Terra (after McGill *et al.*, 1983).

Figure 19

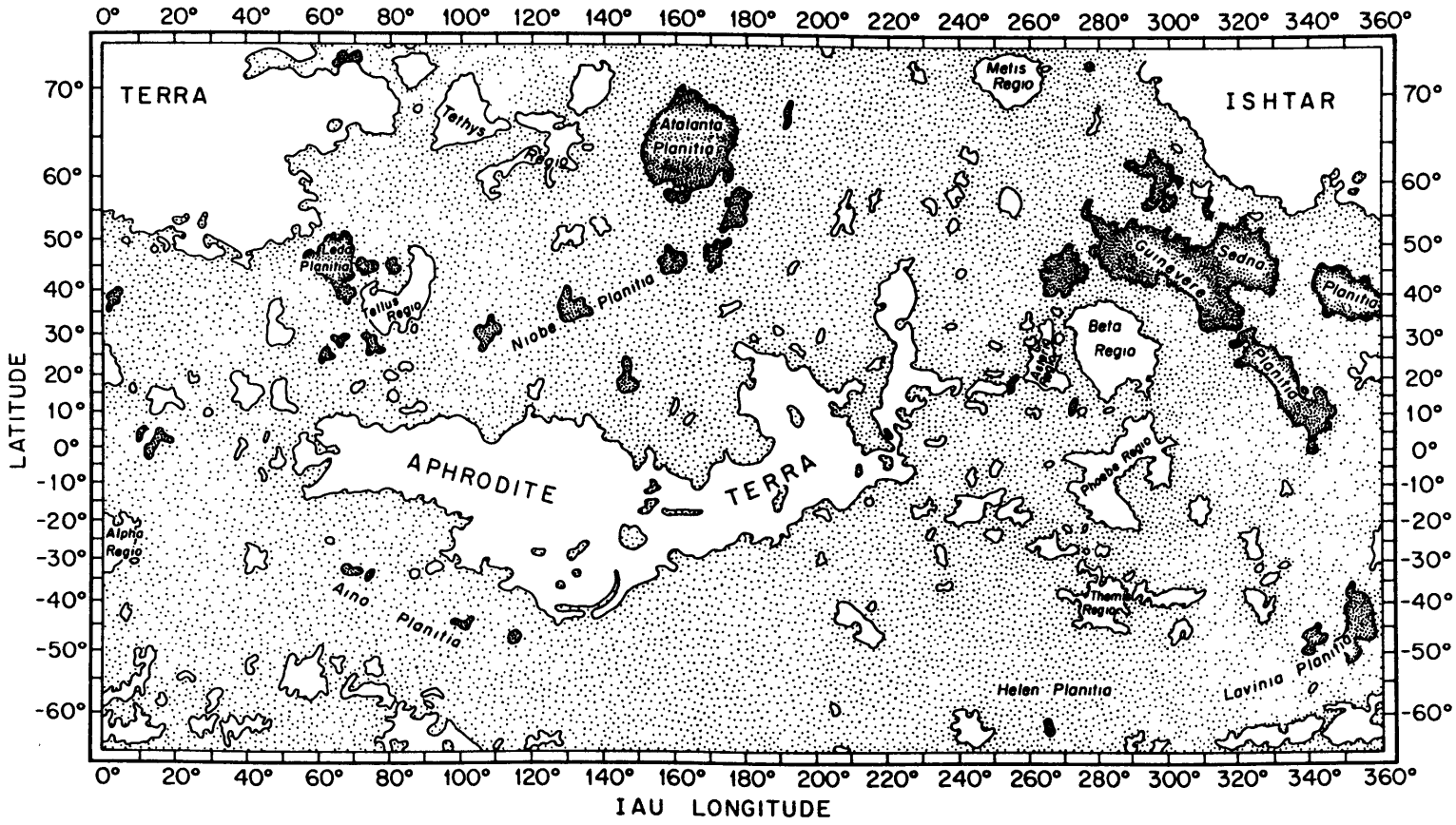
TERRA
ISHTAR
APHRODITE TERRA
Tethys Regio
Atalanta Planitia
Metis Regio
Guinevere Planitia
Sedna Planitia
Beta Regio
Phoebe Regio
Themis Regio
Helen Planitia
Lavinia Planitia
Leda Planitia
Tellus Regio
Niobe Planitia
Alpha Regio
Aino Planitia
LATITUDE
IAU LONGITUDE
0° 20° 40° 60° 80° 100° 120° 140° 160° 180° 200° 220° 240° 260° 280° 300° 320° 340° 360°
70° 60° 50° 40° 30° 20° 10° 0° -10° -20° -30° -40° -50° -60°

Figure 20

Radar images obtained from the Pioneer Venus radar mapper. These images display centimeter scale roughness, and are more nearly comparable to those taken at Arecibo than the data obtained in the altimetric mode.

Figure 20

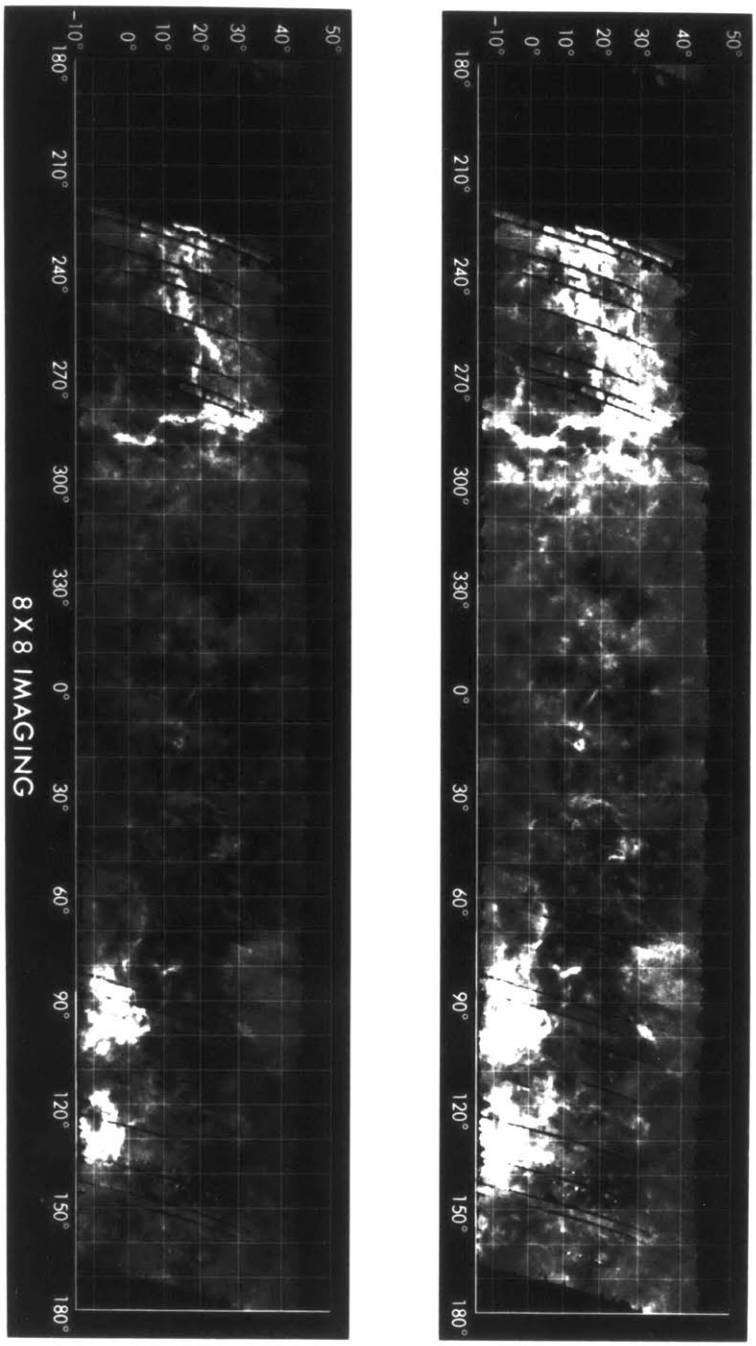
8X8 IMAGING
50°
40°
30°
20°
10°
0°
-10°
180°
210°
240°
270°
300°
330°
0°
30°
60°
90°
120°
150°
180°

Ishtar Terra and Aphrodite Terra are the two elevated regions of continental dimensions, described in detail by Masursky et al. (1980); McGill et al. (1982) present detailed topographic maps which show features not apparent on the global topographic maps.

Ishtar Terra (at least its known extent, since its northern portion may exceed the present coverage) has an area about that of Australia. The plateau Lakshmi Planum extends 2-3 km above the surrounding plains, and dominates the structure. Three features rise above the plateau: Maxwell Montes, Akna Montes, and Freyja Montes.

Centimeter-scale roughness on Maxwell corresponds well with topography. The shape of Maxwell, and the linear banding suggest some structural basis for the roughness. Differential chemical weathering proposed in Section 1 may contribute to Maxwell's small scale roughness. Masursky et al. suggest that Maxwell is a fault-bordered massif, but alternative suggestions include a volcanic complex. The large circular depression on the northeast side may be a volcanic caldera, but the absence of depressions in the high areas of Maxwell argues against a purely volcanic origin. The Arecibo images of Maxwell show a pronounced banding, which have been inferred by Masursky et al. to be caused by roughness differences between block faults. At present, because of the poor resolution of the altimetry data, we do not know if the roughness bands are correlated with topography.

Figure 21

Pioneer Venus map of Hagfors constant, which is inversely related to meter-scale surface undulations. Maxwell and Alpha Regio appear rough at meter scale (as well as centimeter scale in the Arecibo images), while Beta Regio, which is prominent in the Arecibo and ORAD images, is not strikingly rough at meter scale.

Figure 21

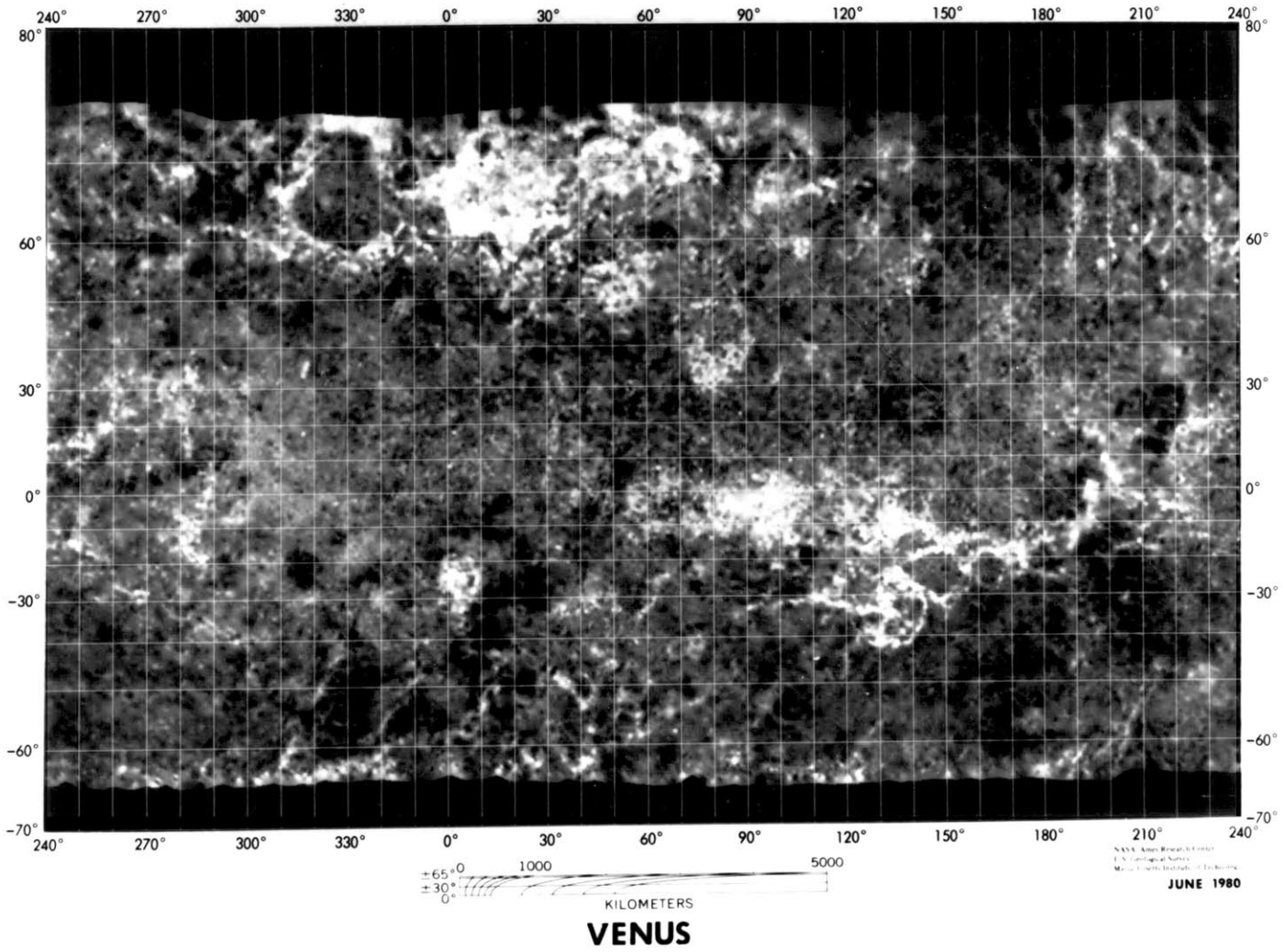

VENUS

Figure 22

Detailed topography of Maxwell Montes, after McGill et al. (1982), and a detailed Arecibo image of Maxwell. The topographic resolution is too low to correlate with the banding seen in the image.

Figure 22

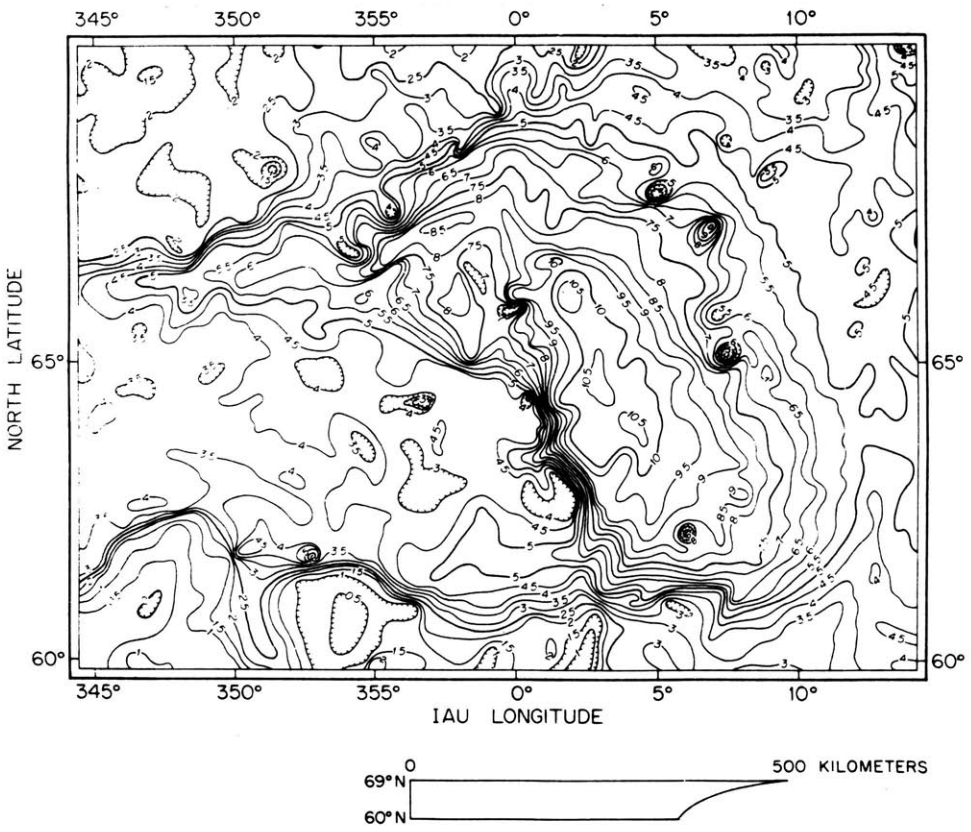
345°
350°
355°
0°
5°
10°
65°
60°
NORTH LATITUDE
IAU LONGITUDE
0
500 KILOMETERS
69°N
60°N

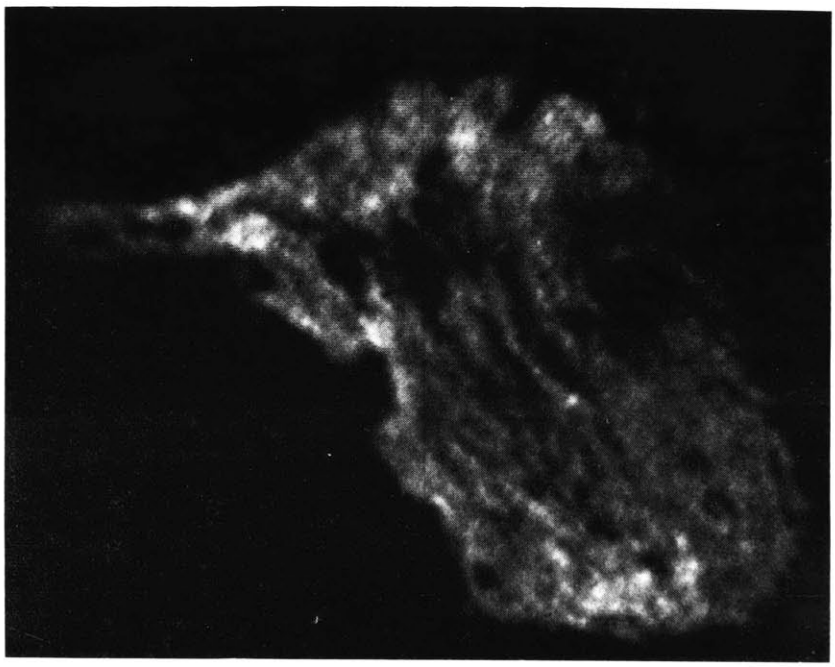

Differential erosion is also a candidate for contributing to these roughness bands.

South of Lakshmi Planum lies a complex terrain, marked by irregular depressions and a shallow elevated region. There are wispy bright streaks against a dark background in Earth-based images, with C factors approaching those on the bounding plateau.

Aphrodite Terra is the extensive equatorial continental structure, about equal in area to South America, or about twice as large as Ishtar Terra. Aphrodite does not contain the extreme elevation found in Terra Ishstar; it is fairly narrow with several semi-isolated areas of high elevation. The two highest elevations occur in the western half. On the map, Aphrodite resembles a legless scorpion, because of the long eastern tail curving toward the northwest, and two short projections at the western end.

At the eastern end of Aphrodite there are a series of remarkable extensive troughs (Artemis, Dali, and Diana Chasmae). The troughs and ridges are over 2000 km long, with relief from bottom to top of more than 5 km, with widths on the order of 100 km.

The characteristic topography of the ridge and trough system is seen in Figure 24. Most workers (McGill, Masursky, et al.) agree that this area must be of tectonic origin, but the altimetry data do not reveal whether the troughs are extensional rifts, or compressional trenches. They may have no terrestrial analogy.

Figure 23

Detailed topography and image of southern half of Lakshmi Planum.

Figure 23

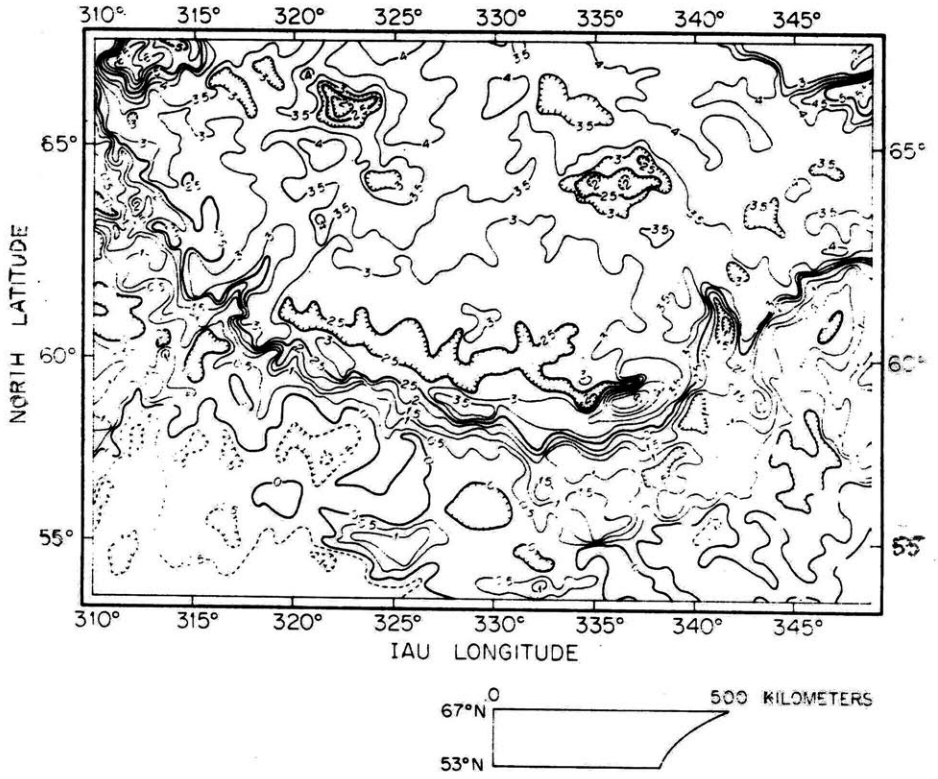
310°
315°
320°
325°
330°
335°
340°
345°
65°
60°
55°
NORTH LATITUDE
IAU LONGITUDE
0
500 KILOMETERS
67°N
53°N

Figure 24

Detailed topography of Diana Chasm.

Figure 24

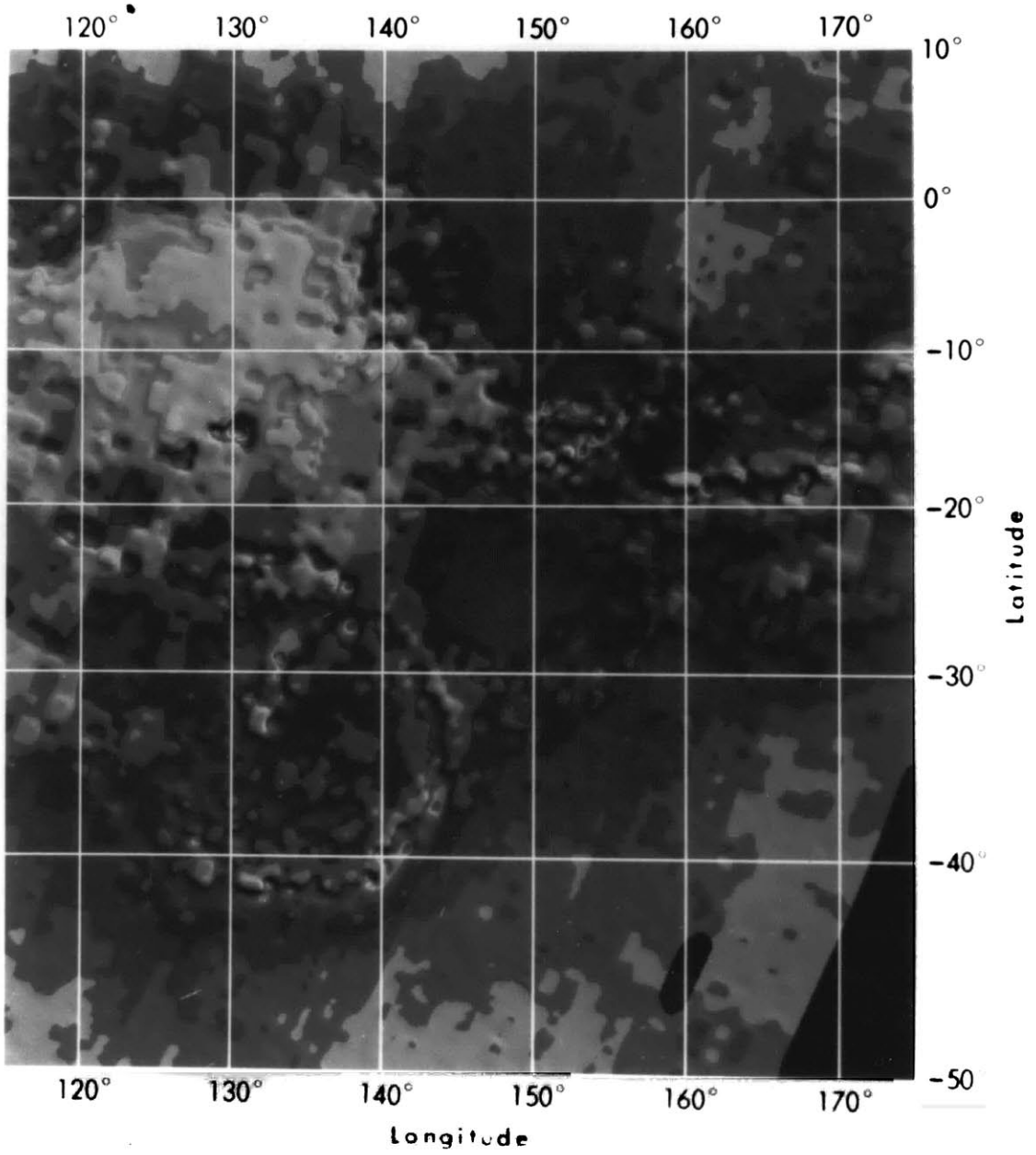

Schaber (1982) has defined a peculiar pitted and hilly topography extending northeastward from the trough ridge complex. The zone has high C factor and centimeter slopes. In this region altimetry coverage is more scarce and some of the highs and lows are defined by only one altimetry footprint. A topographic feature defined by one altimetry footprint could be an anomalous artifact, but many of the pits and hills are produced by paired measurements made in the same orbit or adjacent orbits. Schaber suggests that a continuum may exist between these patched highs and lows, although Schaber and Masursky (1981) call this area a disturbed zone related to the trough and ridge zone. They suggest a common tectonic origin for all.

Beta Regio

Beta Regio was observed to be radar "bright" by Earth based radar prior to the Pioneer Venus mission. Based on these observations Beta Regio was interpreted as being rough on the centimeter scale. Beta Regio is resolvable into two distinct summits lying along a radar bright linear feature. The low average slopes on the flanks of the southern summit, combined with an apparent summit depression, lead Saunders, et al. (1972) to suggest that this feature is a large shield volcano. The Verena 9 and 10 spacecraft obtained measurements of 9, K, and Th, along the eastern flank of Beta indicative of basaltic rock, supporting the volcano hypothesis.

McGill et al.(1982) note that Pioneer Venus topographic data reveal that Beta Regio is much more complex than implied by the shield volcano model. Two summits Rhea Mons and Theia Mons, are visible in topographic maps. The total relief of Beta Regio is about 5km, giving an average flank slope of 0.5°. McGill et al. (1982) note the presence of a series of elongated depressions (2.5 to 0.5 km below the surrounding surface) running the north-south length of Beta Regio. They suggest that the trough that runs 2500km southward through Phoebe Regio is a rift analagous to a continental rift on Earth.

The presence of complex linear depressions in Beta Regio imply a structure more complex than one or two shield volcanos. McGill et al. (1982) cite the presence of rift

features in Beta Regio as evidence for localized tectonic activity, and by analogy with terrestrial rifts, volcanic activity.

The radar properties of Beta imply a smoother surface at meter and centimeter scale than for Maxwell or Aphrodite Terra. Earth based measurements of polarization ratio (Jurgens, et al., 1979, Cambell, et al., 1980) imply that the feature's radar "brightness" may not be entirely due to rocky surfaces, but to differences in intrinsic reflectivity. Pioneer-Venus measurements of C factor reveal substantially less meter-scale roughness for Beta Regio than for Maxwell and Aphrodite, lending support to this hypothesis. Masursky et al., (1980) suggest a "volcanic tectonic" origin for Beta Regio, and note the complexity of the origin by referring to Theia Mons as a "shield-shaped" construct, aligned on a north-south-trending complex of ridges and troughs. This description is broad enough to cover a range of possible origins and given the poor resolution in current data sets more detailed interpretation is difficult.

Figure 25a and b

Detailed topography of Beta Regio showing the twin highs Rhea and Theia Mons and the rifts along the length of the feature.

Figure 25 a and b

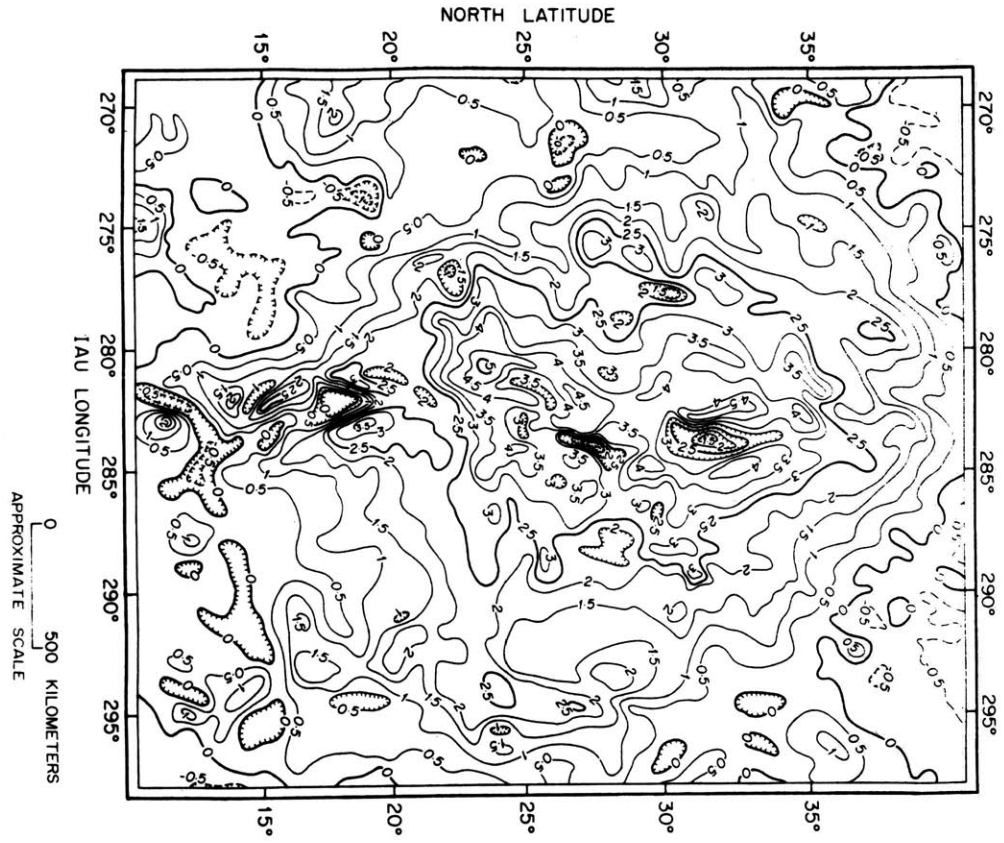

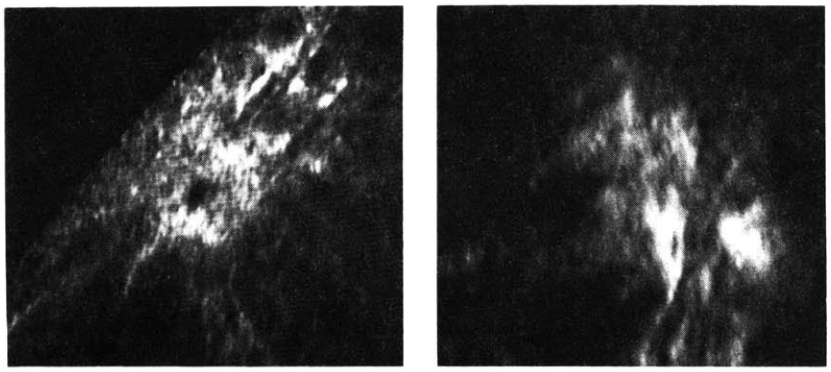

2. Global Reflectivity

As we have seen, use of the Hagfors scattering law allows estimation of ρ_o, and, by inference through the Fresnel relation, ε'. Figure 26 shows the near-global radar reflectivity, smoothed to 100 km resolution, obtained by the radar altimeter.

A globally averaged value of reflectivity of 0.13 ± 0.03 is obtained (weighted by area), with high and low values of 0.4 ± 0.1 and 0.03 ± 0.01, respectively. Pettengill *et al.* (1982) note that diffusely scattering material can reduce the effective reflectivity, by reducing the area effective in specular reflection, and that, as a consequence, the reported values may be somewhat lower than the true values.

Data for selected regions are presented in the form of scatter plots of ρ_o *vs.* $[\alpha=(C)^{-1/2}]$, to see if the scatter in the observations exceed the estimated statistical formal errors. The diagrams can confirm correlations between the estimated parameters, and the location of the centroid of the data points can categorize the surface in terms of gross radar scattering properties. Figure 27 shows a scatter diagram for a portion of Sedna Planitia, a fairly typical region representative of the Venus lowlands, and the rolling uplands as well. The large variation in α (greater than the formal measurement error) suggests a real variation over the area. In agreement with this explanation, no significant correlation between ρ_o and α is seen. The formal correlation between the two parameters is typically about

0.75, but the effect of this correlation is lost in the scatter plot, presumably because of the large intrinsic range of α found in this region.

Sedna Planitia has a dielectric constant of $\varepsilon' \cong 5$, a value commonly measured for dry rock. By comparison, the porous lunar surface has a dielectric constant of about 2.7 (Pettengill, 1978). The lowest value of ρ_o found on Venus (0.03; $\varepsilon' = 2.0$), requires a surface material density on the order of 1 g/cm^3. Only highly porous material will produce dielectric constants this low. A multilayer reflection can not produce a reflectivity as low as 0.03 if there is a lower layer of typical Venus reflectivity accessible to the penetrating radar waves.

Theia Mons, the southern mountain in the Beta Regio area, is one of the most reflective portions of the Venus surface. Theia is bright in Earth-based radar images, but does not display remarkably high α. All of the other areas exhibiting meter-scale roughness, also appear bright in Earth-based images and Pioneer Venus sidelooking images, except for Theia Mons. The scatter in α observed on Theia is about 1.7°, with a near centroid of $\rho o = 0.28 \pm 0.07$, and $\alpha = 5.3° \pm 1°$. The individual points have typical formal errors of 0.06 in ρ and 1° in α. The formal correlation in Theia is 0.92, but the scatter diagram shows more intrinsic variability in α.

The average value of ε' over Theia is 11 ± 4, with a high of 20. As we will see, the only known mechanisms for

Figure 26

Global map of reflectivity of Venus.

Figure 26

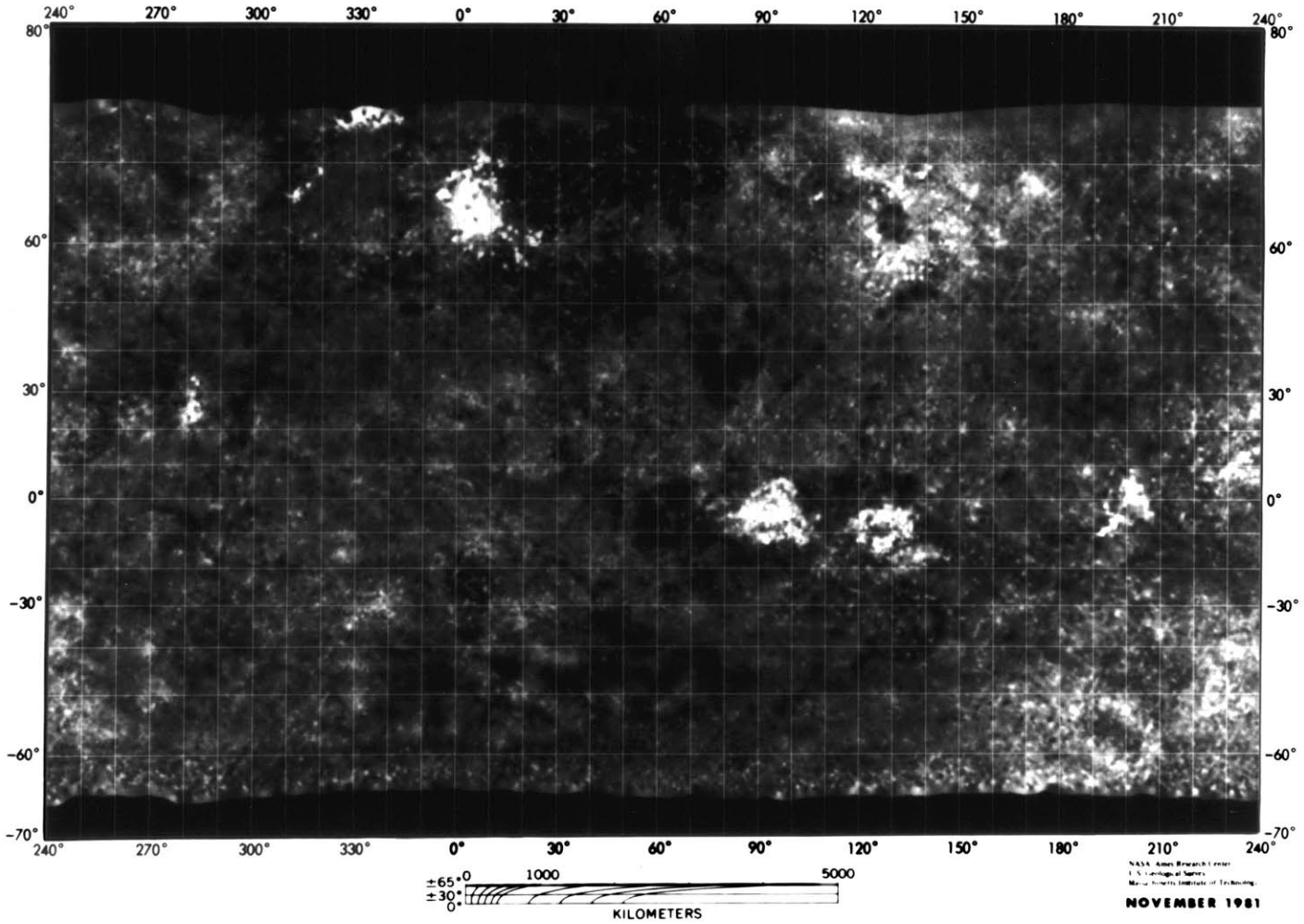

VENUS REFLECTIVITY

Figure 27

Scatter plots of reflectivity versus roughness for Sedna Planitia and Theia Mons.

Figure 27

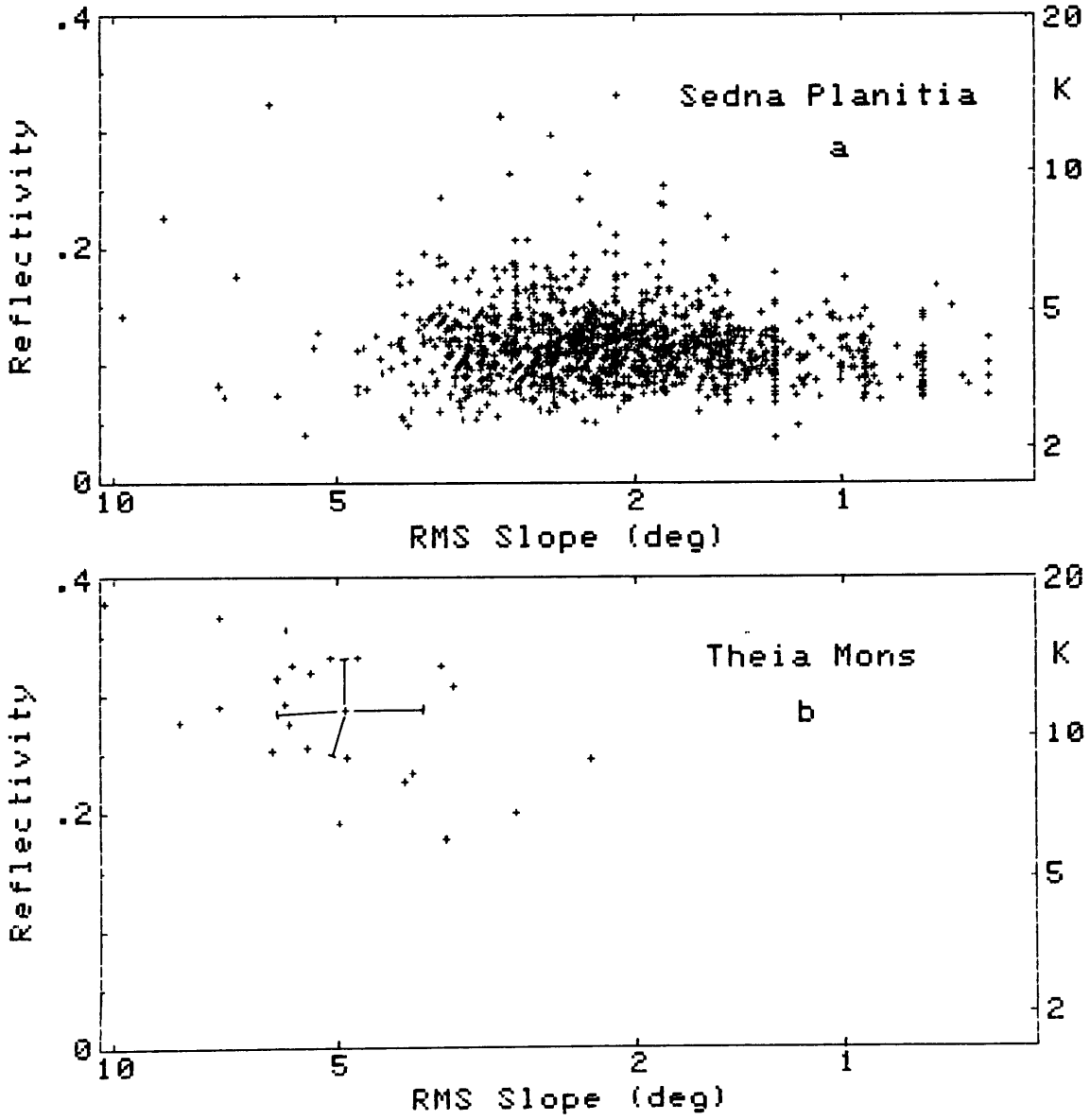
Sedna Planitia
a
Reflectivity
.4
.2
0
10
5
2
1
RMS Slope (deg)
20
K
10
5
2
Theia Mons
b
Reflectivity
.4
.2
0
10
5
2
1
RMS Slope (deg)
20
K
10
5
2

producing such high apparent dielectric constants is the inclusion in the rock volume of a highly polarized substance like water, or by inclusions of conducting material.

E. Dielectric Properties of Materials

1. Previous Work

The dielectric constant is the chief radar-measurable quantity that can tell us about the composition of a material. A study of dielectric constants of relevant geological materials was conducted by Campbell and Ulrichs (1969), which is highly relevant to Venus, since it was conducted using dry terrestrial rocks. The surface of Venus (at ~740K) can safely be assumed to be dry. In fact, Venus and the Moon are probably the best candidates around for radar identification of surface material since Earth and Mars both possess water in various states on or near the surface. The possible presence of water on those surfaces in liquid or hydrated form renders difficult a geochemical inference from a measurement of dielectric constant.

No measurements of dielectric constants for geological materials exist for the specific frequency employed by ORAD (1.76 GHz), but the measurements of Campbell and Ulrichs span the range 450 MHz to 35 GHz, representing the extremes of the frequency band employed in radar astronomy.

Dry silicate rocks exhibit no sharp resonances in this range (Von Hippel, 1954, 1957), and exhibit noticeable losses only at high (10,000GHz) frequencies near the infrared range. The samples measured by Campbell and

Ulrichs were dried at 200°C in a vacuum oven for two days, and measured in a re-entrant cavity calibrated using materials of known and accepted dielectric constant. The following table gives a summary of results measured for solid rocks.

Table 8

Campbell and Ulrichs (1969)

Average Properties of Rocks at 450 MHz and 35 GHz

Rock	Source	450 MHz		35 GHz	
		ε'	tan δ	ε'	tan δ
andesite, hornblende	Mt. Shasta, CA	5.1	0.004	5.0	0.014
anorthosite	Essex County, NY	6.8	0.008	6	0.016
basalt	Lintz, Rhenish-Prussia, Germany	8.9	0.018	9.2	0.09
basalt	Somerset County, NJ	8.0	0.03	8.6	0.07
basalt, amygdaloidal	Keweenaw County, MI	7.2	0.014	7.6	0.023
basalt, hornblende	Chaffee County, CO	6.7	0.013	6.5	0.04
basalt, leucite-nepheline tephrite	Laacher See, Germany	6.5	0.0103	5.3	0.023
basalt, olivine	Jefferson County, CO	8.1	0.017	8.0	0.09
basalt porphyry, olivine	Boulder, CO	8.2	0.016	8.1	0.06
basalt, tholeiitic	Columbia River, NE of Madras, OR	9.6	0.09	8.0	0.112
basalt, vesicular	Chaffee County, CO	7	0.017	5.3	0.04
gabbro, bytownite	Duluth, MN	7	0.02	7	0.018
granite, alkali	Quincy, MA	5.2	0.034	5.3	0.023
granite, aplite	Boulder County, CO	5.2	0.019	4.9	0.009
granite, biotite	Westerly, RI	6	0.02	5.7	0.05
granite, biotite	Llano, TX	5.4	0.007	5.5	0.015
granite, graphic	Auburn, ME	5.0	0.004	5.0	0.008

ε' = real part of dielectric constant
tan δ = loss tangent, the ratio of the imaginary and real parts of the dielectric constant

Table 8 (continued)

Campbell and Ulrichs (1969)

Average Properties of Rocks at 450 MHz and 35 GHz

Rock	Source	450 MHz		35 GHz	
		ε'	tan δ	ε'	tan δ
granite, hornblende	Rockport, MA	6	0.010	5.2	0.01
granite, porphyritic biotite	St. Cloud, MN	5.5	0.011	5.6	0.02
obsidian	Lake County, OR	6.8	0.13	5.6	0.05
obsidian	Newberry Caldera, OR	5.5	0.0134	5.4	0.0381
peridotite, mica	Tompkins County, NY	6.0	0.034	5.3	0.034
peridotite, oliviune (dunite)	Jackson County, NC	6.2	0.01	6.1	0.02
peridotite changing to serpentine	Lowell, VT	7.5	0.008	7.6	0.011
phonolite	Beacon Hill, near				
pumice	Millard County, UT	2.5	0.007	2.4	0.02
rhyolite	Castle Rock, CO	3.38	0.015	3.41	0.007
serpentine	Cardiff, MD	6.4	0.011	6.4	0.04
serpentine	Rogue River, NW of Grant's Pass, OR	7	0.019	6.4	0.06
syenite, augite (larvikite)	Larvik, Norway	8	0.05	6.7	0.2
trachyte	Mineral Hill, near Cripple Creek, CO	5	0.026	5.43	0.025
tuff, grey	near Cripple Creek, CO	6.1	0.06	5.4	0.07
tuff, rhyolitic	Ennis, MT	3.6	0.006	3.4	0.02
tuff, semi-welded	Bend Quarry, OR	2.6	0.011	2.6	0.03
volcanic ash	Chaffee County, CO	3.4	0.07	2.84	0.014
volcanic ash shale	near Florisant, CO	2.7	0.03	2.6	0.015

The effects of temperature on dielectric constant for five types of solid terrestrial rocks were determined. At ambient Venus surface temperatures, a slight rise in ε' (~10%) is noted. The table of dielectric constants for solid rocks indicate a correlation between increasing bulk density and increased dielectric constant. The presence of non-solid rocks, i.e., powder or regolith, will lower the effective dielectric constant. Since planetary surfaces will have regoliths produced by weathering, the dielectric constants of powders are also of great interest to us.

Studies of dielectric properties of powdered rocks, also by Campbell and Ulrichs (1968), Rayleigh (1892), and Krotikov and Troitsky (1963), note that powdering of rocks completely masks the differences between granite and basalts. These workers show that almost all dry powdered rocks of density approximately 1 g/cm^3 have effective dielectric constants very close to 2-2.5.

Krotikov notes that the effective dielectric constant is a regular function of density, for dry powdered rocks, quoting a relationship for density of $(\varepsilon-1)/0.5$. To summarize, dielectric constants of 3.5 or less are indicative of powdered materials, and the effect of powdering and the porosity is far more important than any compositional variation, save for the addition of free iron. Rocks ranging from granite to ultramafic when powdered to 1 g/cm^3 show a quite narrow range of dielectric constant (at 450MHz) of 1.9-2.2. Solid rocks exhibit a range of

dielectric constant from 4 to 10, with metal-rich tholeitic basalt the highest.

The effect of moisture on dielectric properties of rocks is variable. Baldwin (1958), Von Ebert and Langhammer (1981), and McCafferty and Zehlemayer (1971), observed that a monolayer of water adsorbed onto a dielectric surface does not alter the dielectric constant of the bulk material. Beyond about seven layers, free pore water begins to form and pore fluid conduction begins to dominate the electrical properties. Since liquid water in pore spaces is unlikely on Venus, this effect should not be important.

Several groups have investigated the effects of pressure on electrical properties. Dvorak (1973), Dvorak and Schloessin (1973), Duba et al. (1974) and others have investigated the pressure effects in dry rocks, reporting no change in electrical properties for dry rocks up to 8KB.

The geophysical literature contains extensive references to dielectric properties of rocks at frequencies ranging from 10 to 10^6 Hz. These are reviewed by Olhoeft (1982). The data indicate little frequency dependence in the radar (1GHz) range, although a variety of behavior is observed in the lower range 100Hz→10^6Hz. Many of these effects can be attributed to the presence of water, and the pore and crack structure of the rocks. Katsube and Collett (1982) give a concise review of the electromagnetic properties of rocks, at frequencies up to $2x10^8$Hz, frequencies which approach those employed by radar. They

report on the effect of factors such as grain boundaries, moisture, porosity, mineral content, conductive inclusions, and surface and electrode polarization effects.

The presence of conductive minerals, the chemical composition of the individual mineral grains, and the liquid content of pores are the primary factors that determine electrical properties. Katsube and Collett (1973) report that conductive minerals will cause large effects on the bulk dielectric constant of rocks. They claim that conductive mineral content must exceed 10% to be noticeable. This result is confirmed by measurements of meteorites reported by Campbell and Ulrichs, although they do not specify the metallic content of their specimens.

Electrical Properties of Meteorites at 450MHz

Meteorite	Type	ε'	Tan δ
Bonita Springs	H5	43-81	0.13-0.19
Burderheim	L5	9.0-11.9	0.035-0.048
Colby	L5	10.6-11.8	0.045-0.054
Forest City	H5	16-33	0.11-0.22
Holbrook	L5	7.8	0.015
Indarch	E4	130-150	0.065-0.117

Since H chondrites have appreciable Fe-Ni content, conducting paths allow a substantial loss. In the powdered state, the conducting paths in the metallic grains are no longer important, and the electrical conduction is not significant.

Experimental Results

The measurements of meteorites by Campbell and Urlichs indicate that conductive inclusions (FeNi) present in the samples raise the effective dielectric constant. Yet, free metals are not a likely component of the differentiated rocks thought to be present on Venus, if Venus has undergone core formation similar to what occurred on Earth. Sulfides (pyrite, chalcopyrite) have been previously suggested as a geological source for the sulfur in the Venus clouds, and are also conductive. The measurement of the electrical properties of sulfide-bearing rocks is, therefore, obviously most germaine to Venus.

Peacock (1981 M.S. Thesis) obtained samples of volcanic and metamorphic rocks with sulfide inclusions. His samples were selected for electrical analysis in this thesis beacuse of the work already performed to determine their sulfide content. The samples were selected because metamorphic rocks were the most accessible sulfide-rich samples. The two most sulfide-rich samples were selected for this study. These samples 80-70 J and 80-70 K were obtained from a rock cut exposed on the north side of the new Berlin (New Hampshire) High School. The samples were metamorphosed volcanic rocks, although disseminated sulphides can occur in primary volcanic rocks. The other minerals contained were plagioclase, biotite, chlorite, with minor contributions from magnetite and anthophyllite.

Three other samples of a high grade sulfide ore were

also obtained that originated from Sudbury, Ontario, a region of extensive sulfide deposit. The precise geologic setting was unknown. The region contains extensive intrusive and extrusive igneous rocks, and metamorphic rocks of varying grade.

The volume percent of the various sulfides was determined by reflected-light point count.

Sample	FeS_2	Fe_xS_{1-x}	$CuFeS_2$
1 (80-70 J)	5%	2%	<0.2%
2 (80-70 K)	4%	4%	2%
3 Sudbury	45%	<5%	45%
4 Sudbury	20%	<2%	<25%
5 Sudbury	40%	<5%	40%

The samples were cut into hollow core cylinders and measured by the traveling wave method described by Von Hippel (1954). The measurements reported are means of measurements at two orientations (see Appendix C) and were made at room temperature.

Sample 1	1 Ghz	1.7 Ghz
$\varepsilon'/\varepsilon_o$	21±4	14.7±0.2
$\varepsilon''/\varepsilon_o$	29±7	23±10
Tan δ	1.38±0.04	1.5±0.5
σ(mho/cm)	0.017±0.003	0.021±0.009

σ = conductivity

Sample 2

$\varepsilon'/\varepsilon_o$	20±6.5	15.9±0.5
$\varepsilon''/\varepsilon_o$	6.2±0.6	6.4±0.1
Tan δ	0.35±0.14	0.4±0.02
σ	0.0035±0.0004	0.0060±0.0001

Samples 3, 4, and 5 were too conductive to allow determination of ε' and tan δ. The conductivity ranged from 30 to 7500 mho/cm.

The presence of sulfides in the silicate does raise the effective dielectric constant to the range observed for Theia Mons. In fact, the ore-grade samples have so many conducting paths they do not behave as dielectrics. Sample 5 has a bulk conductivity only 10^{-4} that of copper.

The dielectric properties of these samples are actually complicated by the size, shape, and density distribution of the conductive inclusions.

In order to study further the effect of sample inhomogeneity, sample 1 was cut into 5 roughly equal-sized disks each 1.8mm thick, and each disk was measured at two frequencies. The results are shown on the next page.

1Ghz

Sample	ε'	tanδ
1-1	20.314	0.270
1-2	25.475	1.245
1-3	21.181	1.162
1-4	15.713	0.129
1-5	15.669	1.473
mean =	19.670	0.856
standard deviation =	4.125	0.612

1.685 Ghz

Sample	ε'	tanδ
1-1	19.712	0.292
1-2	21.567	0.362
1-3	23.541	0.509
1-4	24.025	0.286
1-5	20.541	0.483
mean =	21.877	0.386
standard deviation =	1.868	0.094

It is clear that frequency of measurement, sample size and the distribution, shape and size of the conductive inclusions all effect values of dielectric constant and loss tangent. The errors caused by inhomogeneity in the sample and the effect of frequency variation are still less than the range of values for reflectivity actually measured by ORAD.

F. Conclusions and Directions for Future Work

The sulfide-bearing rocks measured initially probably have geological histories totally different from any rocks likely to be found in the summit of Theia Mons. It is not possible to distinguish the petrology of any silicate-conductor mixture on the basis of ORAD data; ORAD data will only allow a suggestion that such mixtures are present on the surface. The possible existence of sulfides on Venus as alteration products or as primary minerals was investigated in section 1, where it was seen that pyrite may exist as an alteration product in soil, coexisting with sulfates under a restricted oxygen fugacity (Barsakov, 1980; Lewis and Kreimdendahl, 1980), or as a primary mineral possibly produced by reduction of sulfates produced by reaction of calcic minerals with sulfur dioxide present in the lower atmosphere. Based on currently available data neither case can be excluded.

Sulfides (pyrite, pyrotite, chalcopyrite) have widespread terrestrial occurrence. They occur as primary minerals in igneous rocks, and contact metamorphic rocks, as well as large hydrothermal veins. Sulfide concentration in ordinary basalts is generally low (<0.1% wt.), but high (>5% wt.) concentrations have been observed in the Skaergarrel Intrusion and are though to be of magmatic origin (Deer, Howie and Zussman, 1979), crystallized from an immiscible sulfide liquid associated with a gabbroic silicate liquid. A similar origin is postulated for the Sudbury deposits.

The Samples #3,4, and 5 all originated in the Sudbury complex of Ontario, a region of extensive sulfide deposit. The region is the site of extensive igneous activity with an extremely complex geology. The complex is bowl shaped, with layers of igneous intrusives layered with micropegmatites, gneiss, tuff, and quartzite. Sulfides are found in a contact layer between norite and a micropegmatite layer. Recent evidence even suggests an impact origin for the structure (Boldt, 1967).

Hawley (1962) suggested that massive sulfide deposits could form in cooling of intrusive igneous rocks. Sulfides do occur widely associated with norite and peridotite. The common and close association of sulfide minerals on Earth with rocks of this type suggests that sulfides could be a component of the rock, brought up from depth. A scenario is given by Boldt (1967) and Hawley (1962). They suggest that the sulfides formed from an immiscible liquid which settled to the bottom of the residual silicate liquid left after crystallization of norite. After the norite or the lower portion of it solidified, the whole mass was deformed and the sulfides found their way into fractured zones. This scenario appears to satisfy the gross aspects of the geology of the Sudbury district. The best that can be said for Venus is that, based on Earth analogy, Theia Mons could be an area of sulfide deposit produced by magmatic activity, since almost all large scale, non-hydrothermal, terrestrial sulfides are associated with mafic or ultramafic rocks.

Future work on the electrical properties of Theia Mons must seek to constrain the possible substances contributing to the high effective dielectric constant, like magnetite. Many more samples of sulfide bearing rock must be measured to sort out the effect of rock fabric and mineral grain size, shape, and orientation, on the bulk electrical properties. Measurements must also be conducted at Venus surface temperatures.

Future high resolution radar studies of Venus must take into account the possible presence of highly reflective areas on the surface like Theia Mons. Only high resolution imagery of Theia Mons will confirm the association of highly reflective areas with possible volcanic activity on Venus, by identifying other geological features indicative of volcanism.

IV. Aeolian Transport on Venus

A. Previous Theoretical Studies

Wind may be a dominant mechanism of surface modification on Venus, since Venus lacks running water. Wind transport and wind erosion will be controlled by the spectrum of atmospheric velocity near the surface, and the types of particulate material available on the surface. Wind erosion occurs when the wind force exterted on a particle is great enough to overcome drag and inertia of the particles. The basic theory for this problem was first studied by Bagnold (1941). He defined a critical parameter; the threshold shear velocity

$$U^*t = A\left(\frac{\rho p - \rho a}{\rho a} g\, D\right)^{1/2} \qquad U^*t = (\tau/\rho_a)^{1/2}$$

where A is a threshold parameter similar to a drag coefficient, g is the local gravitational acceleration, D is the particle diameter, ρa is the atmospheric density, ρp is the particle density, and τ is the bed sheer stress. If the surface wind velocity exceeds this threshold velocity particles of a certain size will be set into motion.

A is generally a function of the Reyolds number of the particle A = A(Re)

$$Re = \frac{U^*D\rho}{\mu}$$

where μ is the dynamic viscosity of the fluid. Various

workers (Iverson et al., 1982) have attempted to relate A and Re through experimental data. Application to Venus transport would seem to require experimental data under Venus conditions of temperature, pressures, wind velocity, and viscosity.

Sagan (1975) interpolated data on mineral grains in the terrestrial atmosphere and mineral grains in water to obtain a relation A = A(Re) and a relation of U* to grain diameter D. These calculations ignore such cohesive forces as Van der Waals attraction which are difficult to estimate accurately for Venus.

Using the interpolation, Sagan (1975) finds a threshold shear velocity of 1-2 cm/sec on Venus. This is not necessary equivalent to the minimum free stream wind velocity above the surface required to initiate sediment motion. This velocity must be extracted from a shear velocity by an estimate of the velocity profile through the surface boundary layer. Wind velocities near the Venus surface were determined by tracking the descent of the Pioneer Venus and Venera spacecraft. Wind velocities were also measured in situ by anemometers affixed to the Venera 9 and 10 spacecraft. Wind velocities at the Venera 9 site ranged from 0.4 to 0.7 m/sec and 0.8-1.3 m/sec at the Venera 10 site (Keldish, 1977).

The descent of the Pioneer Venus probes was monitored by differential long baseline interferometery by Counselman et al. (1980). The three dimensional velocity vector of

each probe was determined. Counselman et al. argue that the probe velocity will match the wind velocity to 1 m/sec in the Venus lower atmosphere. A westward wind velocity of 1 m/sec is considered reasonable at the surface. The wind velocity increases with altitude to about 5 m/sec at 10 km altitude.

B. Types of Aeolian Features

Wind ripples are a common result of terrestrial sediment transport, and have been observed on Mars. The study of ripples and other sedimentary features in a controlled laboratory environment has been carried out by numerous workers, (Sharp, 1963, Bagnold, 1954). Greeley (1981) has attempted to study wind ripples in a high pressure CO_2 environment similar to Venus, however no results are available at this time.

Sand movement in wind occurs by three modes: saltation, suspension, and surface creep. Sand transported in saltation moves in jumps over the sediment surface, typically traveling downwind tens to thousands of grain diameters, while rising tens of hundreds grain diameters. Fine particles moving in suspension rarely contacts the bed, while sand moving by surface creep is pushed along the bed surface.

Wind ripples are observed for most terrestrial sand particle sizes. There is no known upper limit of grain diameter for the formation of ripples. Nor do ripples form

under every wind regime. Strong winds will produce flat bed transport, and no ripples. The type of sand sorting can also affect ripple formation, and high density particles can inhibit ripple formations.

Bagnold (1954) made extensive study of wind ripples, and noted five factors which govern ripple height and slope:

1) speed of the wind which promotes saltation;
2) saltation which moves the surface creep;
3) surface grains which move horizontally and vertically according to individual size, density and shape;
4) surface relief which causes spatial variation in the ejection rates of grains and the sand surface; and,
5) state of the sand flux: steady, erosional, or depositional.

C. Scaling Theory

If one postulates the existence of an closed duct open at the ends on the surface of Venus in which sediment transport may be produced, an attempt may be made to define what conditions must be produced in a similar tunnel on Earth such that sediment transport may be exactly scale modeled. Transport of sediment by steady uniform flow in a wide rectangular wind tunnel should be governed by the following variables: duct length, height and width, mean flow velocity U, fluid density ρ, fluid viscosity, μ, sediment size D, sediment density ρs, and acceleration

gravity g. These variables only describe the fluid dynamic properties of the system, not electrostatic forces acting on the sediment grains, or elastic properties, or effects of the tunnel walls. These may or may not be of negligible importance, but are here after ignored. The variables mentioned should describe viscous and pressure forces. and gravity forces on the particles. This set of independent variables is complete: all measures of flow and sediment transport like boundary resistance, pressure gradient, turbulence structure, sediment transport rate, and vertical distribution of sediment are described uniquely.

Four dimensionless variables may be used to characterize the system. One set suggested by Walker (1981) is

$$\rho UD/\mu,\ \rho^2 g D^3/\mu^2,\ L/D,\ \rho_s/\rho$$

The first and second variable are the Reynold's number and the Froude number multiplied by the square of the Reynold's number, respectively. The third variable is the aspect ratio of the tunnel, and the fourth parameter is the ratio of sediment to fluid density. Other equilvalent sets may be produced by rearranging these variables or dividing and multiplying them in different order.

The condition for a dynamic scale model requires that

these parameters be equal for both systems. That is:

$$\frac{\rho r\ Ur\ Dr}{\mu r} = 1; \quad \frac{\rho^2 r\ g_r\ Dr^3}{\mu^2 r} = 1; \quad \frac{Lr}{Dr} = 1; \quad \frac{(\rho_s)r}{\rho r} = 1$$

where r subscript denotes a ratio of two quantities (Venus and Earth).

The particle scale ratio can be expressed as:

$$Dr = \left(\frac{\mu^2 r}{gr\rho^2 r}\right)^{1/3}$$

For pure CO_2 viscosity is a function of temperature approximated by

$$\mu \simeq 1.46 \times 10^{-4}\ (T/300)^{0.95} \text{ poise (Sagan, 1975)}$$

For a surface temperature of 740K the viscosity ratio $\mu_r = 1.9$. Furthermore, we know $g_r = 0.89$ and $\rho_r = 55$, so Dr = 0.11. So a particle on Earth will be 10 times larger than its Venus counterpart.

The ρs ratio = 55 also, so to model materials with densities between 2 and 3 g/cm^3 (i.e. quartz sand $\rho = 2.64\ g/cm^3$) a particle must have a density of about 0.05 g/cm^3. The wind velocity ratio is found directly from the Reynold's number

$$U_r = \mu_r/\rho_r D_r \simeq 0.3\ (D_r = L_r)$$

so the Venus speed is ~ 1/3 that of the Earth model. The problem of modeling aeolian transport on Venus is then reduced to finding the appropriate sediment material. A

Venus surface wind velocity of 1 m/sec (consistent with Pioneer Venus and Venera data) would be scale modeled in our terrestrial tunnel by a wind velocity of roughly 3 m/sec.

1. Other Fluid Dynamical Considerations

The Wall Law

A fluid undergoing steady turbulent flow over a rough surface has a characteristic logarithmic mean-velocity profile given by

$$\frac{U(z)}{U^*} = C\,\mathrm{Ln}\,(z/K) + V$$

where

- $U(z)$ = mean velocity at height z
- C = inverse of von Karman's constant (0.375 for sand transporting flows)
- z = height above the sediment bed
- K = variable length scale related to physical roughness.
- V = constant of integration

If we want to find U^* we may measure the profile $U(z)$ at several different values of z, and fit a line to the data, U^* C is the slope, and V is the intercept. The variable length scale K comes out as a constant whose value is reflected by the intercepts.

2. Experimental Methods

The principle equipment used in this study was a thirty meter long wind tunnel (Walker M.S. thesis). The tunnel was a suction type (see Figure 31.3), and had to be long enough for the full development of the velocity profile and sediment transport. The tunnel was also designed to be wide enough to study ripple patterns, and have easy access to the working section. The tunnel is 30 m long, 1.2 m wide, and 0.6 m high, with a 2.4 m cubical collection chamber and for support.

The walls of the last 5 m of the tunnel are plexiglass, which provides a test section for observations and photography. The fan is a 42" diameter tube-axial type. The flow velocity is adjusted by a movable wall in front of the fan. The wall is also raised and lowered by a hand crank, and two adjustable vents were placed in the collection box for five adjustments.

Velocity measurements were made using a pitot static tube connected to an inclined-tube manometer. The pitot tube has a bore diameter of 0.1 mm, and the alcohol filled manometer has a slope of 20 to 1. The manometer level may be read to ± 1 mm, or about 0.05 m/sec in velocity. The response time is on the order of 60 sec.

Since the displacement is a function of the square of the velocity, accuracy is higher at higher velocities. The pitot-static tube was mounted to a 2.5 cm x 10 cm x 100 cm rounded staff that may be raised and lowered into the flow.

Figure 28

Physical description of the wind tunnel used to study aeolian transport on Venus.

WIND TUNNEL

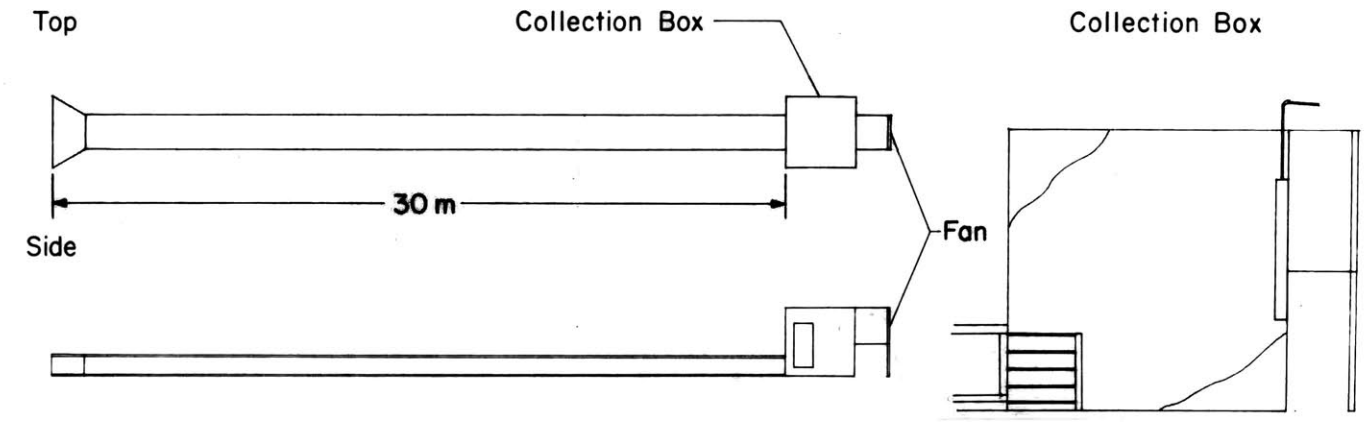

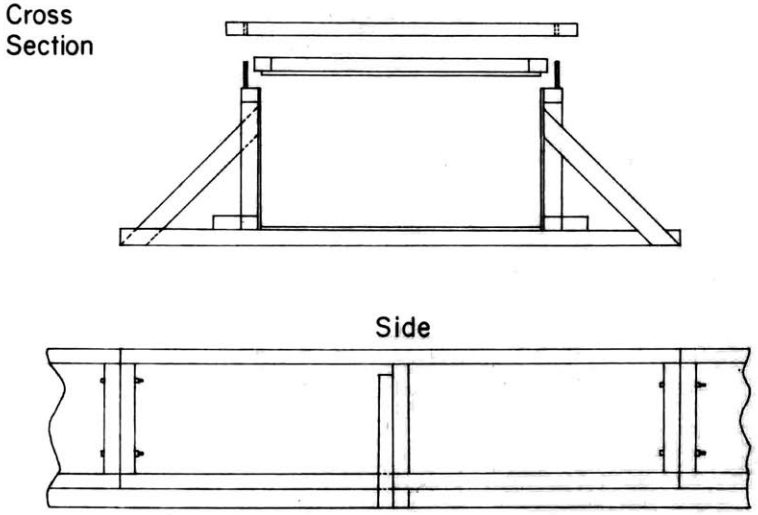

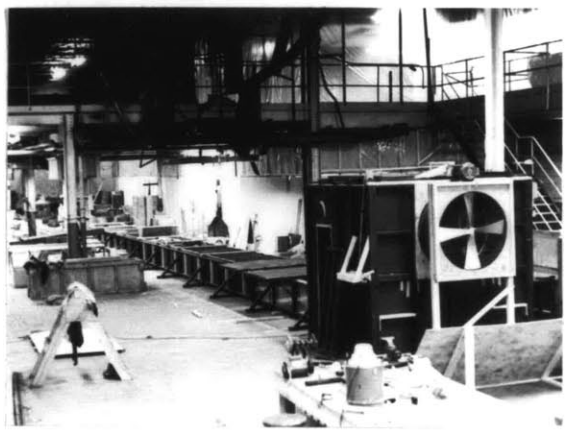

Figure 28

Tunnel Flow Characteristics

The flow in the tunnel is fully developed turbulent duct flow at 5 m distance from the entrance. Flow straighteners (100 cm length of paper tubing) were installed just upstream of the entrance and produced an acceptable two-dimensional flow near the tunnel centerline. There exists secondary circulations in the tunnel, and these were reduced by installation of two horizontal plates 2 cm long, placed 15 cm above the bed and below the roof, upwind from the sand bed.

Experimental Results

The sediment used in the Venus simulation consisted of 3 mm diameter styrofoam beads with an average density of 0.1 ± 0.02 g/cm^3. This density was obtained by weighing twenty beads and measuring their physical dimensions with a micrometer. The beads exhibited noticeable electrostatic attraction to the plexiglass walls of the tunnel at the observation area, but showed no attraction to each other. The air in the laboratory was quite damp, and the beads felt damp to the touch, accounting for their relatively low static potential.

The wind was turned on and the velocity increased until a few beads began to crawl with about 1 grain/100 cm^2 moving. The velocity profile measured at that velocity is given.

h (cm)	$\vec{U}$ m/sec
20	2.09
15	2.00
10	1.92
7.5	1.49
5	1.24
3	1.16
1	-

A linear least squares fit of LnH vs. U gives

$$U = (44.67)\text{Lnh} + 78.06$$

with a correlation coefficient r = 0.986.

No ripples or sedimentary structures were observed up to high wind velocity (~3 m/sec). The transport was quite vigorous with noticeable saltation observable near the bed.

Th U* determined is 16.75 m/sec, while the bed shear stress determined

$$\tau = U^{*2}\rho = 0.05 \text{ dynes/cm}^2$$

for the Venus case

$$U^* \cong 6 \text{ cm/sec and } \tilde{\tau} = 3 \text{ dynes/cm}^2$$

These threshold velocities are higher than those predicted by Sagan (1975) and Greeley (1980) (1-2 cm/sec), but are different by a factor of three. Since the scale only applies for one particle size, (~3/10 mm) smaller particles may also be transported.

Iversen et al. (1982) report a value of 4 cm/sec threshold velocity for 0.3 mm particles on Venus. The actual Venus wind transport will be affected by other surface properties. Local roughness and boulder and block distribution will produce local turbulance, eddies, and vertical motion which can lift particulate matter into a wind stream.

The scale model must also simulate the dynamics of particle interaction to be valid. As indicated previously electrostatic forces between the grains were negligible. An experiment was undertaken to compare the elastic properties of the beads with the elastic properties of quartz grains. Elasticity was determined by measuring the fraction of kinetic energy in a bead which appeared as potential energy after the bead bounces off a styrofoam surface. Terminal velocity was determined by measuring the time the bead required to fall 1 meter and 0.5 meter. Twenty measurements at 1 m yielded 1.12 m/sec ± 0.13 m/sec and twenty measurements at 0.5 meter yielded a terminal velocity of 1.07±0.15 m/sec, fairly good agreement with the first case.

The rebound height was measured by letting the bead bounce off of a styrofoam sheet, and was photographed. The rebound height and direction was not uniform, as it depended on the exact shape of the grain. The highest rebound observed was 2 cm, which yields a range of rebound coefficients

$$\frac{h_{obs}}{\frac{V^2}{2g}} = 0.3\text{-}0.5 \ .$$

A second experiment was performed using quartz grains of 1-3 mm diameter, removed from a quartz conglomerate. Following the same procedure, except substituting a flat glass plate for the styrofoam block yielded 0.5-0.8 rebound coefficient.

These measurements do not take air resistance on the rebound into effect, nevertheless the elastic properties of the styrofoam beads are not extremely different from those of quartz, suggesting that elastic effects should not be greatly important in interpreting the dynamic scale model results.

The reflectivity measurements reveal that portions of the surface are covered by low density materials, but most of the surface reflectivity is closer to that of rocks with low porosity. Terrestrial wind blown sediments generally have a bulk density of about 2.0 g/cm^3, and 30% porosity. Wind blown sediments do not form a continuous layer over the entire planet, but they could form patches.

Wind blown sediments can also be chemically cemented, and this may not be distinguishable by reflectivity. Warner (1980) has suggested that a layer of wind blown, now cemented sediments may cover the surface of Venus at lower elevations. The smooth-flowed, low lying basins may be covered by sedimentary rocks, not basaltic lavas as on the Moon.

The absence of ripples at the scale of the simulation (1/10 m) does not mean that ripples are absent on Venus,

they may simply be larger. The scale of ripples would be determined by the saltation trajectory of the grains. Saltation trajectories observed were short, on the order of 1-2 cm, an order of magnitude lower than seen in sand on Earth.

At the ORAD radar wavelength (17 cm), ripples and dunes larger than our wind tunnel would enlarge the probability of specular reflections. Warner has speculated that the planet-wide zonal winds with consistent west-to-east velocities may produce dunes over the planet with a similar orientation. However, large scale topography may affect this pattern.

The wind tunnel experiment could be improved by obtaining a range of sediment particles with varying diameters and a closer match to the actual density ratio. The scaling might be improved by also changing the gas density by use of a heavy gas (Freon) in a recirculating wind tunnel. This will allow a better match to the observed density ratio and allow a better experimental determination of threshold shear velocity as a function of grain diameter. A larger tunnel would also aid in the study of possible bed forms.

Figure 29

Photographs of dynamical scale model experiment of Aeolian transport.

Figure 29

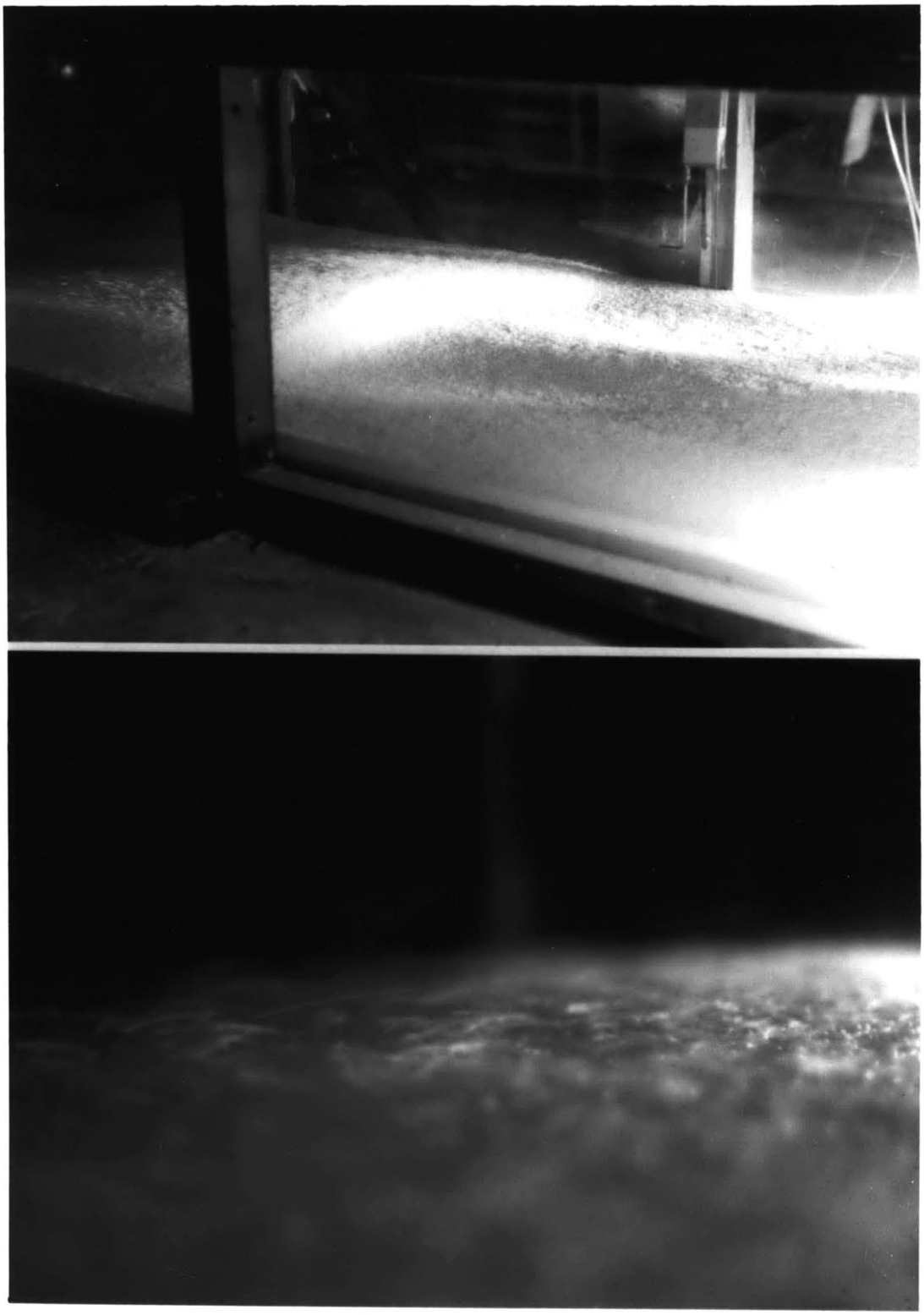

D. Conclusions and Directions for Future Work

Venus research is an open-ended problem and this thesis has only touched the surface of that problem. When dealing with a complex planet and a sparse data set gaps are unavoidable but the path for future investigations may be illuminated.

The most significant result of this work is an inference as to the surface composition at the summit of Theia Mons using radar techniques, the best inference available to date for any planetary surface examined by radar. The connection between this inference (sulfide minerals) and atmosphere-surface interaction is tantalizing.

Research to address the remaining questions about the physical and chemical nature of the Venus surface must take several directions. The chemical interaction of sulfuer bearing gasses and surface minerals needs direct experimental investigation so as to constrain the types of chemical weathering processes ocurring on the surface, and the reasonable modes of occurrence for sulfide minerals.

This knowledge can be gained by improving the reliability and accuracy of in-situ measurements of the chemical composition at the surface atmosphere boundary. It is likely that these problems will be addressed by Soviet workers since Venus surface landers are not planned by the American space program in this century.

Remote sensing of the Venus surface can take several directions. Further analysis of the Pioneer Venus

radiometers data will allow a better constriant on surface reflectivity with less dependence on modeling the surface scattering of radar waves. Radiometric data may also be obtained by ground based observations, and such observations can further constrain the reflective and emissive properties of the surface.

Significant improvement in knowledge of the surface will come about through the acquisition of high quality images by an orbiting spacecraft. Such information will allow an improved understanding of the tectonic and morphological processes shaping the surface and improved estimates of reflectivity, and surface composition.

The exploration strategy of the American and Soviet space programs are complementary, as the in-situ technology has been developed to a high degree by the Soviets, while the orbiting radar technology is developed to a high degree by the Americans. Perhaps these two programs can be better coordinated to yield a more comprehensive picture of Venus. Ultimately this is the only way our overall understanding of the veiled planet will be enhanced.

Appendix A

Equilibrium Thermodynamics

The following data were computed for actual Venus temperatures using data tabulated in Robie (1974) and the JANAF tables.

Free Energy of Formation for Selected Minerals

(KJ/mole)

Mineral	°740K	°700K	°640K
$CaCO_3$	-1015.351	-1025.427	-1040.605
$CaMg(CO_3)_2$	-1924.215	-1945.344	-1977.226
$MgCO_3$	-906.981	-917.866	-934.329
$CaMgSi_2O_6$	-7779.902	-2802.910	-2837.534
$CaAl_2Si_2O_8$	-3669.834	-3699.763	-3744.799
$Ca_2Mg_5Si_8O_{22}(OH)_2$	-10553.861	-10649.984	-10794.813
$CaSO_4$	-1153.517	-1166.775	-1190.026
$KAlSi_3O_8$	-3404.077	-3434.533	-3480.398
$KMg_3Al_3O_{10}F_2$	-5548.019	-5593.399	-5661.722
$NaAlSi_3O_8$	-3377.440	-3407.512	-3452.834
Al_2SiO_5	-2221.031	-2240.674	-2270.260
$KAlSi_2O_6$	-2637.987	-2659.180	-2691.147
Mg_2SiO_4	-1875.270	-1891.067	-1914.862
$MgSiO_3$	-1332.118	-1343.693	-1361.124
Fe_2SiO_4	-1234.390	-1247.269	-1266.684
FeS_2	-138.283	-136.711	-140.815
FeO	-216.192	-218.700	-222.447
$CaSiO_3$	-1424.767	-1435.980	-1452.821

Free Energy of Formation for Selected Minerals

(KJ/mole)

(CONTINUED)

Mineral	°740K	°700K	640K
SiO_2	-776.020	-783.176	-794.002
MgF_2	-994.449	-1001.217	-1011.461
$MgCl_2$	-521.633	-527.749	-537.052
CaF_2	-1102.583	-1109.126	-1119.000
$CaCl_2$	-680.448	-686.437	-695.401
NaCL	-342.668	-346.356	-351.98

Free Energy of Formation for Selected Gases

Gas	°740K	°700K	640K
CO_2	-395.433	-395.359	-395.233
CO	-177.084	-173.496	-168.082
H_2O	-206.661	-208.786	-211.907
SO_2	-300.966	-299.190	-299.733
H_2S	-46.903	-44.100	-43.048
HF	-277.279		-276.767
HCl	-99.001	-98.716	-98.264

Appendix B

Macroscopic Properties of Dielectrics

A circuit of the type below, with a capacitor Co and a sinusoidal voltage source of angular frequency w = $2\pi f$.

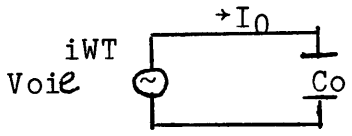

The charging current dQ/dT = d/dT CoV = jwcoV, leads the voltage by a phase angle of 90°

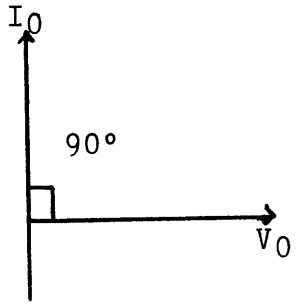

When the capacitor is filled with a substance, the capacitance charges to $C = Co\ \varepsilon'/\varepsilon_0 = CoK'$, where K' is the relative dielectric constant of the material.

In some cases these will exist a loss current component $I\rho = GV$, which is in phase with the voltage. G represents the conductance of the dielectric. The total current traversing the condensor $I = I_c + I_e = (j\omega C + G)V$ is inclined by a power factor angle $\theta<90°$ against the applied voltage V, byu an angle δ from the imaginary axis.

This loss tangent may be written $D = TAN\delta = I_e/I_c$. Since the loss current may result from any energy dissipation process, not just transfer of charge carriers, it is customary to refer to a complex permittivity,

$$\varepsilon^* = \varepsilon' - i\varepsilon''$$

We may write the total current

$$I = (j\omega\varepsilon' + \omega\varepsilon'')\ CoV/\varepsilon o$$

$$I = (i\varepsilon' + \varepsilon'')\ \omega CoV/\varepsilon o$$

$$= \varepsilon^*/\varepsilon o\ i\omega CoV$$

where $\varepsilon^*/\varepsilon o$ becomes k^* the complex relative dielectric constant.

$$K^* = K' - jK''$$

The loss tangent Tanδ then becomes $\varepsilon''/\varepsilon' = K''/K'$

In a parallel plate capacitor, neglecting fringing, has a vacuum capacitance $Co = A/d\ \varepsilon o$, and a current density through the condenser J, under a field $E = V/d$. Therefore, $J = (i\omega\varepsilon' + \omega\varepsilon'')E = \varepsilon^* dE/dT$. The factor $\omega\varepsilon''$ is referred to as the dielectric conductivity $\sigma = \omega\varepsilon''$, which sums over all dissipative effects, and may represent an actual conductivity, caused by migrating charge carriers, or a loss due to friction accompanying the orientation of dipoles.

Appendix C

Measurement of Dielectric Constants

Dielectric constants were measured using the transmission line method described by Van Hipple (1954). Sample preparation involved cutting rock samples into disks with an inner diameter of 0.953cm, and an outer diameter of 2.53cm, so as to accomodate the inner and outer conductors of the transmission line.

The sample is placed into the coaxial line and the electromagnetic waves are allowed to impinge prependicularly on the dielectric boundaries. Dielectric constant ε' and loss tangent are determined by noting the node positions of standing waves setup in the coaxial lines

$$\frac{\varepsilon'}{\varepsilon_o} = \left(\frac{\lambda_o}{2\ell}\right)^2$$

where ℓ is the distance between successive minima, and λ_o is the experimental wavelength. Loss tangent is determined by measuring the inverse standing wave ratio in the line. Corrections must be applied for gaps between the center conductor and the sample, as well as sample thickness. Further details are supplied by Van Hipple (1954).

Measurements were performed with the samples at two orientations (rotated by 180°) and the mean values were computed.

REFERENCES CITED

Adams, W. S. and T. Dunham, Jr., Absorption bands in the infrared spectrum of Venus, Publ. Astron. Soc. Pacific, 44, 243, 1932.

Adel, A. and D. M. Dennison, The infrared spectrum of carbon dioxide. Part I, Phys. Rev., 43, 716, 1933.

Adel, A. and D. M. Dennison, The infrared spectrum of carbon dioxide. Part II, Phys. Rev., 44, 99, 1933.

Aleksandrov, Yu. N., V. K. Golovkov, V. M. Dubrovin, A. L. Zaitsev, V. I. Kaevitser, A. A. Krymov, G. M. Petrov, A. F. Khasyanov, A. M. Shakhovskoi, and O. S. Shamparova, The reflection properties and surface relief of Venus: radar surveys at 39-cm wavelength: Soviet Astronomy, 24, 139-146, 1980 [Astron. Zh., 57, 237-249, 1980].

Arvidson, R. E., Effects of lateral resolution on the interpretability of geologic features sampled by the Pioneer-Venus altimeter, Lunar and Planetary Sci. XII, 31-33, 1981.

Arvidson, R. E., R. Batiza, and E. A. Guinness, Simulation of Pioneer-Venus altimetry using northern Pacific Ocean floor bathymetry, NASA Tech. Memorandum 82385, 77-78, 1980.

Arvidson, R. E. and G. F. Davies, Effects of lateral resolution on the identification of volcanotectonic provinces on Earth and Venus, Geophys. Res. Lett., 8, 741-744, 1981.

Avduevskii, V. S., N. F. Borodin, V. N. Vasil'ev, A. G. Godnev, V. P. Karyagin, V. A. Kovev'yanov, V. P. Kortunenko, R. S. Kremnev, V. M. Pavlova, M. K. Cheremukhina, Parameters of Venus' atmosphere at Venera 11 and 12 landing sites (an analysis of the results of measurements made by these automatic interplanetary stations), Cosmic Res., 17, 539, 1980.

Bagnold, R. A., The physics of blown sand and desert dunes, New York, Wm. Marrow, 265 pp., 1941.

Barker, E. S., Comparison of simultaneous CO_2 and H_2O observations of Venus, J. Atmos. Sci., 32, 1971, 1975.

Barker, E. S., Observations of Venus water vapor over the disk of Venus: the 1972-74 data using H_2O lines at 81097 Å and 8176 Å, Icarus, 25, 268, 1975.

Barker, E. S., Detection of SO_2 in the UV spectrum of Venus, Geophys. Res. Lett., 6, 117, 1979.

Barker, E. S. and M. A. Perry, Semiperiodic variations in CO_2 abundance on Venus, Icarus, 25, 282, 1975.

Barsukov, V. L., I. L. Khodakovsky, V. P. Volkov, and K. P. Florensky, The geochemical model of the troposphere and lithosphere of Venus based on new data, Space Res., 20, 197, 1980.

Barsukov, V. I., V. P. Volkov, and I. L. Khodakovsky, The mineral composition of Venus surface rocks, LPSC 11, 765-773, 1980.

Barth, C. A., J. D. Pearce, K. K. Kelly, L. Wallace, and W. G. Fastie, UV emissions observed near Venus from Mariner 5, Science, 158, 1675, 1967.

Belton, M. J. S., and D. M. Hunten, A search for O_2 on Mars and Venus, A.P.J., 153, 963, 1968.

Boldt, J., The Winning of Nickel, Methuen and Co., 1967.

Campbell, D. B., R. B. Dyce and G. H. Pettengill, New radar image of Venus, Science, 193, 1123-1124, 1976.

Campbell, D. B. and B. A. Burns, Earth-based radar imagery of Venus, Journ. Geophys. Res., 85, 8271-8281, 1980.

Campbell, D. B., B. A. Burns, and V. Boriakoff, Venus: further evidence of impact cratering and tectonic activity from radar observations, Science, 204, 1424-1427, 1979.

Campbell, M. J. and J. Ulrich, Electrical properties of rocks and their significance for lunar radar observations, Journ. Geophys. Res., 74, 5867, 1969.

Carpenter, R. L., Study of Venus by CW radar - 1964 results, Atron. Journ., 71, 142-152, 1966.

Connes, J. and P. Connes, Near-infrared planetary spectra by Fourier spectroscopy, I. Instrtuments and results, J. Opt. Sco. Am., 56, 896, 1966.

Connes, P. and G. Michel, Astronomical Fourier spectrometer, Appl. Optics, 14, 2067, 1975.

Connes, P., J. Connes, W. S. Benedict, and L. D. Kaplan, Traces of HCl and HF in the atmosphere of Venus, Astrophys. J., 147, L1230, 1967.

Connes, P., J. Connes, L. D. Kaplan, and W. S. Benedict, Carbon monoxide in the Venus atmosphere, Astrophys. J., 152, 731, 1968.

Conway, R. R., R. P. McCoy, C. A. Barth, and A. L. Lane, IUE detection of sulphur dioxide in the atmosphere of Venus, Geophys. Res. Lett., 6, 629, 1979.

Counselman, C. C., S. A. Gourevitch, R. W. King, and G. B. Loriot, Zonal and meridional circulation of the lower atmosphere of Venus determined by radio interferometry, Journ. Geophys. Res., 85, 8026-8030, 1980.

Cruikshank, D. P., Sulphur compounds in the atmosphere of Venus, II: upper limits for the abundance of COS and H_2S, Comm. Lun. Planet. Lab., No. 98, U. Ariz., 1967.

Deer, Howie, and Zussman, An Introduction to the Rock Forming Minerals, Longman, 1966.

Donahue, Hoffman, Hodges, Watson, Venus was wet, Science, 216, p. 631, 1982.

Donahue, T. M., The upper atmosphere of Venus: a review, J. Atmos. Sci., 25, 5678, 1968.

Donahue, T. M. Deuterium in the upper atmospheres of Venus and Earth, J. Geophys. Res., 74, 1128, 1969.

Durrance, S. T., R. R. Conway, C. A. Barth, and A. L. Lane, IUE high-resolution observation of the Venus dayglow spectrum 1280-1380 Å, Geophys. Res. Lett., 8, 111, 1981.

Dyce, R. B. and G. H. Pettengill, Radar determination of the rotation of Venus and Mercury, Astron. Journ., 72, 351-359, 1967.

Ekonomov, A. P., B. E. Moshkin, Yu. M. Golovin, N. A. Parfent'ev, and N. F. San'ko, Spectrophotometric experiments on Venera II and Venera 12 descent modules, Cosmic. Res., 17, 590, 1980.

Elachi, C., Spaceborne imaging: geologic and oceanographic applications, Science, 209, 1073-1082, 1980.

Esposito, L. W., Ultraviolet contrasts and the absorbers near the Venus cloud tops, J. Geophys. Res., 85, 8151, 1980.

Esposito, L. W., Absorbers seen near the Venus cloud tops from Pioneer Venus, Adv. Space Res., 1, 163, 1981.

Esposito, L. W., J. R. Winick and A. I. Stewart, Sulfur dioxide in the Venus atmosphere: distribution and implications, Geophys. Res. Lett., 6, 601, 1979.

Evans, J. V., Radar studies of planetary surfaces, Ann. Rev. Astron. Astrophys., 7, 201-249, 1969.

Evans, J. V. and T. Hagfors, eds., Radar Astronomy, New York, McGraw-Hill, 620 pp., 1968.

Fink, U., H. P. Larson, G. P. Kuiper, and R. F. Poppen, Water vapor in the atmosphere of Venus, Icarus, 17, 617, 1972.

Florensky, C. P., L. B. Ronca and A. T. Basilevsky, Geomorphic degradations on the surface of Venus: an analysis of Venera 9 and Venera 10 data, Science, 196, 869-871, 1977a.

Florensky, C. P., V. P. Volkov, and O. V. Nikolaeva, A geochemical model of the Venus troposphere, Icarus, 33, 537, 1978.

Florensky, C. P., L. B. Ronca, A. T. Basilevsky, G. A. Burba, O. V. Nikolaeva, A. A. Pronin, A. M. Trakhtman, V. P. Volkov, and V. V. Zazetsky, The surface of Venus as revealed by Soviet Venera 9 and 10, Geol. Soc. Amer. Bull., 88, 1537-1545, 1977b.

Forsyth, D. W., Lithospheric flexure, Rev. Geophys. Space Phys., 17, 1109-1114, 1979.
the upper mantle, Journ. Geophys. Res., 80, 2553-2564, 1975.

Gelman, B. G., V. G. Zolotukhun, N. I. Lamonov, B. V. Levchuk, A. N. Lipatov, L. M. Mukhin, D. F. Nenarokov, V. A. Rotin, and B. P. Okhotnikov, An analysis of the chemical composition of the atmosphere of Venus on an AMS of the Venera 12 using a gas chromatograph, Kosmich. Issled., 17, 708, 1979 (Cosmic. Res., 17, 585, 1980).

Goldstein, R. M., Preliminary Venus radar results, Radio Sci., 69D, 1623-1625, 1965.

Goldstein, R. M. and H. Rumsey, Jr., A radar snapshot of Venus, Science, 169, 974-977, 1970.

Goldstein, R. M., R. R. Green, and H. C. Rumsey, Venus radar images, Journ. Geophys. Res., 81, 4807-4817, 1976.

Goldstein, R. M., R. R. Green, and H. C. Rumsey, Venus radar brightness and altitude images, Icarus, 36, 334-352, 1978.

Gooding, J. L., Chemical weathering on Mars, thermodynamic stabilities of primary minerals (and their alteraction products) from mafic igneous rocks, Icarus, 33, 483, 1978.

Gooding, J. L., Experimental studies of weathering in a hot CO_2 atmosphere, NASA Tech. Memo #84211, 1981.

Greeley, R. J., B. R. White, R. Leach, R. Leonard, J. B. Pollack, and J. D. Iversen, Venus aeolian processes: saltation studies and the Venusian wind tunnel, NASA Tech. Memorandum 82385, 275-277, 1980a.

Greeley, R. J., R. Leach, and J. B. Pollack, Venus: consideration of aeolian (windblown) processes, Lunar Planet. Sci. XI, 360-363, 1980b.

Green, D. H., Experimental melting studies on a model upper mantle composition at high pressure under water-saturated and water-undersaturated conditions, Earth Planet. Sci. Lett., 19, 37-53, 1973.

Gull, T. R., C. R. O'Dell, and R. A. R. Parker, Water vapor in Venus determined by airborne observations of the 8200 Å band, Icarus, 21, 213, 1974.

Hagfors, T., Remote probing of the Moon by infrared and microwave emissions and by radar, Radio Sci., 5, 219-227, 1970.

Hagfors, T. and J. V. Evans, Radar studies of the Moon, In: Radar Astronomy, Evans, J. V. and T. Hagfors, eds., New York, McGraw-Hill, 219-273, 1968.

Harker, R. I. and O. F. Tuttle, Experimental data on the PCO_2-T curve for the reaction: calcite + quartz wollastonite + CO_2, Am. Journ. Sci., 254, 239-249, 1956.

Hawley, J., The Sudberg ores: Their Mineralogy and Origin, Mineralogical Association of Canada, 1962.

Head, J. W., S. E. Yoter, and S. C. Solomon, Topography of Venus and Earth: a test for the presence of plate tectonics, Lunar Planet. Sci. XII, 430-432, 1981.

Hoffman, J. H., G. M. Keating, H. Niemann, V. Oyama, J. Pollack, A. Seiff, A. I. Stewart, and U. von Zahn, Composition and structure of the atmosphere of Venus, Space Sci. Rev., 20, 307, 1977.

Hoffman, J. H., R. R. Hodges, Jr., and K. D. Duerksen, Pioneer Venus large probe neutral mass spectrometer, J. Vac. Soc. Technol., 16(2), 692, 1979.

Hoffman, J. H., R. R. Hodges, T. M. Donahue, and M. B. McElroy, Composition of the Venus lower atmosphere from the Pioneer Venus mass spectrometer, Journ. Geophys. Res., 85, 7882-7890, 1980.

Hoffman, J. H., V. I. Oyama, and U. Von Zahn, Measurements of the Venus lower atmosphere composition: a comparison of results, Journ. Geophys. Res., 85, 7871, 1980.

Hoffman, H. J., D. Krankowsky, D. Linkert, K. Pelka, and U. von Zahn, The Pioneer Venus bus neutral gas mass spectrometer (BNMS), IEEE, Trans. Geoscience and Remote Sensing, GE-18, 122, 1980.

Hunten, D. M. and T. M. Donahue, Hydrogen loss from the terrestrial planets, Ann. Rev. Earth Planet. Sci., 4, 265, 1976.

Hunten, D. M., M. J. S. Belton, and H. Spinrad, Water vapor on Venus - reply, Astrophys. J., 150, L125, 1967.

Istomin, V. G., K. V. Grechnev, V. A. Kochnev, and L. N. Ozerov, Kosmich. Issled., 17, 703, 1979.

Istomin, V. G., K. V. Grechnev, and V. A. Kotchnev, Mass spectrometer measurements of the composition of the lower atmosphere of Venus, Space Res., 20, 215, 1980.

Istomin, V. G., K. V. Grechnev, and V. A. Kochnev, Mass-spectrometery of the Venus lower atmosphere: krypton isotopes and other recent results of processing the data of measurements on-board the Venera 11 and 12 spacecrafts, paper presented at the COSPAR Conference, 1980.

Iverson, J. D. and B. R. White, Saltation threshold on Earth, Mars, and Venus, Sedimentology, 111-119, 1982.

Iversen, J. D., R. J. Greeley, and J. B. Pollack, Windblown dust on Earth, Mars, and Venus, Journ. Atmos. Sci., 33, 2425-2429, 1976a.

Iversen, J. D., J. B. Pollack, R. J. Greeley, and B. R. White, Saltation threshold on Mars: the effect of interparticle force, surface roughness, and low atmospheric density, Icarus, 29, 381-393, 1976b.

JANAF thermochemical tables, Dow Chemical Co., Midland, MI, 1971.

Janssen, M. A. and R. L. Poynter, The microwave absorption of SO_2 in the Venus atmosphere, Icarus, 46, 51, 1981.

Kakar, R. K., J. W. Waters, and W. J. Wilson, Venus: microwave detection of carbon monoxide, Science, 191, 379, 1976.

Katsube, T. J. and L. S. Collett, Electromagnetic propagation characteristics of rocks, in: The Physics and Chemistry of Minerals and Rocks, Strens, R. G. J., ed., John Wiley and Sons, 1982.

Katsube, T. J. and L. S. Collett, Proc. 4th Lunar Sci. Conf., 311, 1973.

Keldysh, M. V., Venus exploration with the Venera 9 and Venera 10 spacecrafts, Icarus, 30, 605-625, 1977.

Keller, G. V., Electrical properties of rocks and minerals, In: Handbook of Physical Constants, Clark, S. P., Jr., ed., Geol. Soc. Am. Mem. 97, 553-577, 1966.

Khodakovsky, I. L., V. P. Volkov, I. Yu. Sidorov, M. V. Borisov, and M. V. Lomonosov, Venus: preliminary prediction of the mineral composition of surface rocks, Icarus, 39, 352-363, 1979.

Krasnopolsky, V. A. and V. A. Parshev, On the chemical composition of the Venus troposphere and the cloud layer based on Venera 11, 12 and Pioneer Venus measurements, Space Res. Inst., Acad. Sci., USSR, PR-514, 1979.

Krasnopolsky, V. A. and V. A. Parshev, Chemical composition of Venus' troposphere and cloud layer based on Venera 11, Venera 12, and Pioneer Venus measurments, Cosmic Res., 17, 630, 1980.

Kriedelbaugh, M., Experimental study of reaction kinetics for reaction calcite + quartz = wollastonite + CO_2, American Journal of Science, 273, 757-777, 1973.

Kridelbaugh, S. J., Experimental Study of the reaction Quartz + Celcite = Wollastonite + Carbon Dioxide at elevated temperature and pressure, American Journal of Science 273, 757-777 (1973).

Krotikov, V. D., Several electrical characteristics of the Earth's rocks and a comparison with the characteristics of the surface layer of the Moon, Izv. Vuzov. Radiofizika 5/6, 1057-1061, 1962.

Kuz'min, A. D. and M. Ya. Marov, Physics of the planet Venus, NASA Tech. Trans. TT F-16, 226, 328 pp., 1975 [Fizika Planety Venera, Moscow, Nauka Press, 408 pp., 1974].

Lambert, R. St. J., Archean thermal regimes, crustal and upper mantle temperatures, and a progressive evolutionary model for the Earth, In: The early history of the Earth, B. F. Windley, ed., London, John Wiley and Sons, 363-373, 1976.

Lawrence, G. M., C. A. Barth, and V. Argabright, Excitation of the Venus night airglow, Science, 195, 573, 1977.

Lewis, J. S., Estimate of the surface conditions on Venus, Icarus, 8, 434-456, 1968.

Lewis, J. S., Venus: atmospheric and lithospheric composition, Earth Planet. Sci. Lett., 10, 73-80, 1970.

Lewis, J. S., Metal/silicate fractionation in the solar system, Earth Planet. Sci. Lett., 15, 286-290, 1972.

Lewis, J. S. and F. A. Kreimendahl, Oxidation state of the atmosphere and crust of Venus from Pioneer Venus observations, Icarus, 42, 330-337, 1980.

Malin, M. C. and R. S. Saunders, Surface of Venus: evidence of diverse landforms from radar observations, Science, 196, 987-990, 1977.

Masursky, H., E. Eliason, P. G. Ford, G. E. McGill, G. H. Pettengill, G. G. Schubert, Pioneer Venus radar results: geology from images and altimetry, J. Geophys. Res., 85, 8232-8260, 1980.

Masursky, H., A. L. Dial, Jr., G. G. Schaber, and M. E. Strobell, Venus: a first geologic map based on radar altimetric and image data, Lunar. Planet. Sci. XII, 661-663, 1981a.

Masursky, H., G. G. Schaber, A. L. Dial, and M. E. Strobell, Tectonism and volcanism on Venus deduced from Pioneer Venus images and altimetry, Trans. Am. Geophys. Union, 62, 385, 1981b.

McElroy, M. B. and D. M. Hunten, the ratio of deuterium to hydrogen in the Venus atmosphere, J. Geophys. Res., 74, 1720, 1969.

McGill, G. E., Tectonics of Venus, NASA Tech. Memorandum, 80339, 39-41, 1979a.

McGill, G. E., Venus tectonics: another Earth or another Mars?, Geophys, Res. Lett., 6, 739-741, 1979b.

McGill, G. E., Evidence for continental-style rifting from the Beta region of Venus, NASA Tech. Memorandum, 82385, 79-80, 1980.

McGill, G. E., S. J. Steenstrup, C. Barton, and P. G. Ford, Continental rfiting and the origin of Beta Regio, Venus, Geophys. Res. Lett., 8, 737-740, 1981.

McGill, G. E., J. L. Warner, M. C. Malin, R. E. Arvidson, E. Eliason, S. Nozette, and R. D. Reasenberg, Topography, Surface Properties and Tectonic Evolution in Venus, ed. D. Hunten, L. Colin, T. Donahue, U. of Arizona Press, Tucson, 1982.

Mueller, G., and Kridelbaugh, S. J., Kinetics of CO_2 Production on Venus, Icarus, 19, 531-551, 1973.

Mueller, R. F., Chemistry and petrology of Venus: preliminary deductions, Science, 141, 1046-1047, 1963.

Mueller, R. F., Planetary problems: origin of the Venus atmopshere, Science, 163, 1322-1324, 1969.

Mueller, R. F. and S. K. Saxena, Chemical Petrology, New York, Springer-Verlag, 1977.

Nozette, S. and J. S. Lewis, Venus: chemical weathering of igneous rocks and buffering of atmospheric composition, Science, 216, 181-183, 1982.

Olhoeft, G. R., Electrical properties of rocks, in: The Physics and Chemistry of Minerals and Rocks, Strens, R. G. J., ed., John Wiley and Sons, 1982.

Orville, P., Crust-atmosphere interactions, In: The atmosphere of Venus, J. E. Hansen, ed., NASA Spec. Publ. SP-382, 190-195, 1975.

Oyama, V. I., Large probe gas chromatograph (LGC), In: Pioneer Venus experiment descriptions, L. Colin and D. M. Hunten, eds., Space Sci. Rev., 20, 465, 1977.

Oyama, V. I., G. C. Carle, F. Woeller, Corrections in the Pioneer Venus sounder probe gas chromatographic analysis of the lower Venus atmosphere, Science, 208, 399, 1980.

Oyama, V. I., G. C. Carle, F. Woeller, J. B. Pollack, R. T. Reynolds, and R. A. Craig, Pioneer Venus gas chromatography of the lower atmosphere of Venus, J. Geophys. Res., 85, 7891, 1980.

Peacock, S., The systematics of sulfide, mineralogy and the regionally metamorphosed Ammonoosuc Volcanics, Ms. Thesis, M.I.T., 1981.

Pettengill, G. H., R. B. Dyce and D. B. Campbell, Radar measurements at 70 cm of Venus and Mercury, Astron. Journ., 72, 330-337, 1967.

Pettengill, G. H. P. G. Ford, W. E. Brown, W. M. Kaula, C. H. Keller, H. Masursky, and G. E. McGill, Pioneer Venus radar mapper experiment, Science, 203, 806-808, 1979a.

Pettengill, G. H., P. G. Ford, W. E. Brown, W. M. Kaula, H. Masursky, E. Eliason, and G. E. McGill, Venus: preliminary topographic and surface imaging results from the Pioneer Orbiter, Science, 205, 91-93, 1979b.

Pettengill, G. H., E. Eliason, P. G. Ford, G. B. Loriot, H. Masursky, and G. E. McGill, Pioneer Venus radar results: altimetry and surface properties, J. Geophs. Res., 85, 8261-8270, 1980.

Pettengill, G. H., P. G. Ford, and S. Nozette, Venus: global surface radar reflectivity, Science, 217, 640-642.

Phillips, R. J. and K. Lambeck, Gravity fields of the terrestrial planets: long-wavelength anomalies and tectonics, Rev. Geophys. Space Phys., 18, 27-76, 1980.

Phillips, R. J., W. M. Kaula, G. E. McGill, and M. C. Malin, Tectonics and evolution of Venus, Science, 212, 879-887, 1981.

Phillips, R. J. and Malin, M. The Interior of Venus, Tectonic Implications in Venus, ed. D. M. Hunten, L. Colin, and T. M. Donahue, U. of Arizona Press, Tucson, 1982.

Pollack, J. B., O. B. Toon, and R. Boese, Green house models of Venus' high surface temperature, as constrained by Pioneer Venus measurements, J. Geophys. Res., 85, 8223, 1980.

Prinn, R. G., Photochemistry of HCl and other minor constituents in the atmosphere of Venus, J. Atmos. Sci., 28, 1058, 1971.

Prinn, R. G., Venus: composition and structure of the visible clouds, Science, 182, 1132, 1973.

Prinn, R. G., Venus: chemical and dynamical processes in the stratosphere and mesosphere, J. Atmos. Sci., 32, 1237, 1975.

Prinn, R. G., Venus: chemistry of the lower atmosphere prior to the Pioneer Venus mission, Geophys. Res. Lett., 5, 973, 1978.

Prinn, R. G., On the possible roles of gaseous sulfur and sulfanes in the atmosphere of Venus, Geophys. Res. Lett., 6, 807, 1979.

Prinn, R. G. Chemistry of the atmosphere of Venus, EOS, 61, 965, 1980.

Ringwood, A. E. and D. L. Anderson, Earth and Venus: a comparative study, Icarus, 30, 243-253, 1977.

Robie, R. A., B. S. Hemingway, and J. R. Fisher, Thermodynamic properties of minerals and related substances at 298.15°K and 1 bar (10^5 pascals) pressure and at higher temperatures, U.S.G.S. Bull., 1452, 1979.

Rogers, A. E. E. and R. P. Ingalls, Venus: mapping the surface reflectivity by radar interferometry, Science, 165, 797-799, 1969.

Rumsey, H. C., G. A. Morris, R. R. Green, and R. M. Goldstein, A radar brightness and altitude image of a portion of Venus, Icarus, 23, 1-7, 1974.

Sagan, C., Wind blown dust on Venus, J. Atmos. Sci., 1975.

Saunders, R. S. and M. C. Malin, Venus: geologic analysis of radar images, Geologica Romana, 15, 507-515, 1976.

Saunders, R. S. and M. C. Malin, Geologic interpretation of new observations of the surface of Venus, Geophys. Res. Lett., 4, 547-550, 1977.

Schaber, G. G., Geologic application of radar data to planetary exploration, Geologica Romana, 15, 363-365, 1976.

Schaber, G. G. and J. M. Boyce, Probable distribution of large impact basin on Venus: comparison with Mercury and the Moon, In: Impact and explosion cratering, D. J. Roddy, R. O. Peppin, and R. B. Morrill, eds., New York, Pergamon Press, 603-612, 1977.

Schaber, G. G. and H. Masursky, Large-scale equatorial and mid-latitude surface disruptions on Venus: preliminary geologic assessment, Lunar Planet. Sci. XII, 929-931, 1981.

Seiff, A., D. B. Kirk, R. E. Young, R. C. Blanchard, J. T. Findlay, G. M. Kelly, and S. C. Sommer, Measurements of thermal structure and thermal contrasts in the atmosphere of Venus and related dynamical observations: results from the four Pioneer Venus probes, J. Geophys. Res., 85, 7903-7933, 1980.

Selivanov, A. S., A. S. Panfilov, M. K. Naraeva, V. P. Chemodanov, M. I. Bokhonov, and M. A. Gerasimov, Photometric analysis of panoramas on the surface of Venus, Cosmic Res., 14, 596-603, 1976.

Sill, G. T., Sulfuric acid in the Venus clouds, Comm. Lun. Planet. Lab., No. 171, Univ. Arizona, 1972.

Sill, G. T., The composition of the ultraviolet dark markings on Venus, J. Atmos. Sci., 32, 1201, 1975.

Sjogren, W. L., R. J. Phillips, P. W. Birkeland, and R. N. Wimberly, Gravity anomalies on Venus, J. Geophys. Res., 85, 8295-8302, 1980.

Smith, J. V., Planetary crusts: a comparative review, Proc. Conf. Lunar Highlands Crust, Geoch. Cosmoch. Acata, Supp. 12, 441-456, 1980.

Surkov, Y. A., B. M. Andreichikov, and O. M. Kalinkina, Gas-analysis equipment of the automatic interplanetary stations Venera 4, 5, 6, and 8, Space Sci. Instrum., 3, 301, 1977.

Surkov, Yu. A., Geochemical studies of Venus 9 and 10 automatic interplanetary stations, Lunar Planet. Sci. VIII, 2665-2685, 1977.

Surkov, Yu. A., B. M. Andreichikov, and O. M. Kalinkina, Composition and structure of the cloud layer of Venus, In: Space Research XIV, ed., Berlin, Akad Verlag, 679-687, 1974.

Surkov, Yu. A., F. F. Kirnozov, V. N. Glazov, A. G. Dunchenko, and L. P. Tatsil, The content of natural radioactive elements in Venusian rock as determined by Venera 9 and Venera 10, Kosmicheskie Issledovaniya, 14, 704-709, 1976a.

Surkov, Yu. A. et al., 1976b.

Tauber, M. E. and D. B. Kirk, Impact craters on Venus: Icarus, 28, 351-357, 1976.

Tullis, J. A., High temperature deformation of rocks and minerals, Rev. Geophys. Space Phys., 17, 1137-1154, 1979.

Turcotte, D. L., Convection, Rev. Geophys. Space Phys., 17, 1090-1098, 1979.

Turcotte, D. L., R. J. Willemann, W. F. Haxby, and J. Norberry, Role of membrane stresses in the support of planetary topography, J. Geophys. Res., 86, 3951-3959, 1981.

Urey, H., The planets, their origin and development, New Haven, Yale Univ. Press, 1953.

Vinogradov, A. P., Yu. A. Surkov, and F. F. Kirnozov, The content of uranium, thorium and potassium in the rocks of Venus as measured by Venera 8, Icarus, 20, 253-259, 1973.

Von Hippell, A. R., Dielectric materials and applications, MIT Press, 1954.

Von Zahn, U., S. Kumar, H. Niumann, and R. Prinn, Composition of the Venus Atmosphere In: Venus, eds., D. Hunten, L. Colin, T. Donahue, V. I. Mapoz, U. Arizona Press, Tucson, 1982.

Walker, D., An experimental study of wind ripples, Ms. Thesis, M.I.T., 1981.

Wallace, L., F. E. Stuart, R. H. Nagel, and M. D. Larson, A search for deuterium on Venus, Astrophys. J., 168, L29, 1971.

Warner, J. L., Venus: do sediments cover lowlands?, Bull. Amer. Astron. Soc., 12, 691, 1980.

Weertman, J., Height of mountains on Venus and the creep properties of rock, Physics Earth Planet. Int., 19, 197-207, 1979.

Weertman, J. and J. R. Weertman, High temperature creep of rock and mantle viscosity, Ann. Rev. Earth Planet. Sci., 3, 293-317, 1975.

Wilson, W. J., M. J. Klein, R. K. Kahar, S. Gulkis, E. T. Olsen, and P. T. P. Ho, Venus, I. Carbon monoxide distribution and molecularline searches, Icarus, 45, 624, 1981.

Winick, J. R. and A. I. F. Stewart, Photochemistry of SO_2 in Venus' upper cloud layers, J. Geophys. Res., 85, 7849, 1980.

Wood, C. Venusian volcanism: environmental effects on style and landforms, NASA Tech. Memorandum 80339, 244-276, 1979.

Wyllie, P. J., The dynamic earth, New York, John Wiley and Sons, Inc., 416 pp., 1971.

Young, A. T., Are the clouds of Venus sulfuric acid?, Icarus, 18, 564, 1973.

Young, A. T., The clouds of Venus, J. Atmos. Sci., 32, 1125, 1975.

Young, A. T., An improved Venus cloud model, Icarus, 32, 1, 1977.

Young, L. D. G., High resolution spectra of Venus, a review, Icarus, 17, 632, 1972.

Young, L. D. G., A new interpretation of the Venera 11 spectra of Venus, paper presented at An International Conference on the Venus Environment, Palo Alto, USA, 1981.

Zohar, S. and R. M. Goldstein, Venus map: a detailed look at the feature B, Nature, 219, 357-358, 1968.